AFWL-TR-76-327

AFWL-TR-76-327

TORIC RESONATOR EXPERIMENTAL STUDY

Perkin-Elmer Corporation
Electro-Optical Division
Norwalk, CT 06856

July 1977

Final Report

Approved for public release; distribtuion unlimited.

AIR FORCE WEAPONS LABORATORY
Air Force Systems Command
Kirtland Air Force Base, NM 87117

This final report was prepared by the Perkin-Elmer Corporation, Electro-Optical Division, Norwalk, Connecticut, under Contract F29601-75-C-0141, Job Order 30151802, with the Air Force Weapons Laboratory, Kirtland Air Force Base, New Mexico. Captain Van Workum (ALO) was the Laboratory Project Officer-in-Charge.

When US Government drawings, specifications, or other data are used for any purpose other than a definitely related Government procurement operation, the Government thereby incurs no responsibility nor any obligation whatsoever, and the fact that the Government may have formulated, furnished, or in any way supplied the said drawings, specifications, or other data is not to be regarded by implication or otherwise as in amy manner licensing the holder or any other person or corporation or conveying any rights or permission to manufacture, use, or sell any patented invention that may in any way be related thereto.

This report has been reviewed by the Information Office (OI) and is releasable to the National Technical Information Service (NTIS). At NTIS, it will be available to the general pulbic, including foreign nations.

This technical report has been reviewed and is approved for publication.

JOHN A. VAN WORKUM
Captain, USAF
Project Officer

FOR THE COMMANDER

JAMES D. DILLOW
Lt Colonel, USAF
Chief, Advanced Beam Control Branch

ARMAND D. MAIO
Lt Colonel, USAF
Chief, Advanced Laser Technology Division

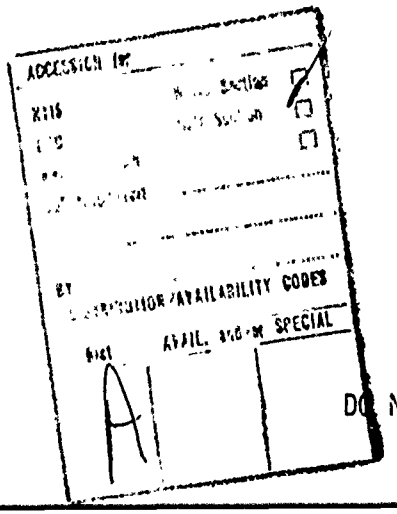

DO NOT RETURN THIS COPY. RETAIN OR DESTROY.

UNCLASSIFIED

SECURITY CLASSIFICATION OF THIS PAGE (When Data Entered)

REPORT DOCUMENTATION PAGE	READ INSTRUCTIONS BEFORE COMPLETING FORM
1. REPORT NUMBER: AFWL-TR-76-327	2. GOVT ACCESSION NO. / 3. RECIPIENT'S CATALOG NUMBER
4. TITLE (and Subtitle): TORIC RESONATOR EXPERIMENTAL STUDY.	5. TYPE OF REPORT & PERIOD COVERED: Final Report.
	6. PERFORMING ORG. REPORT NUMBER
7. AUTHOR(s)	8. CONTRACT OR GRANT NUMBER(s): F29601-75-C-0141 new
9. PERFORMING ORGANIZATION NAME AND ADDRESS: Perkin-Elmer Corporation, Main Avenue, Norwalk, Conneticut 06856	10. PROGRAM ELEMENT, PROJECT, TASK AREA & WORK UNIT NUMBERS: 63000F, 30151802
11. CONTROLLING OFFICE NAME AND ADDRESS: Air Force Weapons Laboratory (ALO), Kirtland Air Force Base, NM 87117	12. REPORT DATE: July 1977 ✓
	13. NUMBER OF PAGES: 134
14. MONITORING AGENCY NAME & ADDRESS (if different from Controlling Office) 135p.	15. SECURITY CLASS. (of this report): Unclassified
	15a. DECLASSIFICATION/DOWNGRADING SCHEDULE

16. DISTRIBUTION STATEMENT (of this Report)

Approved for public release; distribution unlimited.

17. DISTRIBUTION STATEMENT (of the abstract entered in Block 20, if different from Report)

18. SUPPLEMENTARY NOTES

19. KEY WORDS (Continue on reverse side if necessary and identify by block number)

Optics
Resonators
Lasers
Annular Laser
Toric Resonator

20. ABSTRACT (Continue on reverse side if necessary and identify by block number)

An experimental study of several unstable resonator concepts for annular gain volume lasers has been performed. The annular geometry is potentially advantageous for lasers employing radial flow of gain media across the optical resonator axis. The objectives of this study were to determine the ability of each resonator concept to support a single low-order transverse mode, and to measure its sensitivity to various misalignments and figure errors. The configurations tested were the 'converging wave' resonator of Chodzko, and several variations of the half-symmetric unstable resonator with an intracavity axicon

DD FORM 1 JAN 73 1473 EDITION OF 1 NOV 65 IS OBSOLETE

UNCLASSIFIED

SECURITY CLASSIFICATION OF THIS PAGE (When Data Entered)

(Blk 20)

(HSURIA). Several different annular gain cells were designed and used in these test including an annular dye cell (visible) and a flash photolysis DF (IR) gain cell, each stimulated by a central flash lamp. The "converging wave" resonator did not produce the desired single low order transverse mode and its characteristics were sensitive to small misalignments (≈ 10 μrad). Results obtained for the HSURIA show evidence of fundamental mode output (≤ 2λ/D divergence) and high sensitivity to misalignments. Modification of the cavity with a hollow corner reflector in place of the spherical feedback mirror significantly reduces this misalignment sensitivity.

TABLE OF CONTENTS

TABLE OF CONTENTS (Continued)

LIST OF ILLUSTRATIONS

LIST OF ILLUSTRATIONS (Continued)

LIST OF ILLUSTRATIONS (Continued)

LIST OF ILLUSTRATIONS (Continued)

SECTION I

INTRODUCTION

1. PROGRAM OBJECTIVES

Because of the trend in high-energy lasers toward using gain volumes that are annular cylinders, suitable optical methods need to be developed to extract power efficiently and to produce near-uniform phase front output from such gain regions.

The objective of this contract was to determine experimentally the feasibility of various resonator cavity designs for use with high-energy, high-tube-Fresnel-number, radial flow lasers.

2. DESIGN APPROACH

It was required to design, fabricate, and assemble a suitable laser test-bed to simulate a high-gain, high-Fresnel-number, radial flow laser and to investigate and report on the results of several resonator configurations on the test-bed. The investigations and reports were to include studies of beam quality, mirror misalignment sensitivity, mode control, and alignment techniques.

Resonators to be included were orginally:

(1) Spherical mirror (converging wave)

(2) Half-symmetric unstable resonators with internal axicon (HSURIA) with various feedback elements

(3) Toric unstable resonators

The (confocal) toric unstable resonator was judged to have a low probability of success and was deleted from the program because of time and budgetary considerations.

Originally, a visible wavelength dye laser had been intended for use with all the desired resonator configurations. The advantages of being able

to work in the visible region from the standpoint of alignment and diagnostic capability are obvious. It became apparent, however, that the problem of obtaining the necessary optical quality of beam compactor elements seriously compromised the performance of HSURIA resonators operating in the visible. Perkin-Elmer was unable to obtain a two-element axicon to the $\lambda/10$ zero to peak tolerances required for operation at 5900 Å within the time and cost constraints of the contract. The HSURIA resonator designs were therefore modified to be used with a government-supplied W-axicon. The W-axicon, however, still exhibited excessive aberration in the visible so an additional test was added for the HSURIA configuration using an HF/DF laser test bed. The HF/DF laser operated at 3.8 μm where the optical quality of the W-axicon met specifications.

The resonator configurations (shown in Figures 1 through 6) and the gain cells used are listed in Table 1.

TABLE 1. RESONATOR EXPERIMENTS PERFORMED

Resonator	Gain Cell
Spherical Mirror (Figure 1)	Dye (Annular)
HSURIA (Figure 2)	Dye (Annular)
HSURIA (Figure 5)	Dye (Compacted)
HSURIA/C^3* (Figure 3)	Dye (Annular)
HSURIA/C^3 (Figure 4)	Dye (Compacted)
HSURIA/C^3 (Figure 6)	HF/DF (Annular)

*HSURIA/C^3 denotes an HSURIA that uses a corner-cube feedback element.

These resonator configurations were selected on the basis of their predicted ability to produce fundamental transverse mode outputs of near-diffraction-limited quality. The experiments were performed to verify this hypothesis and, furthermore, to determine each resonator's sensitivity to component misalignments.

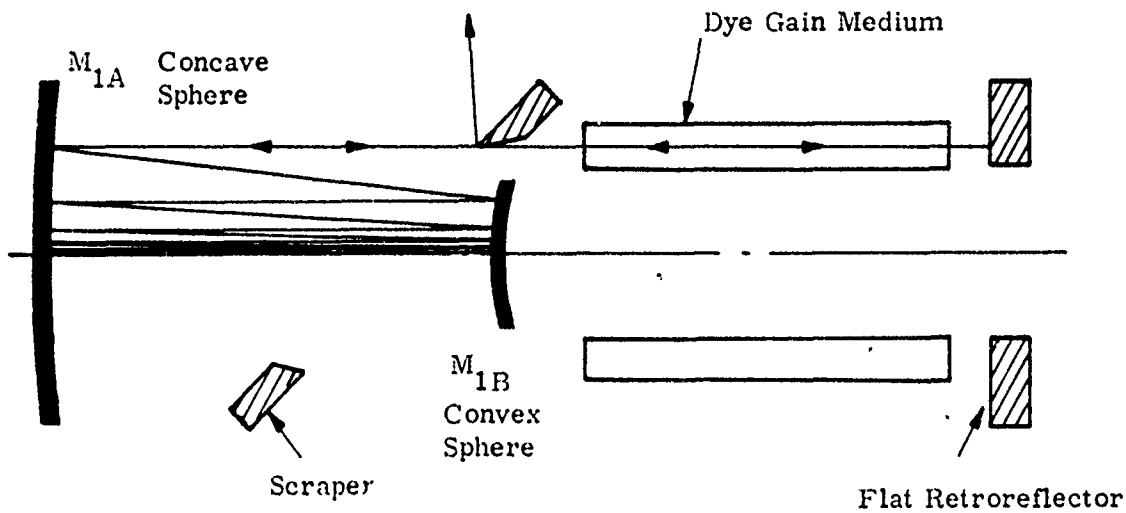

Figure 1. Spherical Mirror (Converging Wave) Resonator

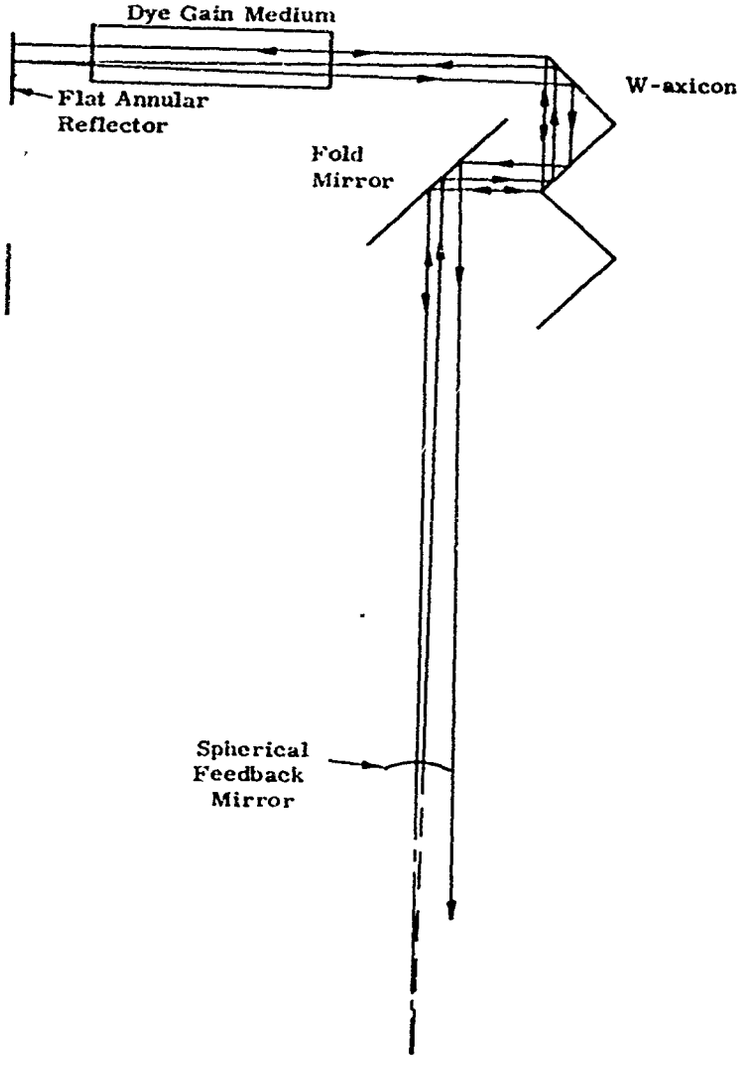

Figure 2. HSURIA Using W-axicon and Convex Spherical Feedback Element

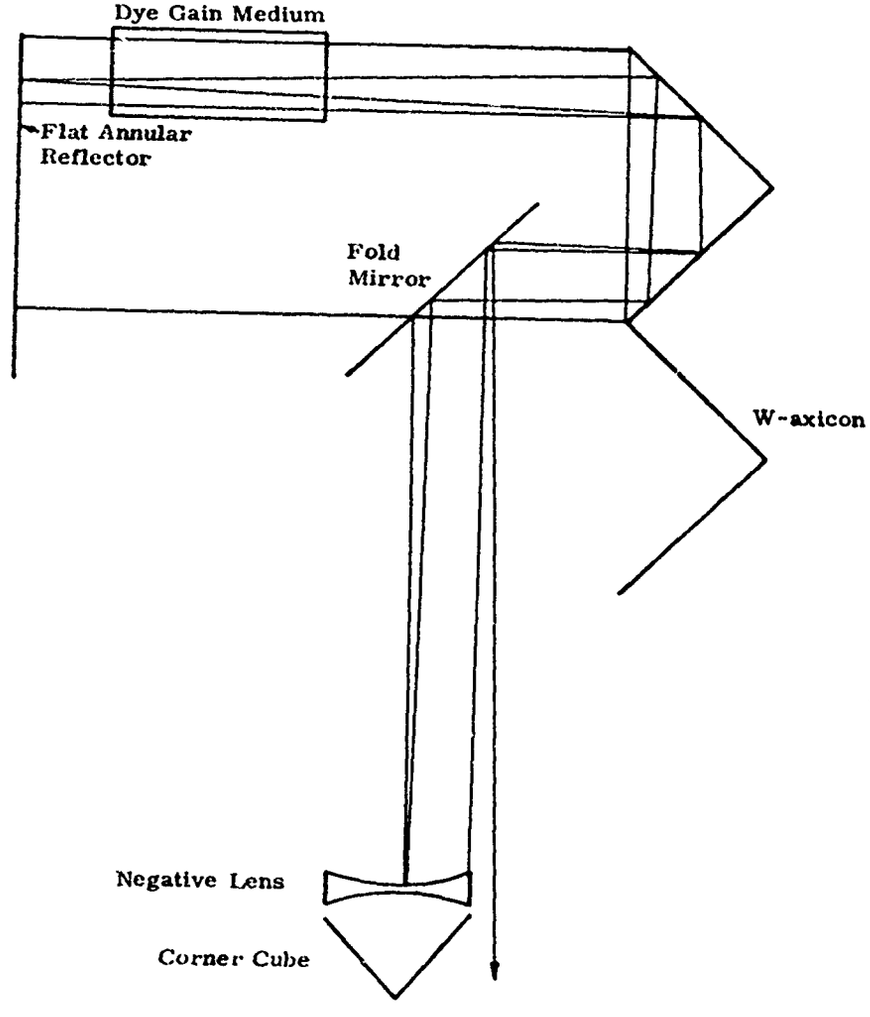

Figure 3. HSURIA Using W-axicon and Negative Lens and Corner-Cube Feedback Element

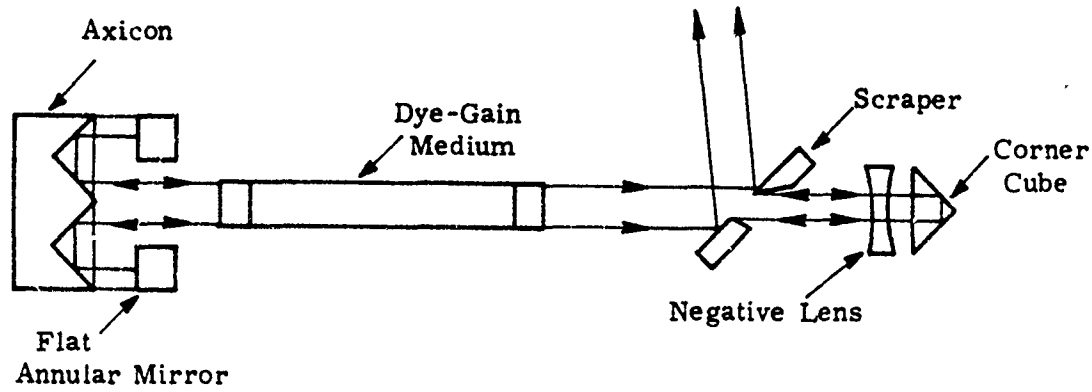

Figure 4. HSURIA with Corner-Cube and Negative-Lens Feedback

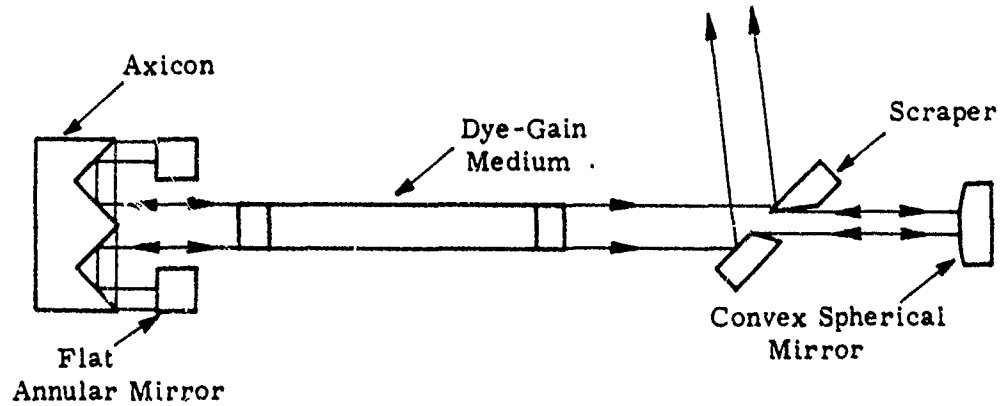

Figure 5. HSURIA with Convex Spherical Mirror Feedback Element

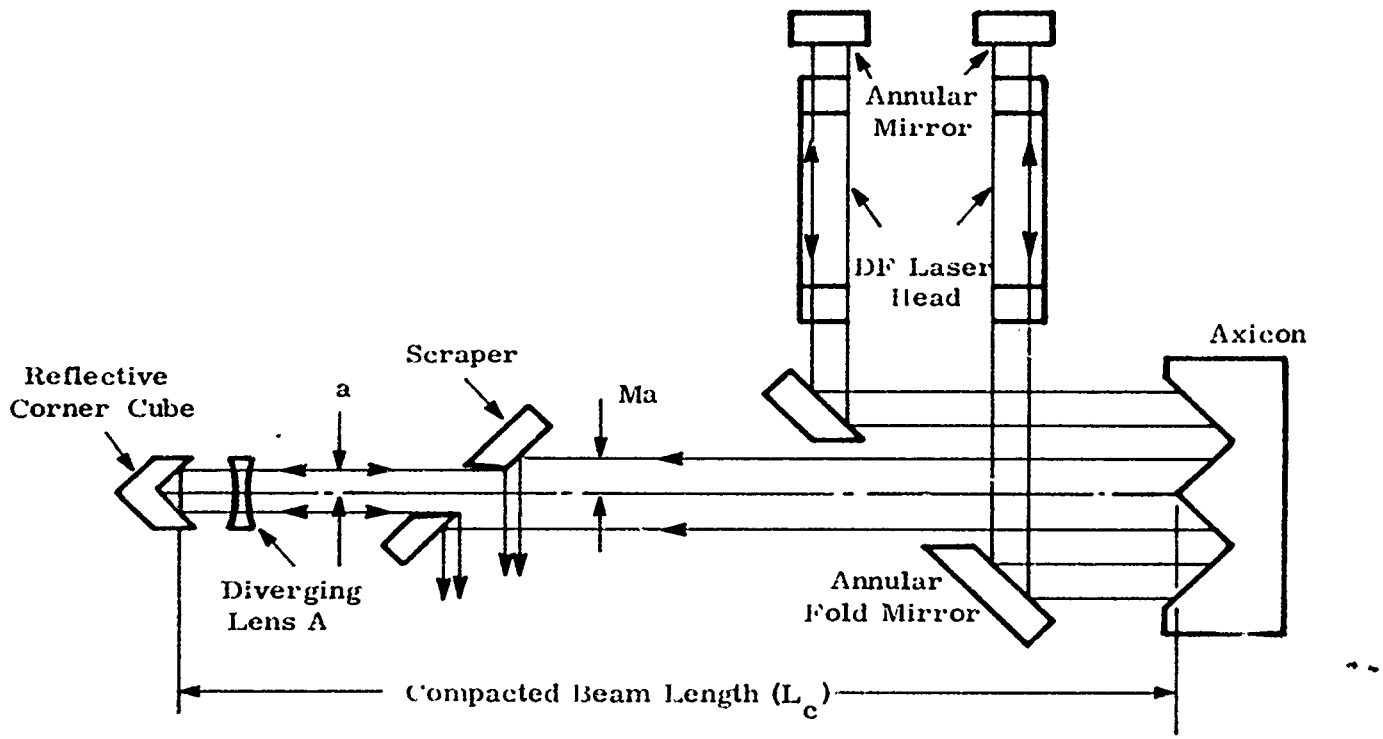

Figure 6. HF/DF Laser HSURIA with Corner-Cube Feedback Element

SECTION II

OPTICAL AND MECHANICAL COMPLIANCE WITH SPECIFIED TOLERANCES

1. CONTRACT REQUIREMENTS FOR PERFORMANCE OF OPTICAL COMPONENTS

Layouts for the various resonators tested are shown in Figures 7, 8, and 9 for the purpose of identification of the optical components required. The individual optical specifications for the components identified in the three figures are shown in Figures 10 through 22.

The requirements of the contract for optical component quality for resonators used with the dye laser to achieve the desired experimental results are that resonator mirrors shall deviate from the nominal surface figure by less than one-tenth of the shortest wavelength of the dye laser and that windows will introduce not more than $\lambda/10$ phase error anywhere across the wavefront when transmitting a plane wave of the smallest wavelength of the dye laser. The gain medium is rhodamine 6G dye in ethanol, which lases at 5900 Å. A maximum tolerance of $\lambda/10$ at 6328 Å on the peak-to-peak surface error on mirrors and on the peak-to-peak error introduced by windows was called for in the optical component procurements. This represents $\lambda/20$ maximum deviation from nominal surface figure or from transmitted wavefront at 6328 Å (zero-to-peak error) and is slightly greater than one-half the allowed error at the rhodamine 6G lasing frequency.

The requirements for optical component quality for resonators used with the HF/DF laser are the same as for the dye laser except that the wavelength of operation was defined as the shortest of those exhibited by the HF/DF laser. The gain medium is HF/DF gas, which lases at 3.8 μm. The maximum tolerance of $\lambda/4$ at 6328 Å on the peak-to-peak surface error on mirrors and on the peak-to-peak error introduced by windows was called for in the optical component procurements specifically procured for use at 3.8 μm. This represents $\lambda/8$ maximum deviation from nominal surface figure or from transmitted wavefront at 6328 Å (zero-to-peak error) and is slightly greater than one-fifth the allowed error at the HF/DF lasing frequency.

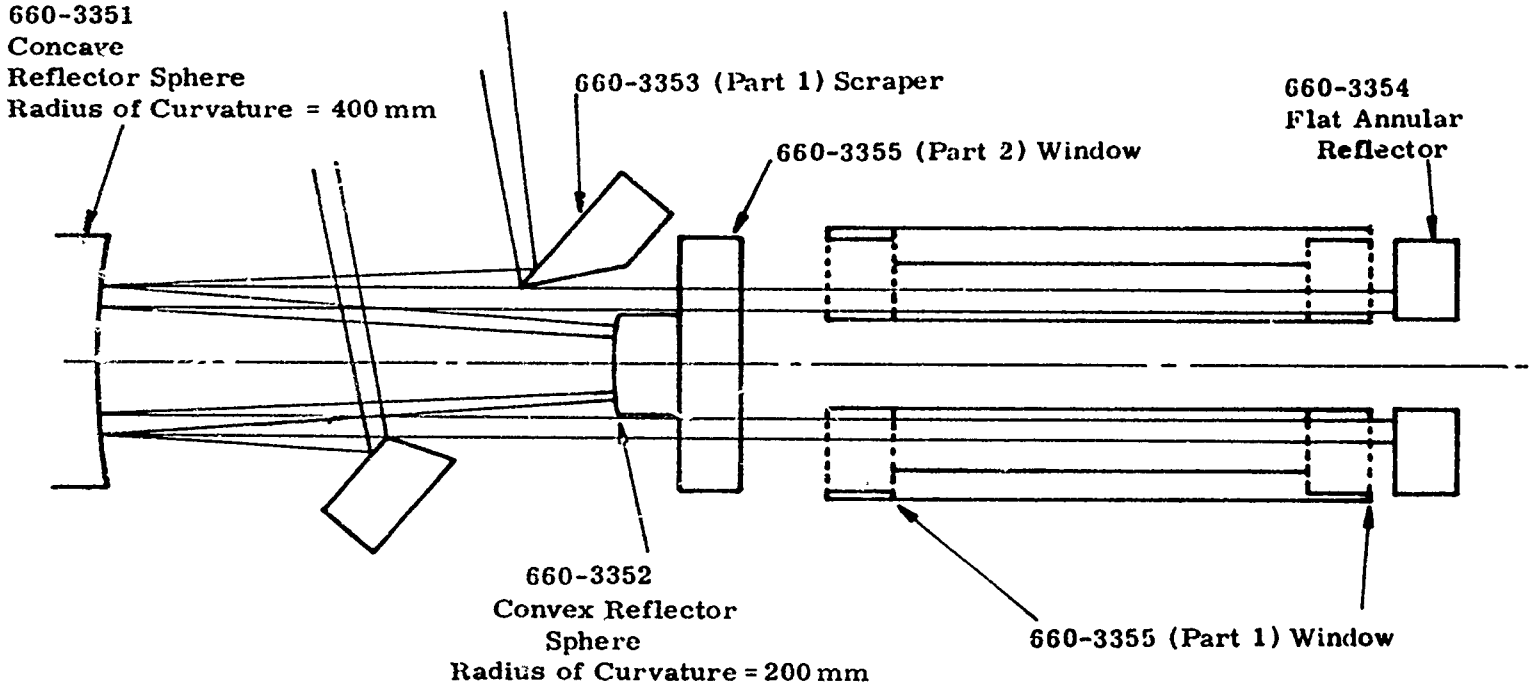

Figure 7. Spherical Mirror Resonator Optical Component Identification

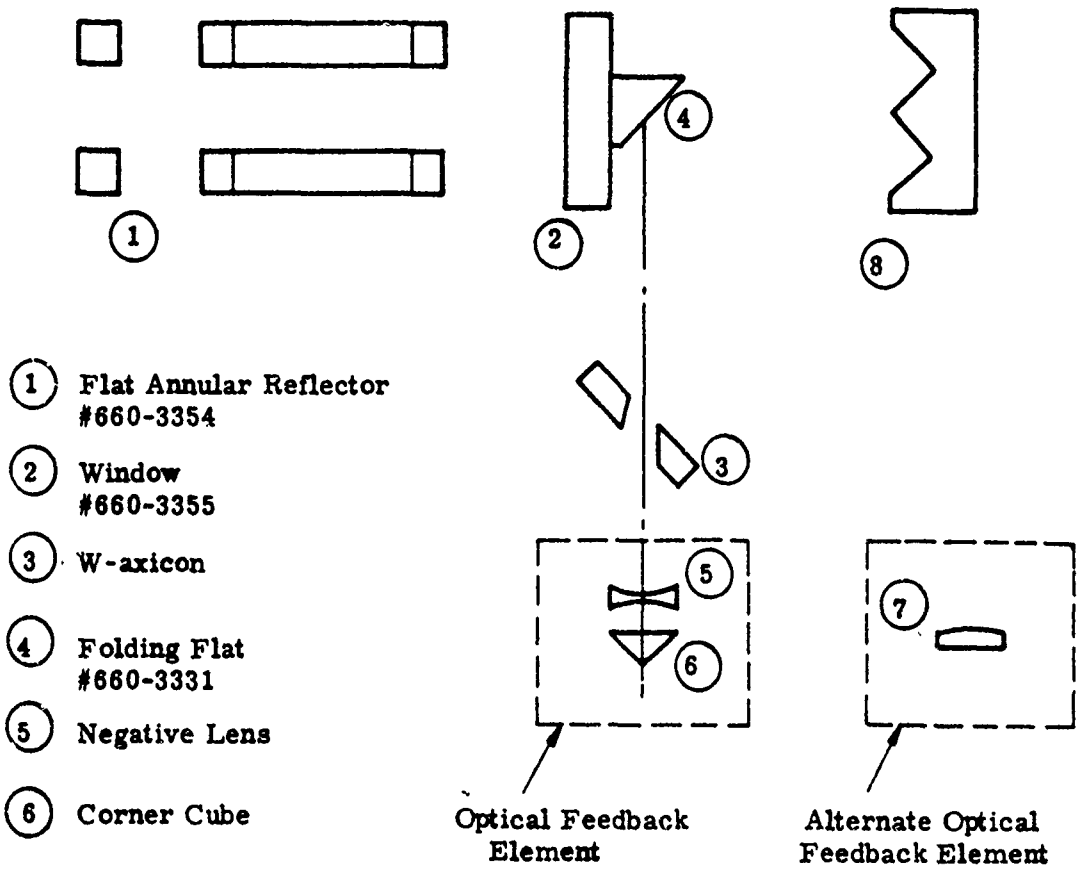

Figure 8. Major Components Used in Dye Laser with W-axicon HSURIA Experiments

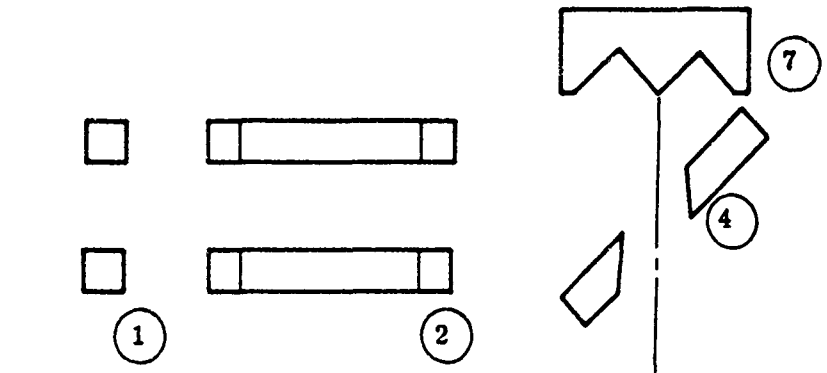

1. Flat Annular Reflector #660-3354
2. Windows
3. Scraper #660-3353, Part 2
4. Scraper #660-3353, Part 1
5. Negative Lens
6. Corner Cube
7. W-axicon

Figure 9. Major Optical Components Used in HF/DF Laser with W-axicon HSURIA Experiments

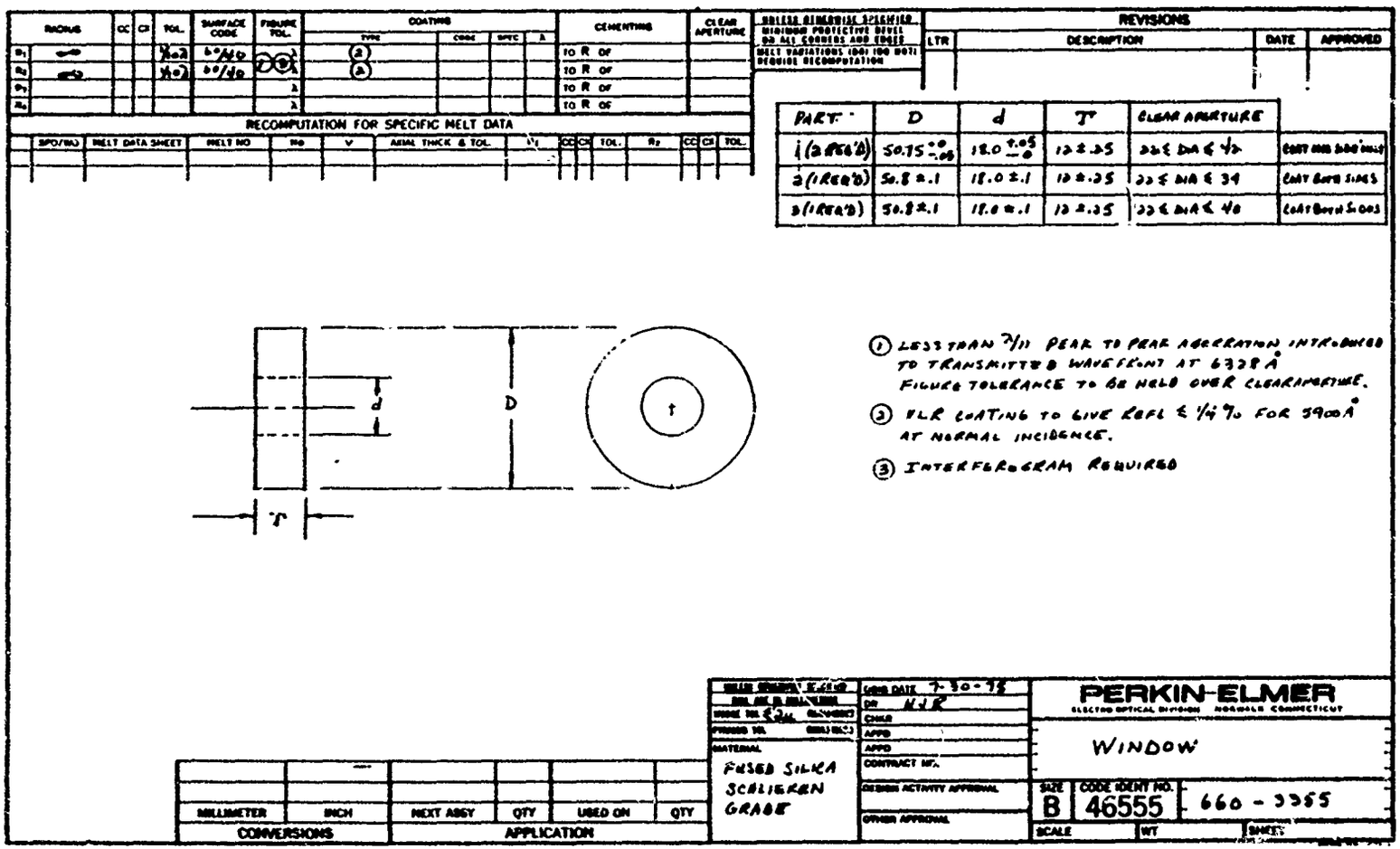

Figure 10. Window Specifications

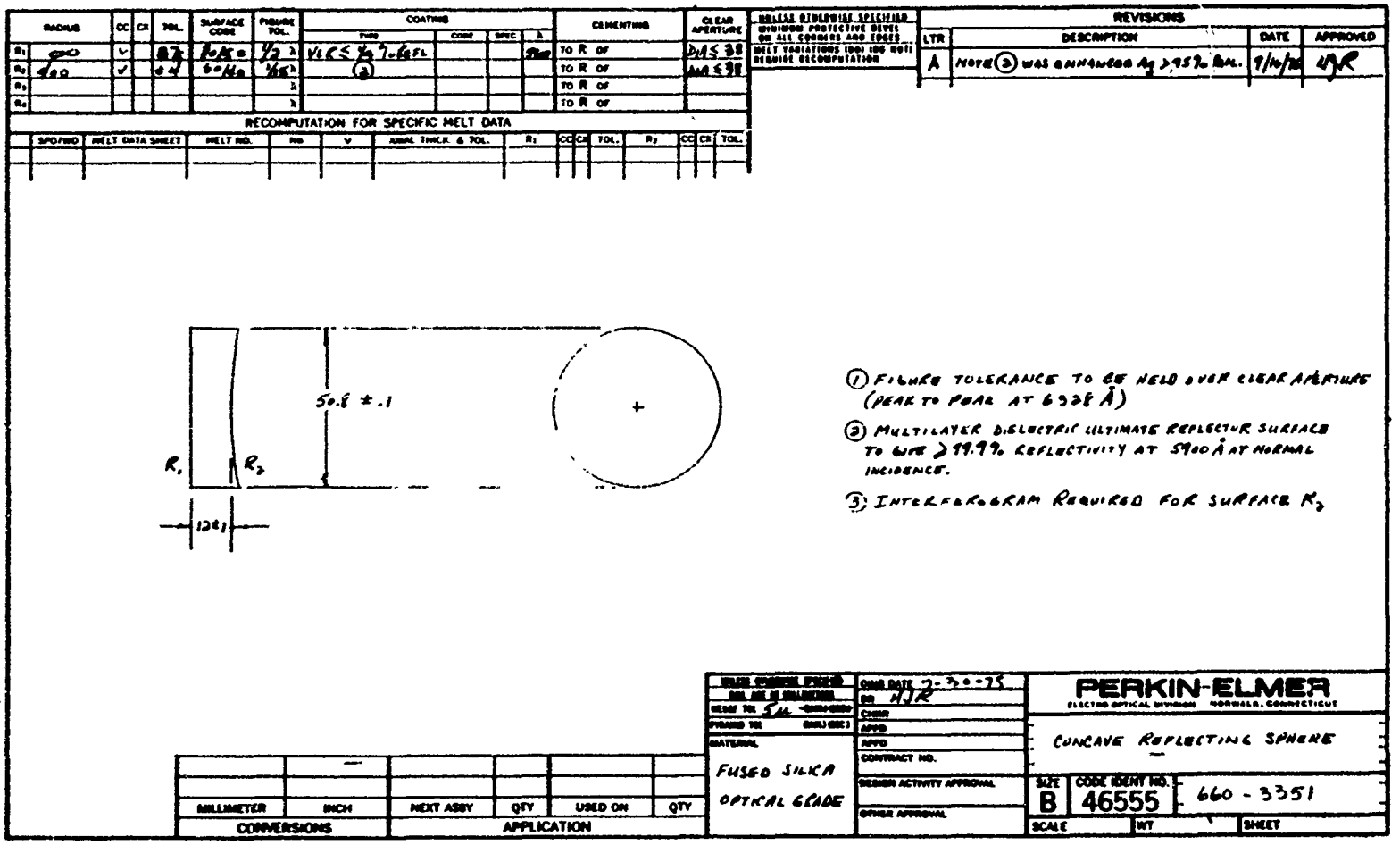

Figure 11. Concave Reflecting Sphere Specifications

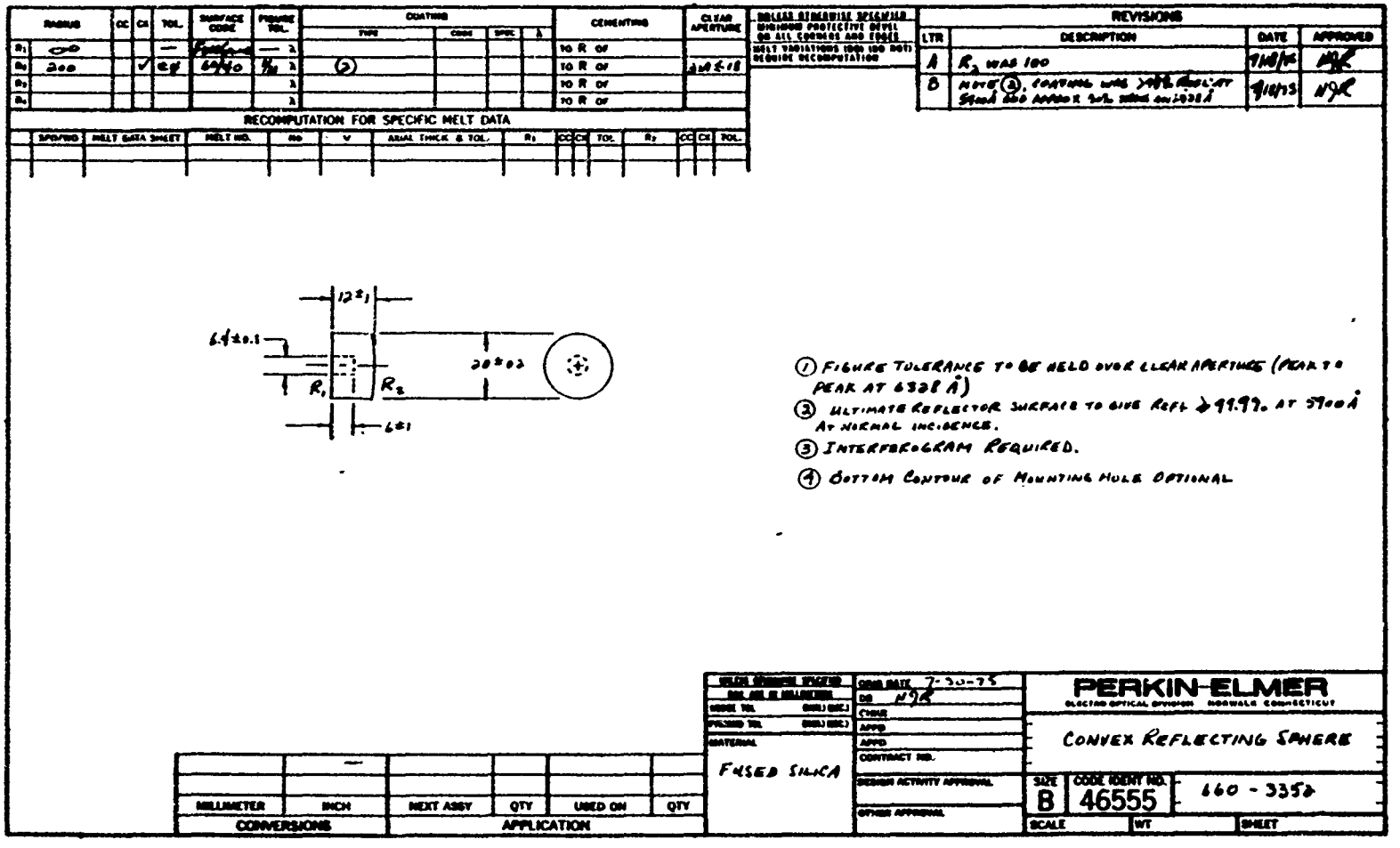

Figure 12. Convex Reflecting Sphere Specifications

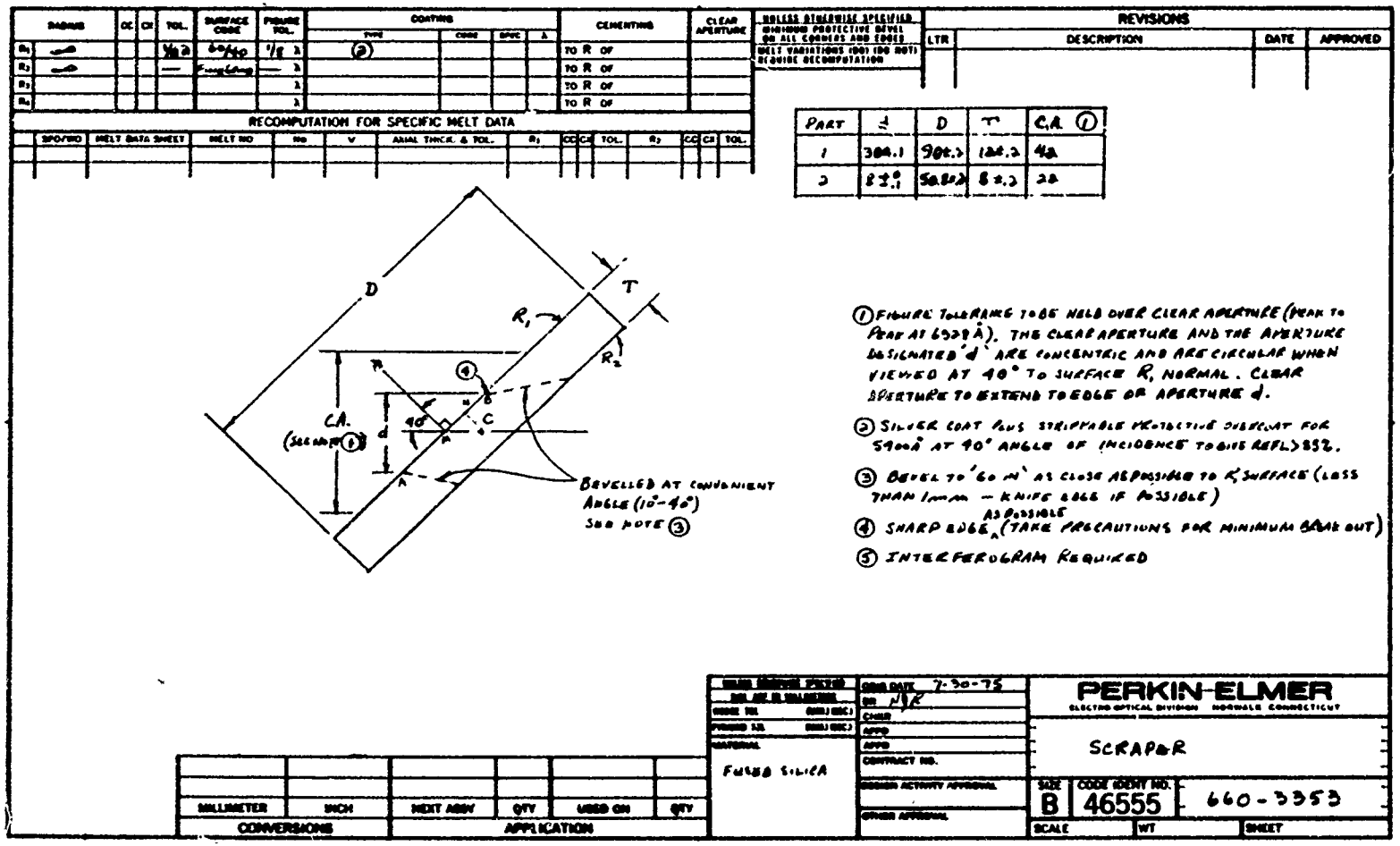

Figure 13. Scraper Specifications

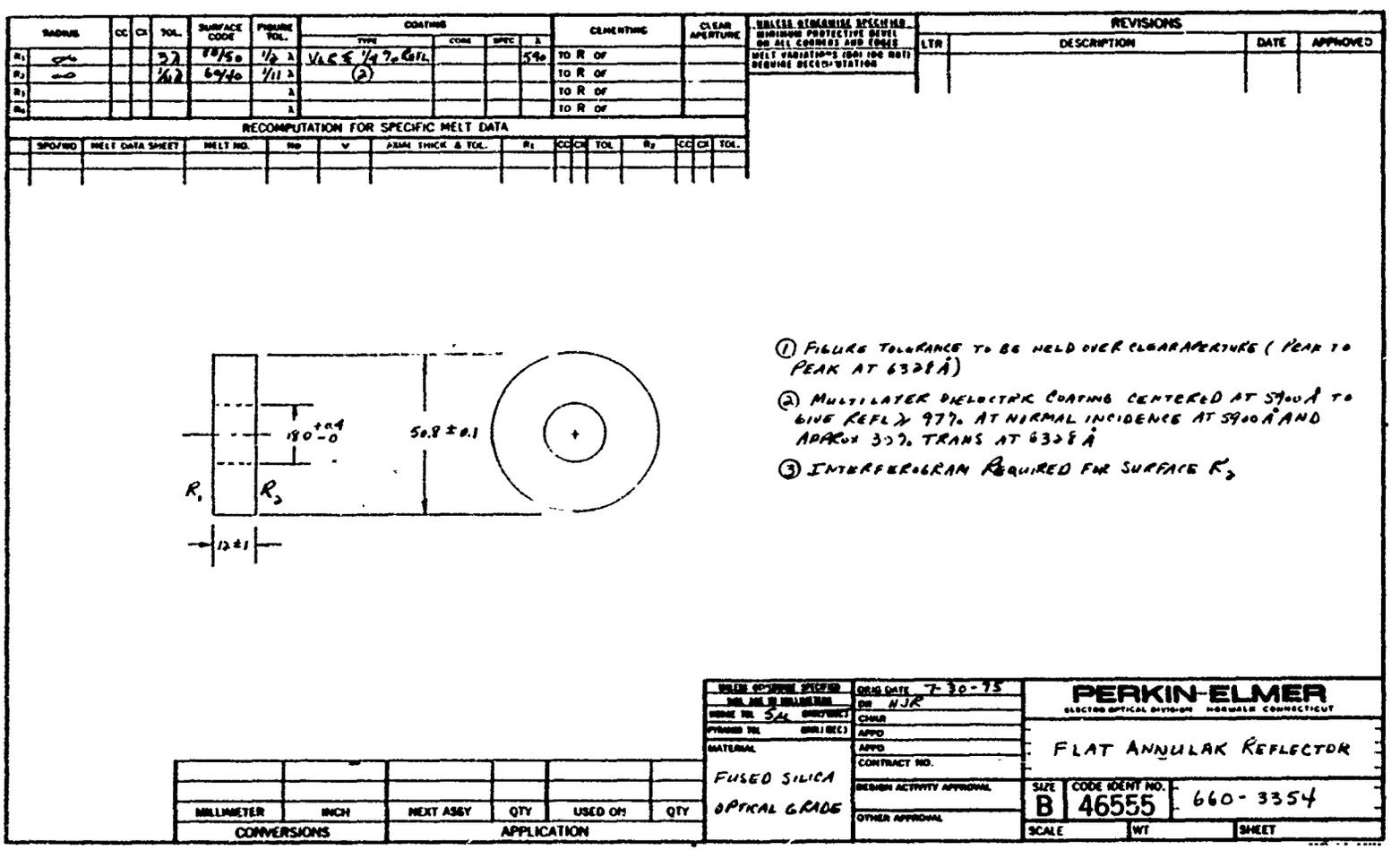

Figure 14. Flat Annular Reflector Specifications

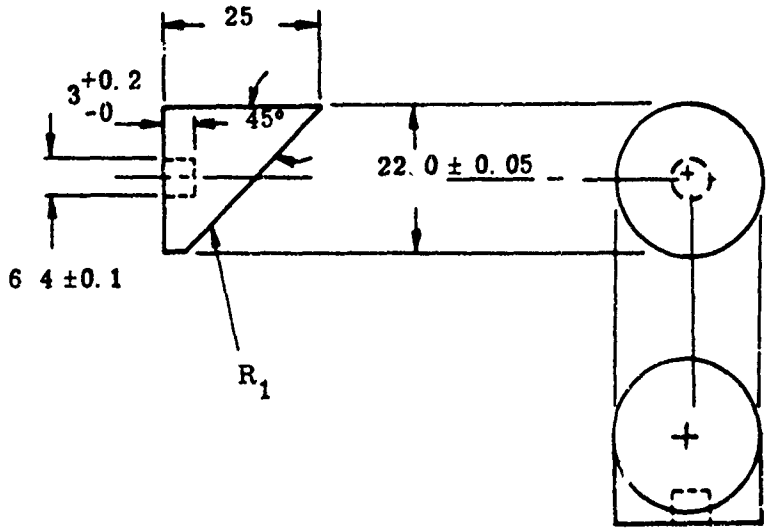

All Dimensions in Millimeters

Material: Fused Silica

Figure Surface R_1 Flat to $\lambda/10$ pk-to-pk at 6328Å Over 16-mm Clear Aperture Diameter. Minimum Bevel Edge of R_1 Surface

Coat Figured Surface R_1 for Maximum Reflectance at 5900Å

Bottom Contour of Mounting Hole Optional

Figure 15. 45° Fold Mirror Specifications (Dwg. No. 660-3331)

Material: Fused Silica

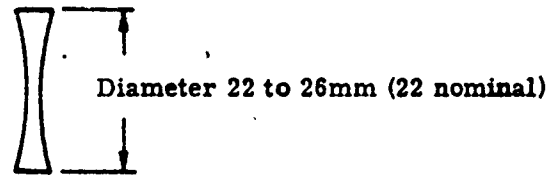

1. 16 mm Diameter Clear Aperture
2. Focal Length = 4.5 ± 0.5 Meters (0.2 to 0.25 diopters)
3. 1/10λ Maximum Peak-to-Peak Deviation From Best-Fit Sphere Introduced to Wavefront Across Clear Aperture At 6328Å
4. AR Coat Both Surfaces for λ = 5900Å

Figure 16. Negative Lens Specifications

Material: Fused Silica or BK-7

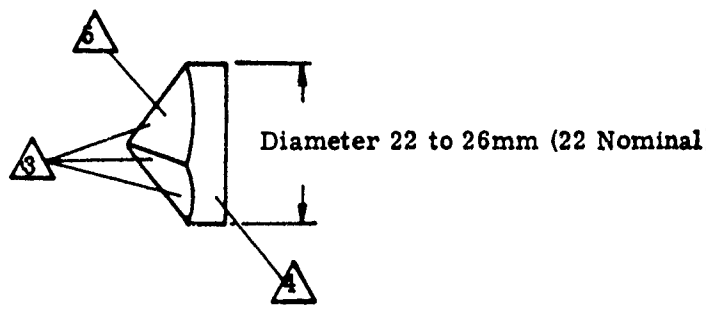

1. Clear Aperture Diameter ≤ 16mm
2. One Arc-Second Maximum Tilt Introduced to Wavefront
3. No Break on Back Edges or Apex
4. AR Coat Front Surface for λ = 5900 Å
5. Metallic Coating on Back Surfaces for Mirror Reflection

Figure 17. Refractive Corner-Cube Specifications

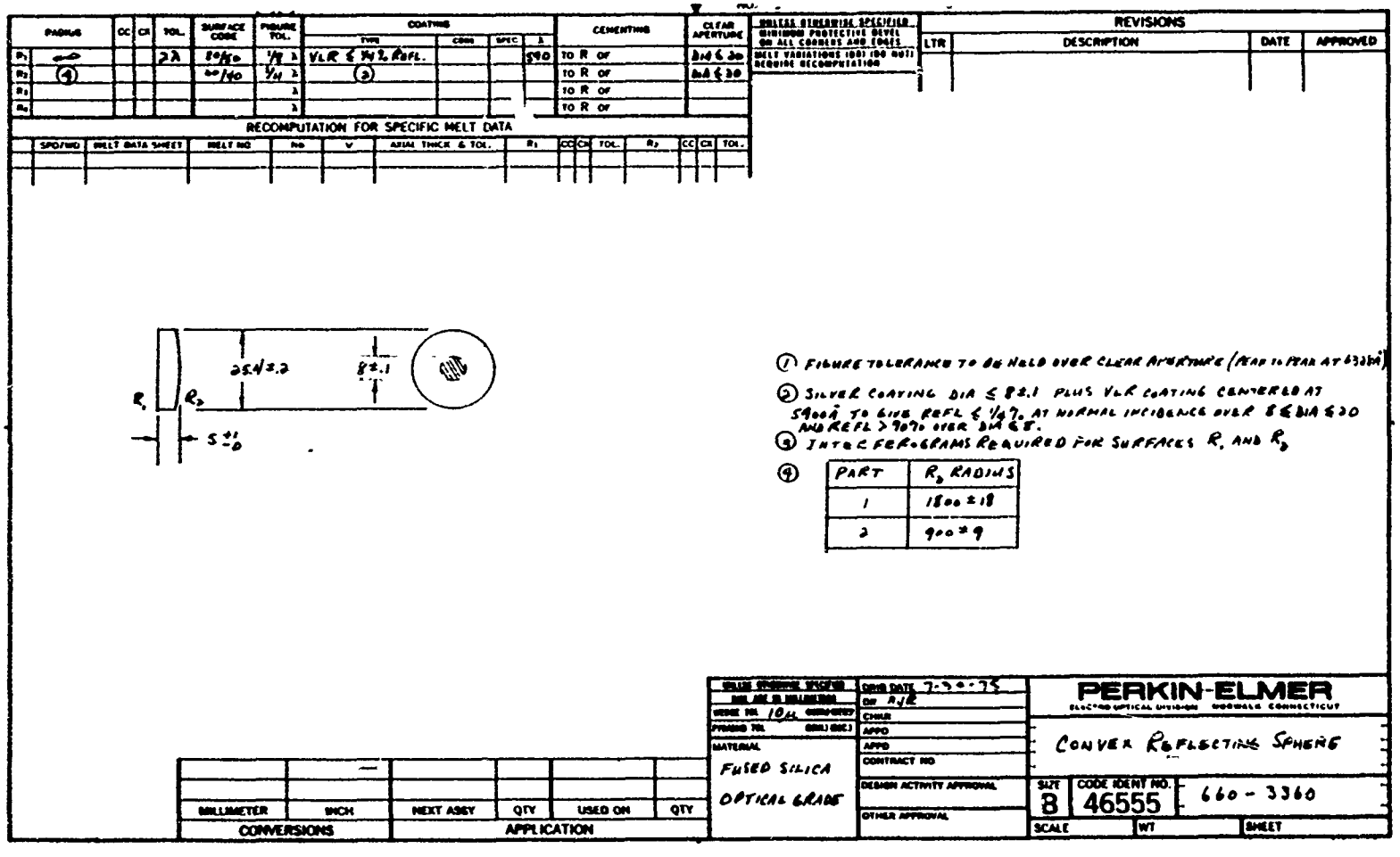

Figure 18. Convex Reflecting Sphere Specifications

All Dimensions in Inches

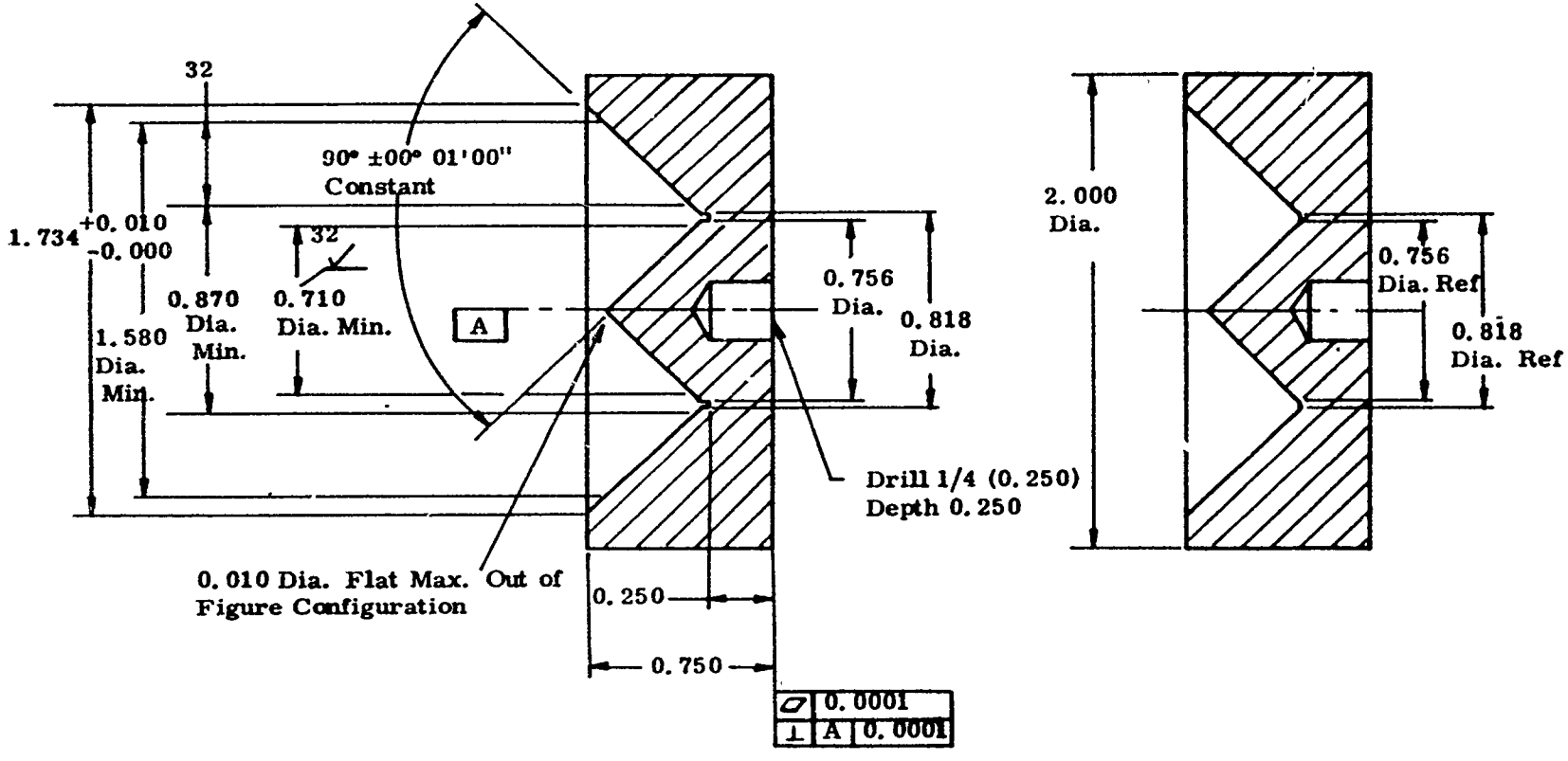

Material - OFHC Copper QQ-C-502 Alloy 102

Figure 19. W-axicon Specifications

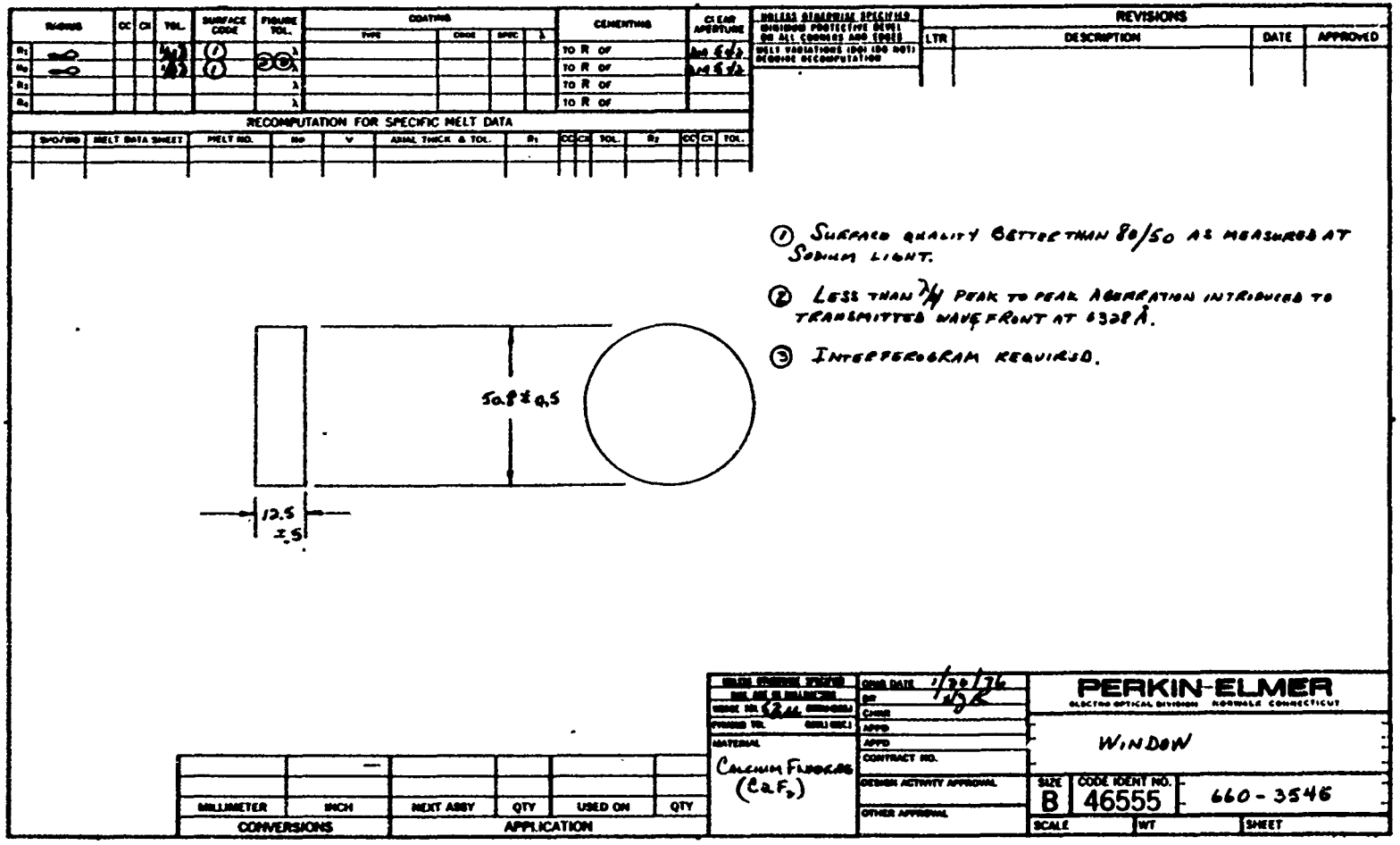

Figure 20. CaF_2 Window Specifications

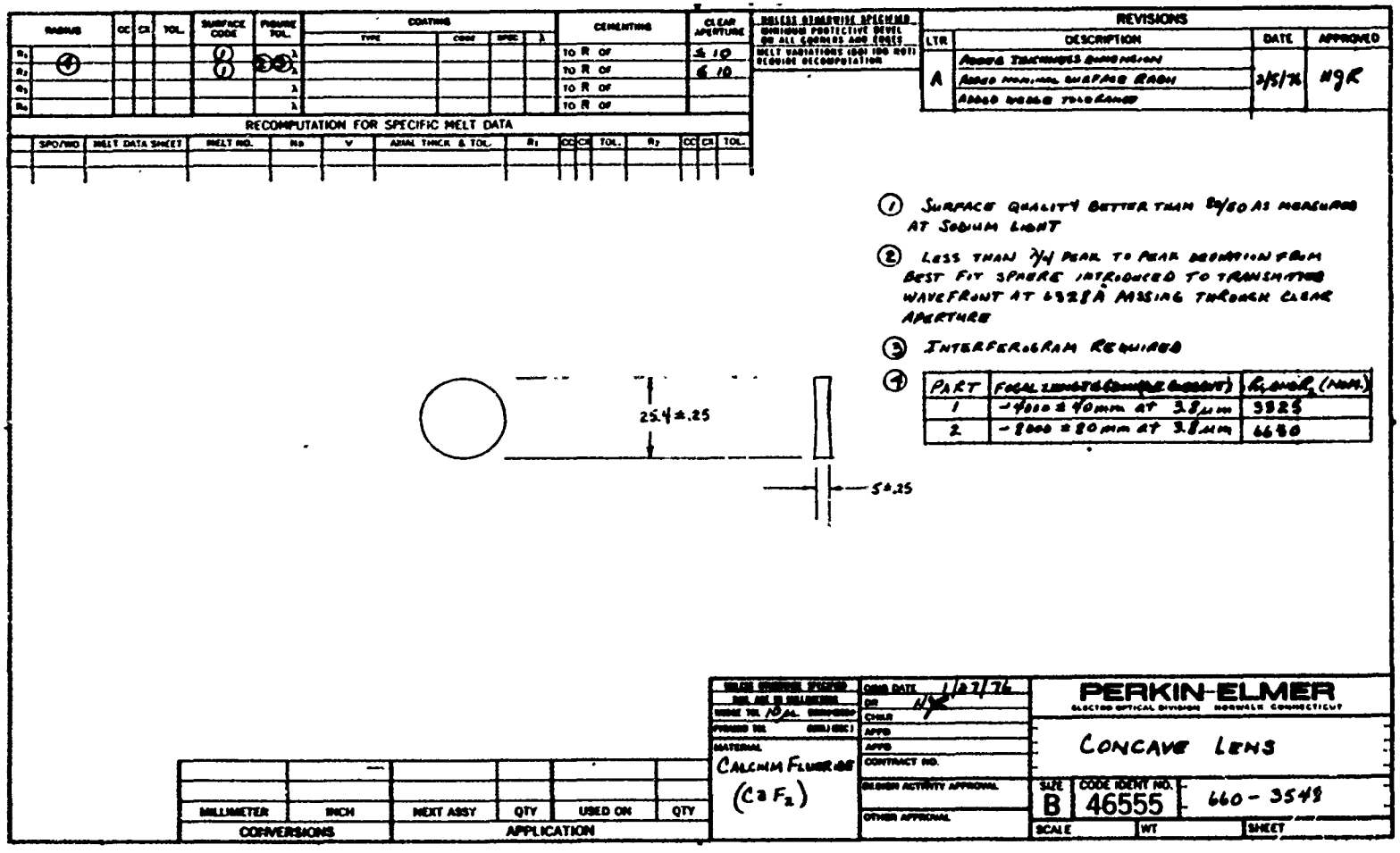

Figure 21. CaF_2 Negative Lens Specifications

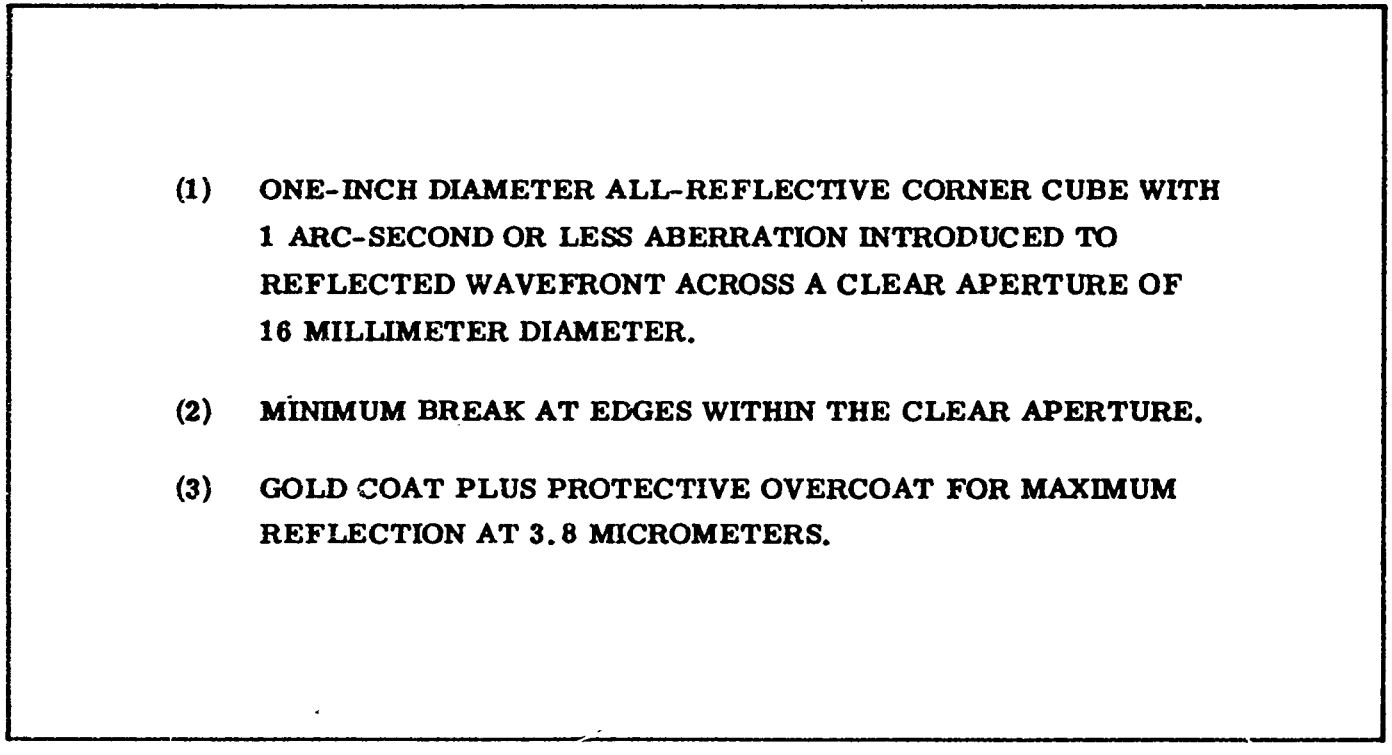

Figure 22. All-Reflective Corner Cube Specifications

As far as practicable the HF/DF laser resonators used mirrors and mounts designed for the dye laser and as can be seen in Figures 7, 8, and 9 several of the optical elements are used in more than one resonator configuration.

2. TEST RESULTS FOR PERFORMANCE OF OPTICAL COMPONENTS

Interferograms showing the optical quality actually obtained in manufacture of the resonator elements are shown in Figures 23 through 41. Interferograms were obtained at 6328 Å by contacting the element with a test flat or test sphere, by using a Twyman-Green interferometer, or with a Spherical Wave Interferometer (SWIM), which is similar to a Fizeau interferometer in that it is a multiple beam configuration that yields sharper fringes than a Twyman-Green.

The interferograms indicate satisfactory quality for all individual components (better than $\lambda/20$ zero-to-peak aberration at 6328 Å) with the exception of the W-axicon. The W-axicon introduced approximately 1 wavelength peak-to-peak aberration to the wavefront in double pass off an annular flat mirror, which is equivalent to 1/12 wavelength at 3.8 μm and just meets the acceptability standard at that wavelength.

The performance of the dye laser as a compound optical element can be seen in the interferograms made with the SWIM interferometer (Figures 24, 25, and 26) showing the aberrations introduced by the dye solution in the dye laser head. Optimum wavefront quality in this case was achieved at a flow rate of 1.2 liters/minute as indicated in Figure 26.

3. TRANSLATION AND ROTATIONAL ADJUSTMENTS

Mechanical mounts used to obtain the high resolution motions required in tilt and translation were obtained from Aerotech, Inc. Tilt resolution obtainable with the AOM110-3 Azimuth Elevation Gimbal Mount is 0.1 arc-second (0.5 microradian) over a range of 12 degrees (1.0-microradian resolution over 0.2-degree range required). Translation resolution obtainable with the ATS301 Linear Translation Stage is 1 microinch over a range of 1 inch (20-microinch resolution over 0.2-inch range required).

Window No. 1

Window No. 2

Figure 23. Dye-Laser Head Window Test Results. Interferograms are double-pass (fringe separation is $\lambda/2$, λ = 6328 Å)

Figure 24. Dye-Laser Head Optical Quality, Without Fluid (windows only)

Figure 25. Transmitted Wavefront Through Stagnant Fluid (ethanol, pump speed = 0 ℓ/min). Note the severe degradation due presumably to thermal gradients

0.9 ℓ/min

1.2 ℓ/min

1.5 ℓ/min

2.0 ℓ/min

Figure 26. Transmitted Wavefront for Various Fluid Flow Rates Through the Dye-Laser Head. Dye-laser head capacity is 75.4 cm^3 (0.075 ℓ)

Interferogram obtained by contacting with test sphere.

$\lambda/8$ power due to difference in radius of curvature between concave sphere and test sphere.

$\lambda/15$ peak-to-peak variation from best-fit sphere at 6328 Å.

Figure 27. Concave Reflecting Sphere (Dwg. No. 660-3351)

Interferogram obtained by contacting with test sphere.

$\lambda/2$ power due to difference in radius of curvature between convex sphere and test sphere.

$\lambda/12$ peak-to-peak variation from best-fit sphere at 6328 Å.

Figure 28. Convex Reflecting Sphere (Dwg. No. 660-3352)

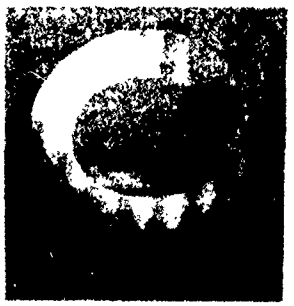

Interferogram obtained by contacting with test flat.

$\lambda/8$ peak-to-peak variation from flat at 6328 Å.

Figure 29. Scraper (Dwg. No. 660-3353, Part 1)

Interferogram obtained with Twyman-Green interferometer.

$\lambda/15$ peak-to-peak variation from flat at 6328 A.

Figure 30. Flat Annular Reflector (Dwg. No. 660-3354)

Interferogram obtained with Twyman-Green interferometer.

$\lambda/20$ peak-to-peak wavefront aberration introduced by window at 6328 A.

Figure 31. Window (Dwg. No. 660-3355, Part 2)

Interferogram obtained with Twyman-Green interferometer.

$\lambda/20$ peak-to-peak wavefront aberration introduced by window at 6328 A.

Figure 32. Window (Dwg. No. 660-3355)

Interferogram obtained by contacting with test flat.

$\lambda/15$ peak-to-peak variation from flat at 6328 Å.

Figure 33. Scraper (Dwg. No. 660-3353, Part 2)

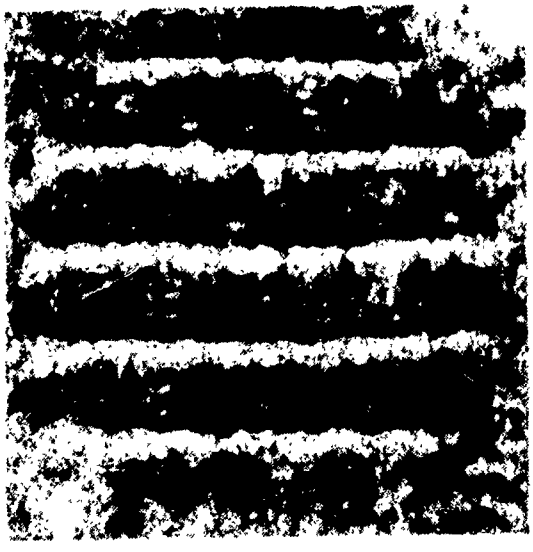

$\lambda/11$ peak-to-peak aberration introduced to wavefront on double pass at 45°.

Figure 34. Fold Mirror (Dwg. No. 660-3331)

Interferogram obtained with Twyman-Green interferometer.

$\lambda/15$ peak-to-peak aberration introduced to wavefront over central 8-mm diameter.

Figure 35. Negative Lens

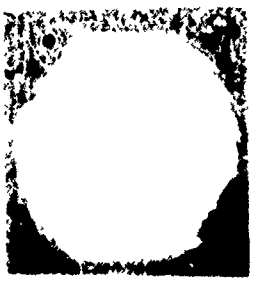

Interferogram obtained with Twyman-Green interferometer.

$\lambda/15$ peak-to-peak aberration introduced to wavefront at 6328 A.

Figure 36. Refractive Corner Cube

Interferogram obtained with
Twyman-Green interferometer.

$\lambda/11$ peak-to-peak variation
from best fit sphere at
6328 Å across 25-mm diameter.

Figure 37. Convex Sphere (Dwg. No. 660-3360)

λ/20 peak-to-peak wavefront aberration introduced by window at 6328 Å.

(a) Window No. 1

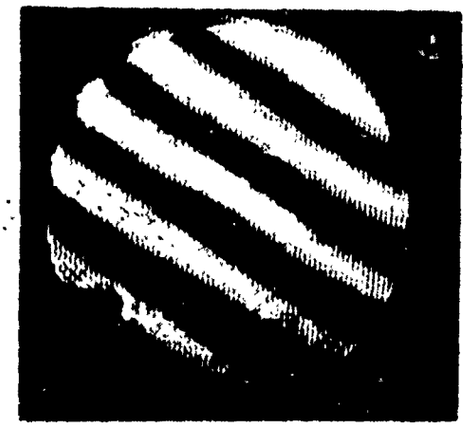

λ/20 peak-to-peak wavefront aberration introduced by window at 6328 Å.

(b) Window No. 2

Figure 38. Interferograms of CaF_2 Windows (Dwg. No. 660-3545) Used in HF/DF Laser Head (Interferograms obtained with Twyman-Green interferometer)

(a) 4-Meter Focal Length CaF_2 Lens

(b) 8-Meter Focal Length CaF_2 Lens

Figure 39. Negative Lens (Interferograms obtained with Twyman-Green interferometer. Less than $\lambda/20$ peak-to-peak aberration at 6328 Å introduced to wavefront over central 8-mm dia.)

Interferogram obtained with Twyman-Green interferometer.

$\lambda/15$ peak-to-peak variation from flat at 6328 Å.

Figure 40. Reflective Corner Cube

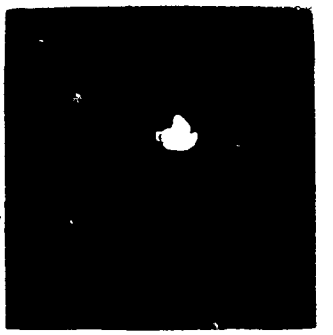

METAL CONE

CONE A (12/16/75) FROM Y12

Single Pass
Far-Field Image Corrected
for Aperture Size

Cone

Flat

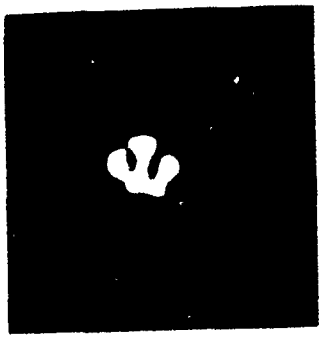

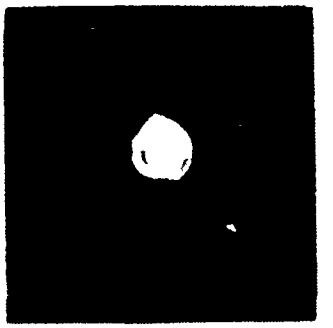

Double Pass Off
Annular Mirror

Cone

Flat

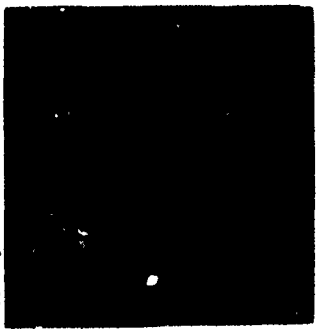

INTERFEROGRAM AGAINST PLANE
WAVEFRONT OF CONE AND ANNULAR
FLAT REFLECTED WAVEFRONT

Linear Wedge

Null

Figure 41. W-axicon Test Results

A typical mounting configuration is shown in Figure 42 where the W-axicon element is shown mounted on one AOM110-3 Gimbal Mount and two ATS301 Linear Translation Stages allowing control of position in two degrees of tilt and two degrees of translation.

4. CONCLUSIONS

The fabrication of optical components to meet requirements for the cylindrical resonators investigated did not present any difficulties except for the W-axicon and axicon elements, which could not be obtained to the tolerances required for performance in the visible with the dye laser. The W-axicon supplied was, however, satisfactory for use at 3.8 μm with the HF/DF laser.

This identifies the beam compacting element as one of the critical optical devices requiring investigation into, and development of, fabrication techniques to obtain diffraction-limited performance with larger scale HSURIA resonator cavities.

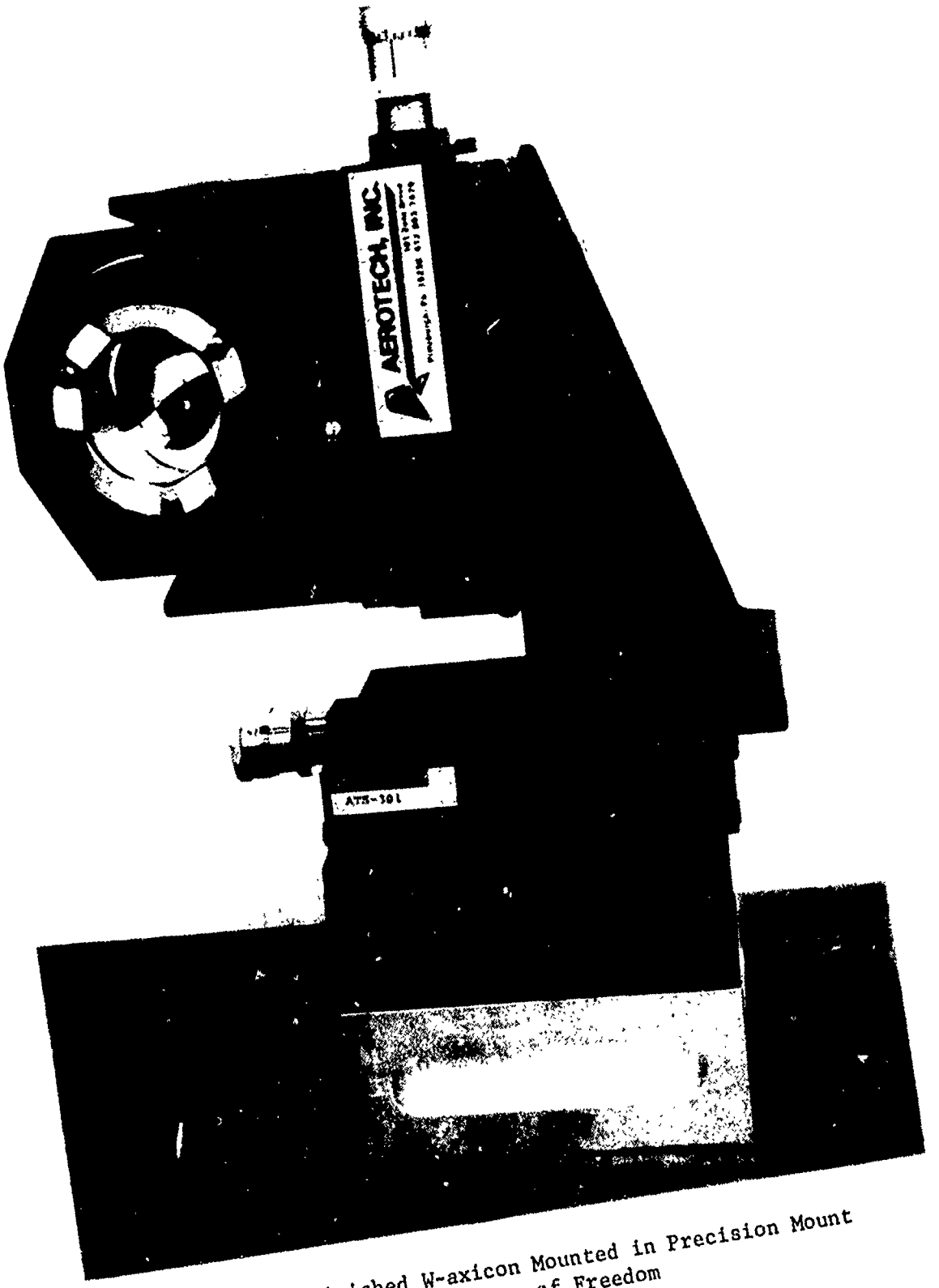

Figure 42. Finished W-axicon Mounted in Precision Mount with Four Degrees of Freedom

SECTION III

DYE LASER EXPERIMENTS

1. DYE-LASER HEAD DESIGN

a. Optical Pumping Requirements of the Dye Laser Medium

In order to minimize risk in the laser design, components and system parameters were chosen to be consistent with previous successful devices. Conventional dye laser systems with circular mode volumes and unstable optical resonators have the following nominal operating parameters:

Dye cell:	8 mm ϕ, 10 cm long
Dye concentration:	5×10^{-5} moles/liter
Dye:	Rhodamine 6G (several similar components)
Solvent:	Ethanol, Flow Rate: 2 ℓ/min
Output coupling:	25-75% (70% typical)
Threshold pumping energy:	1 to 3 joules/cm^3

A conventional linear flash lamp was chosen (Xenon Corp., Model 851A) with a 89-mm bore length and 5-mm bore diameter. The lamp with its pyrex jacket for water or air cooling has a 15-mm outer diameter. This dimension, plus some additional allowance for mounting supports, sets a limiting inner dimension for the annular dye cell. The inner dimension was therefore chosen to be 22 mm. The thickness of the annulus is determined by the pumping requirements. For this reason the annular width of 4 mm was chosen to be consistent with earlier experience. The outer diameter of the annular dye cell (active region, not a physical bound) is therefore 30 mm. The dye volume, V, is

$$V = \pi \ell \, (r_o^2 - r_i^2) = (3.14)(8.0)(1.5^2 - 1.1^2) \approx 23.4 \text{ cm}^3,$$

where ℓ is the useful length of the flash lamp. The threshold energy should therefore be in the range of 25 to 70 joules depending upon the output coupling of the resonator.

The flash lamp can be safely fired at 100 joules/pulse with an expected lifetime of several thousand shots. The energy storage system used for driving the lamp was designed to be similar to earlier units used for dye lasers. It consists of a low-inductance coaxial capacitor mounted in a canister with a spark gap as reported by Furumoto and Ceccon (Ref. 1). The capacitor was Capacitor Specialists Model 25W019 (0.3 microfarad, 25 kilovolts, 10-nanohenry self-inductance). The spark gap was designed to hold off 15 to 17 kV without pressurization and over 25 kV with 10 psi of dry nitrogen. The spark gap uses a conventional spark plug as a trigger wire inserted through the ground electrode of the gap. An EG&G Model TM-11A trigger module drives the spark gap to initiate the discharge. The capacitor is resistively charged by a Universal Voltronics Model BAL-32-10 high-voltage DC power supply. Special high-voltage ceramic resistors are used to isolate the power supply from the capacitor and limit the charging current. The electrical driver circuit is shown in Figure 43. The charging resistors across the lamp serve a dual purpose. They allow the capacitor to charge without drawing current through the lamp. Secondly, they act as a fuse in the event that the lamp does not fire (because of a gas leak or broken lead). The completed electrical storage unit (capacitor and internal spark gap) is shown in Figure 44. An exploded view of the energy storage unit is shown in Figure 45. The flash lamp is shown with mounts in an exploded view in Figure 46.

b. Dye-Laser Head Mechanical Design

A section view of the dye-laser head assembly is shown in Figure 47. The critical dimensions for the annular dye cell were defined above. The cell has a length of 80 mm, an inner diameter of 22 mm, and an outer diameter of 42 mm. The housing is stainless steel with a liner of polypropylene and a quartz tube as the inner wall (surrounding the flash lamp). Fluid connections and tubing are made of polypropylene for compatibility with the solvent and dye. The liner has a series of inlet and outlet holes (16 each) to disperse the fluid and make the flow more uniform. The windows are made of Schlieren-grade fused silica with the following specifications:

1. H.W. Furumoto and H.L. Ceccon, "Optical Pumps for Organic Lasers," Appl. Opt. 8, 1613 (1969).

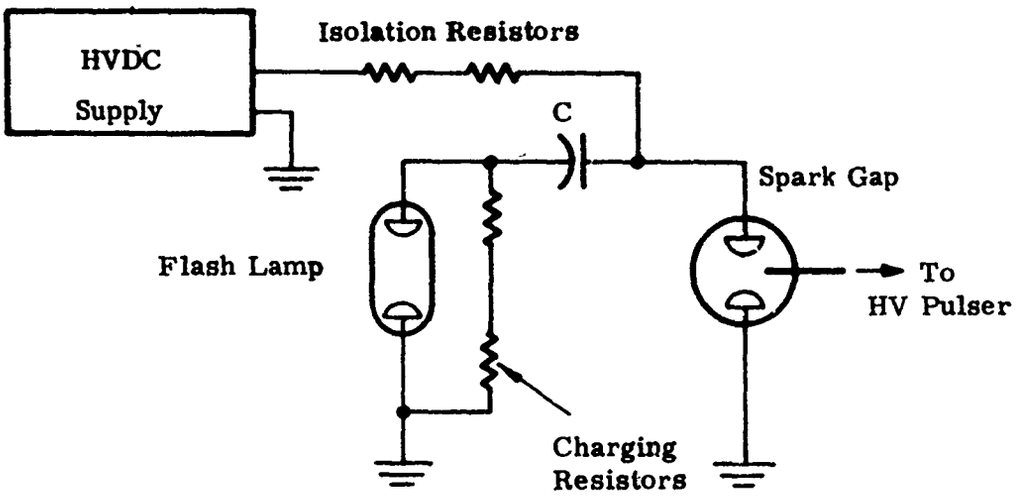

Figure 43. Electrical Driver Circuit

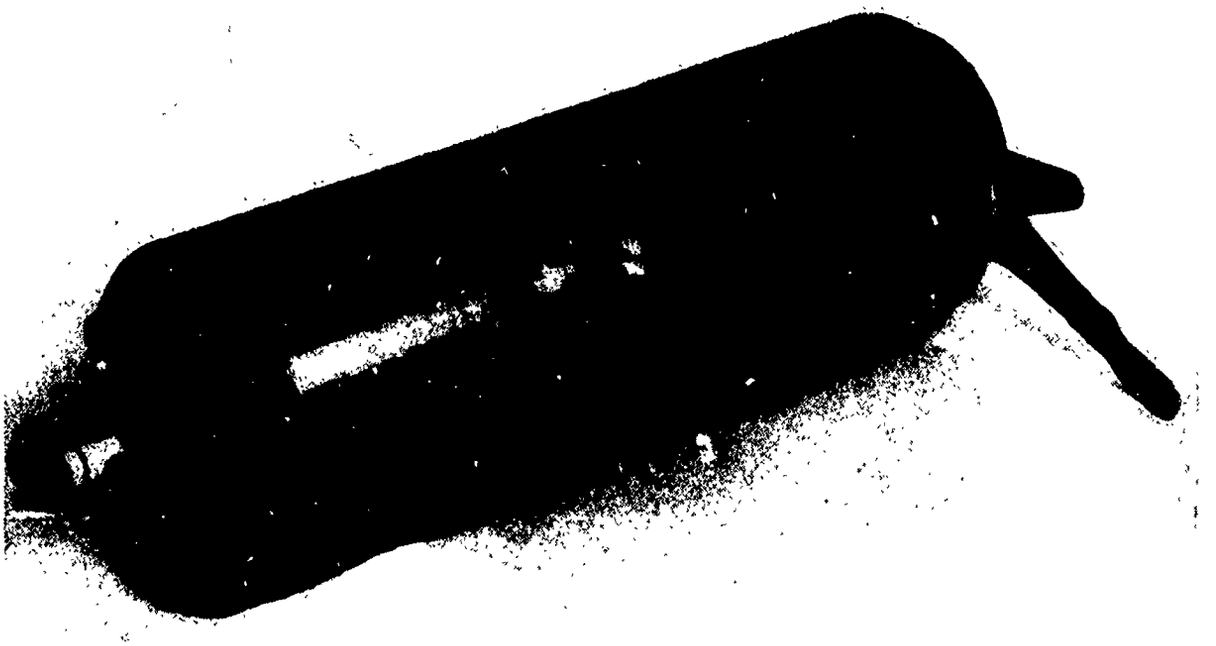

Figure 44. Energy Storage Unit with Coaxial Capacitor and Spark Gap

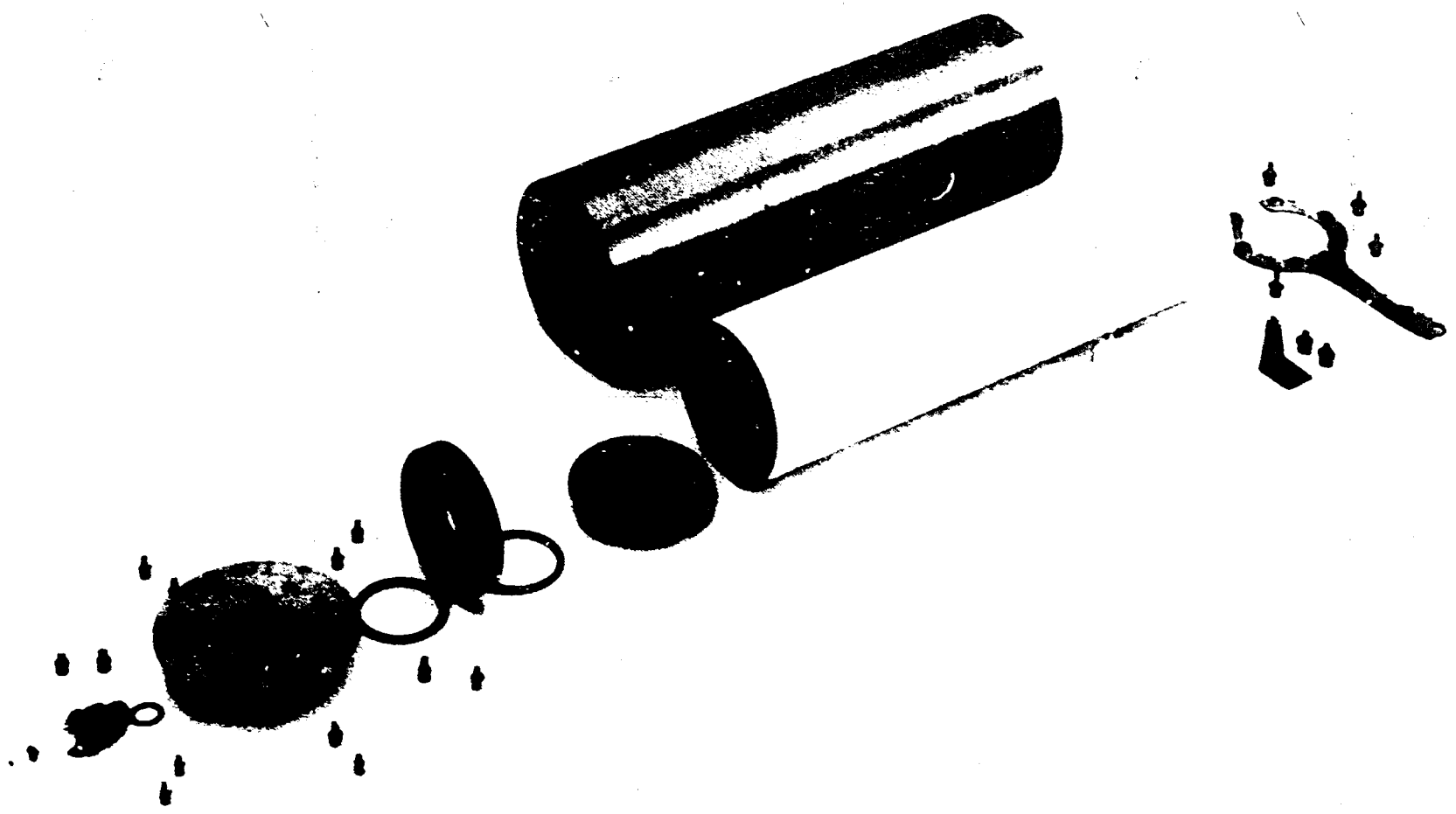

Figure 45. Exploded View of Energy Storage Unit

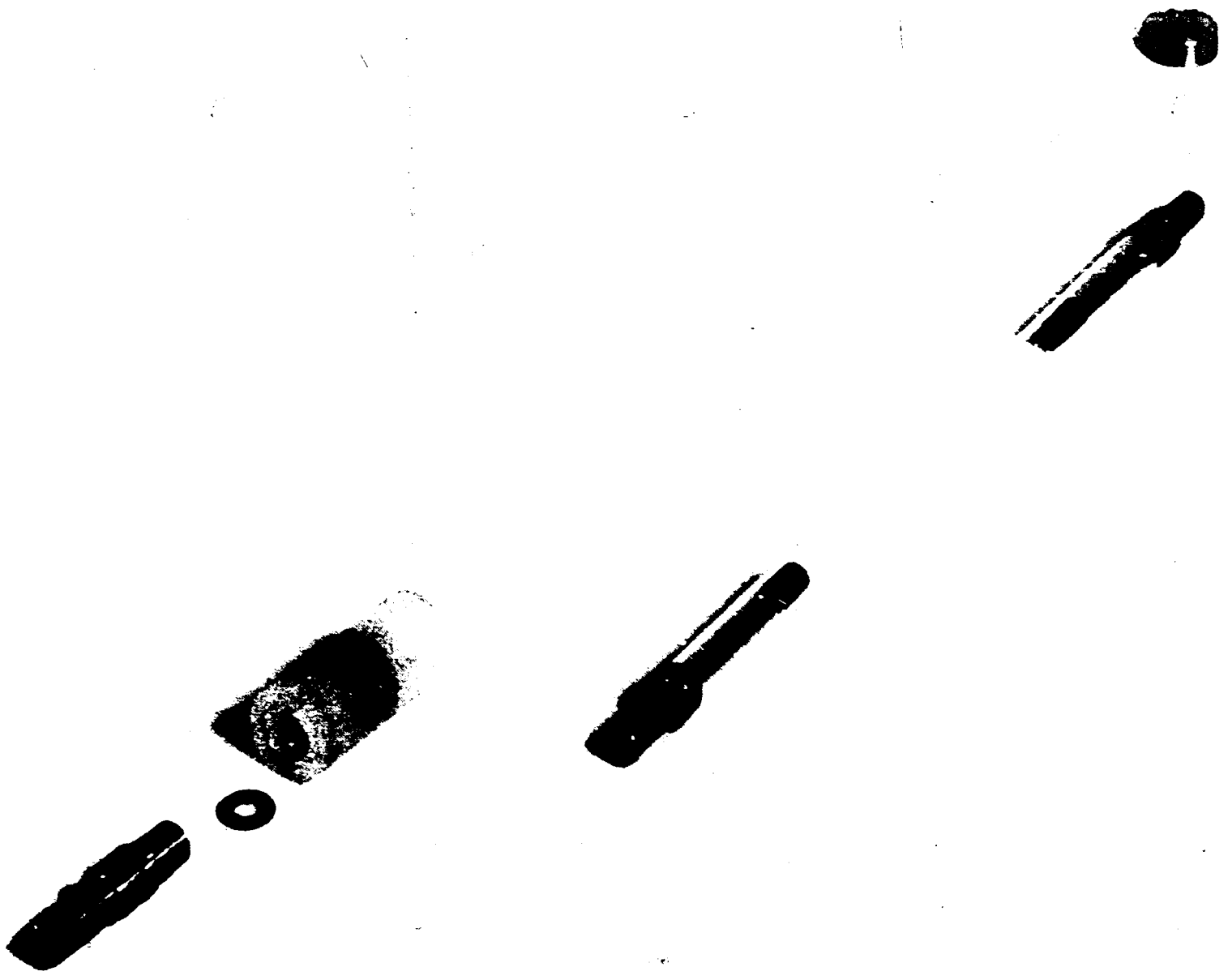

Figure 46. Flash Lamp with Mounts and Jacket

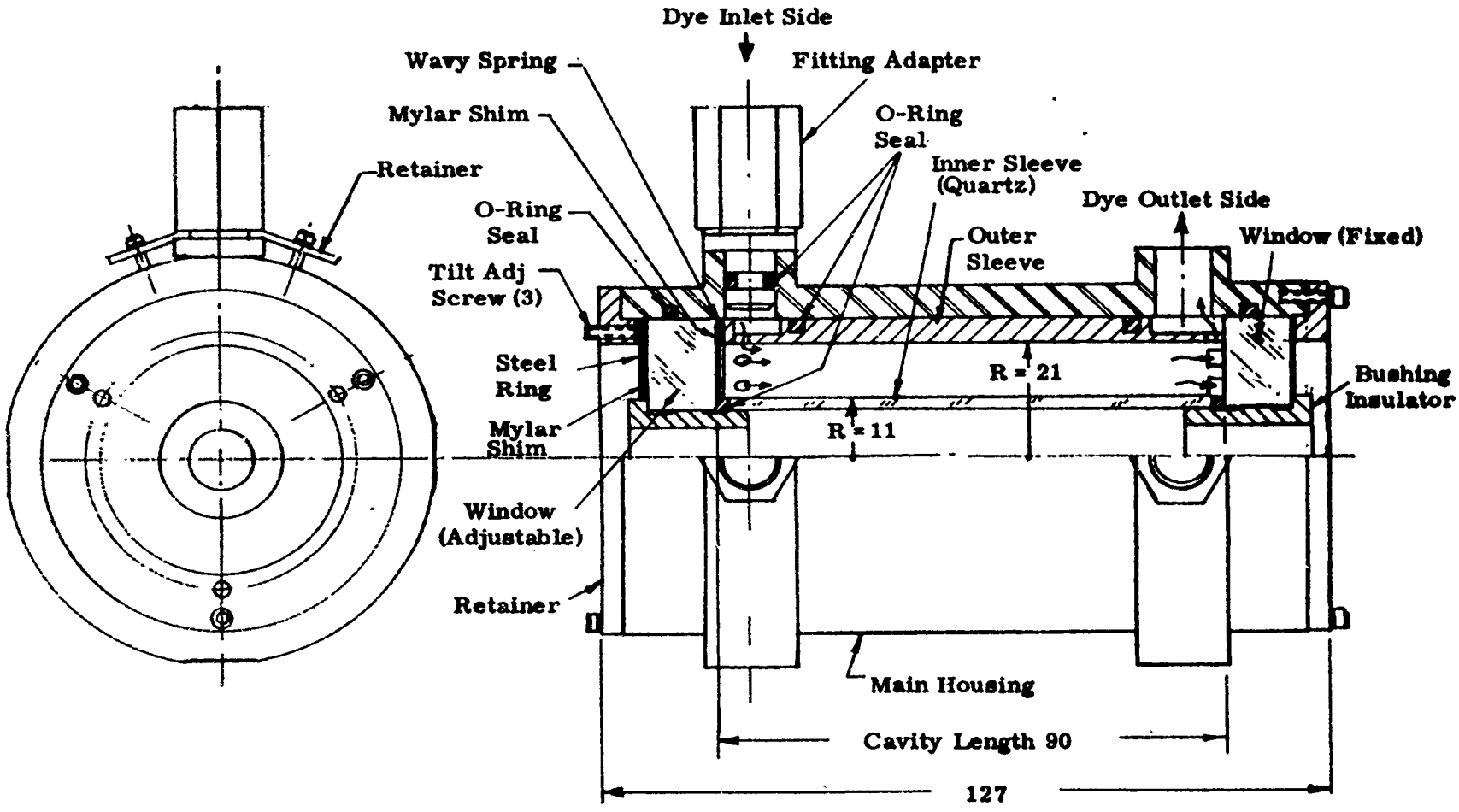

Figure 47. Dye-Laser Head Assembly

Clear aperture:	20 ≤ Diameter ≤ 42 mm
Thickness:	12 mm, wedge free (≤ λ/10 across aperture
Figure:	λ/10 p-p (transmitted wavefront), λ = 0.59 μm
Coating:	Antireflection, one surface

The assembled dye-laser head with its fluid connectors is shown in Figure 48. The window outer diameter of 42 mm can be used to visualize the overall size of the dye-laser head. An exploded view of the head is shown in Figure 49.

2. DYE-LASER HEAD TESTS

a. Electrical System Tests

The electrical system was assembled and tested with the flash lamp as shown earlier in Figure 43. No mechanical difficulties were encountered. The insulator (nylon) mounted on the flash lamp was found susceptible to arcing and was redesigned accordingly. The system was tested up to a maximum voltage of 24 kilovolts without problems. Spark gap pressurization was necessary above 18 kV to prevent self-firing. Dry nitrogen was used at 5 to 10 psi to hold off the discharge.

The flash-lamp output was monitored with a silicon PIN photodiode. Oscilloscope traces indicated a pulse full width of approximately 1.0 μs and a rise time (10% to 90% peak) of 200 ns. This was certainly well within the design goals of 2.0 μs and 500 ns, respectively. No transient degradation of the laser medium during the laser pulse was therefore anticipated.

b. Checkout with a Plane-Parallel Resonator

The dye laser head was tested with a pair of flat mirrors as shown in Figure 50 to establish the threshold pumping energy, efficiency (energy in versus energy out) and uniformity. A dye concentration of 2.0×10^{-4} mole/liter was chosen based upon previous experience. The resonator mirrors were high quality flats (better than λ/20 p-p) and coated for 100% and 80% reflectivity. Some difficulty was encountered with dye contamination which resulted in very short dye lifetime (tens of shots) and high pumping threshold

Figure 48. Assembled Dye-Laser Head

Figure 49. Dye-Laser Head, Exploded View

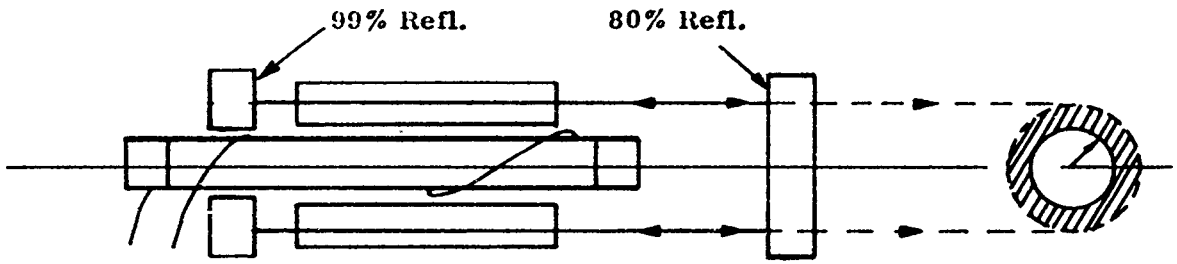

Figure 50. Plane-Parallel Resonator Arrangement for Testing Medium Effects

energy. Insertion of an in-line filter (0.3 μm) and replacement of the originally selected pump by an all-plastic model solved the problem.

The resultant threshold energy was found to be 13 joules (9.5 kV). This was somewhat lower than expected and may indicate certain advantages of this geometry for efficient optical pumping. (Similar experiments in elliptical cavities require nearly twice the pumping energy.)

The efficiency of the laser was measured and the results are shown in Figure 51. Several points should be noted. The output mirror reflectivity of 80 percent is probably higher than it should be for optimum output. Experience indicates optimum reflectivity of approximately 30 percent. Also we see that saturation of the medium has not been achieved since the curve of Figure 51 shows no flattening.

The head was tested in the stable, plane-parallel resonator configuration of Figure 9 to determine the gain in the dye-laser medium as a function of distance from the cylinder axis. To determine the radial extent and variation of the gain region during lasing, photographs were taken of the laser output coupled out through the partially reflecting resonator end mirror of the plane-parallel resonator of Figure 50 while varying flash-lamp pumping power, dye concentration, end mirror reflection, and camera aperture. The relative variation of light intensity in the outcoupled laser beam as determined from the photographs is plotted in Figures 52, 53 and 54 as a function of radial distance from the inner diameter of the gain region.

Ideally, a uniform gain across the dye medium is desired. The width of the region between the inner wall of the dye-laser head and the outer boundary defined by the diameter of the scraper hole is 4 mm. For the optimum dye concentration (1.5×10^{-4} conc.) and using the case of the 16-percent reflectivity corresponding to a conservative estimate of the losses in the spherical mirror resonator, the gain decrease across a 4-mm cylinder wall width can be extrapolated from Figure 54 to be approximately 10^4. This means that the outermost ray, parallel to the axis of the spherical mirror resonator which is 4 mm from the inner wall of the cylindrical gain medium and just grazes the inside edge of the scraper, will have very little energy in it; this may excessively reduce the fraction of energy coupled out by the scraper for the desired mode of resonance.

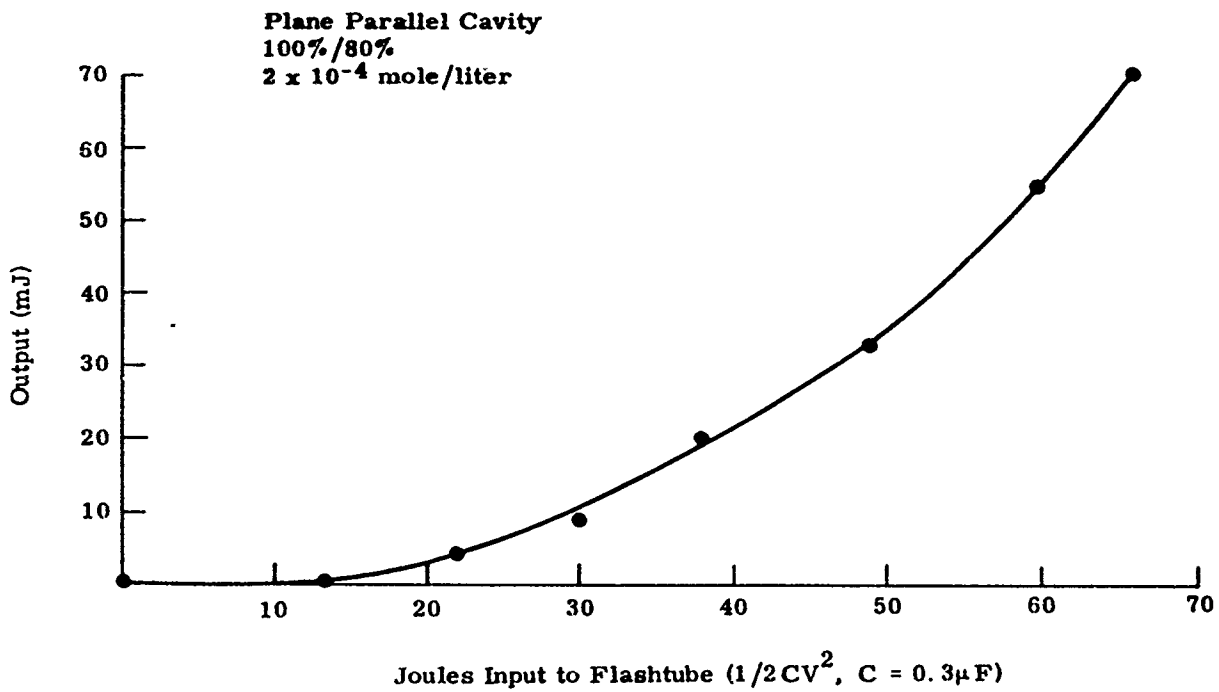

Figure 51. Laser Efficiency Measured with Stable Resonator

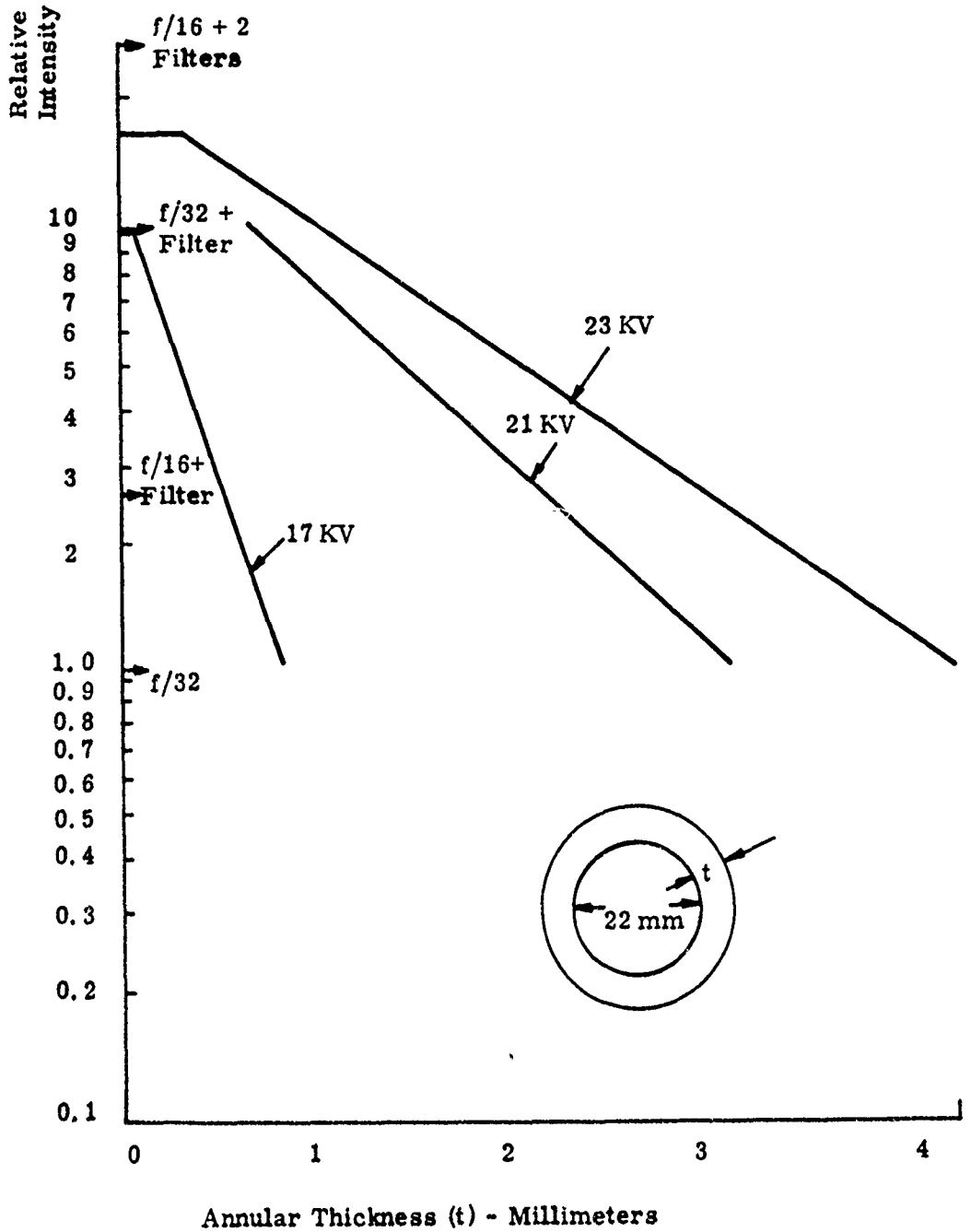

Figure 52. Intensity as a Function of Radial Distance from the Inner Diameter of the Gain Region for 80% End Mirror Reflectivity and 0.5×10^{-4} Dye Concentration

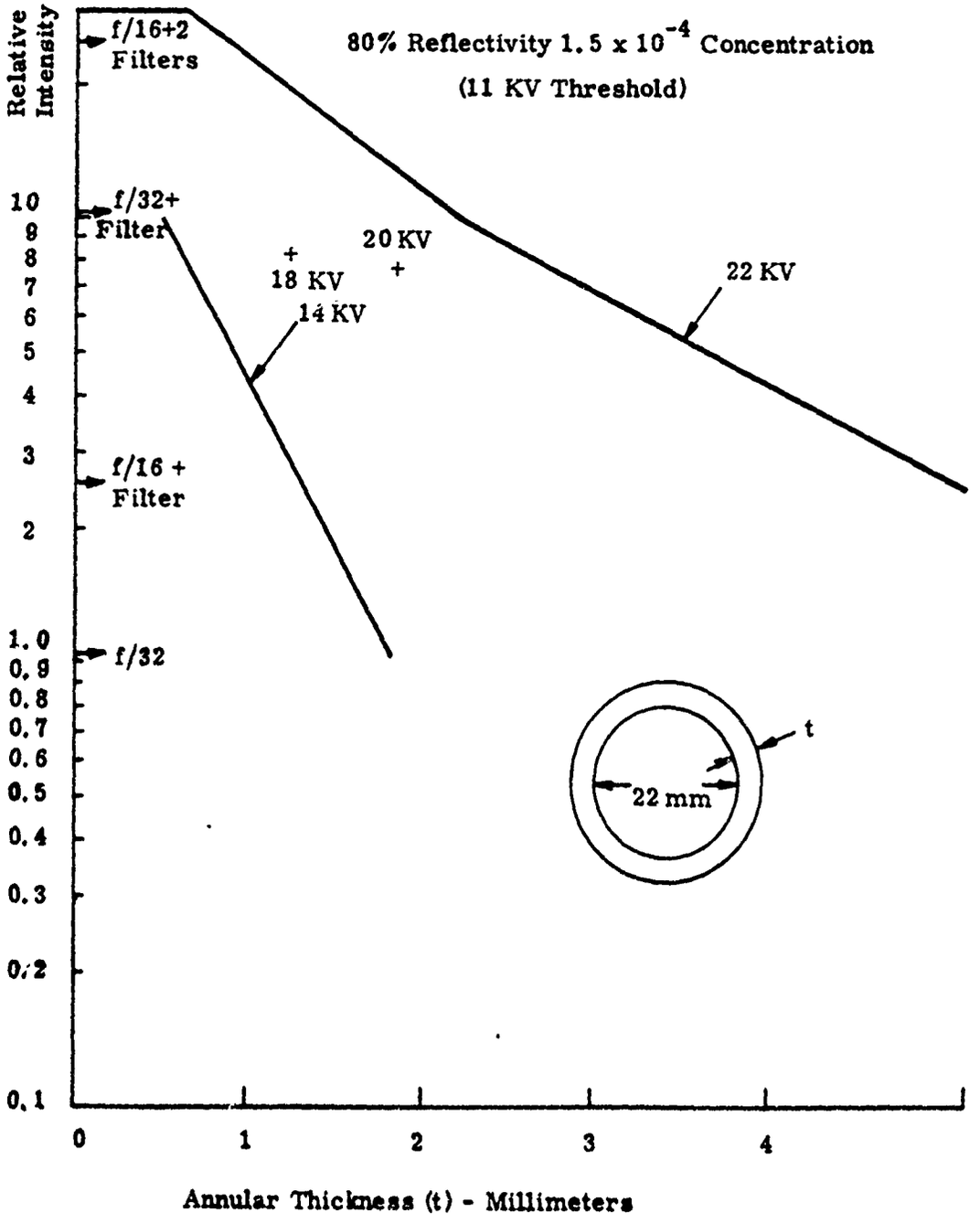

Figure 53. Intensity as a Function of Radial Distance from the Inner Diameter of the Gain Region for 80% End Mirror Reflectivity and 1.5×10^{-4} Dye Concentration

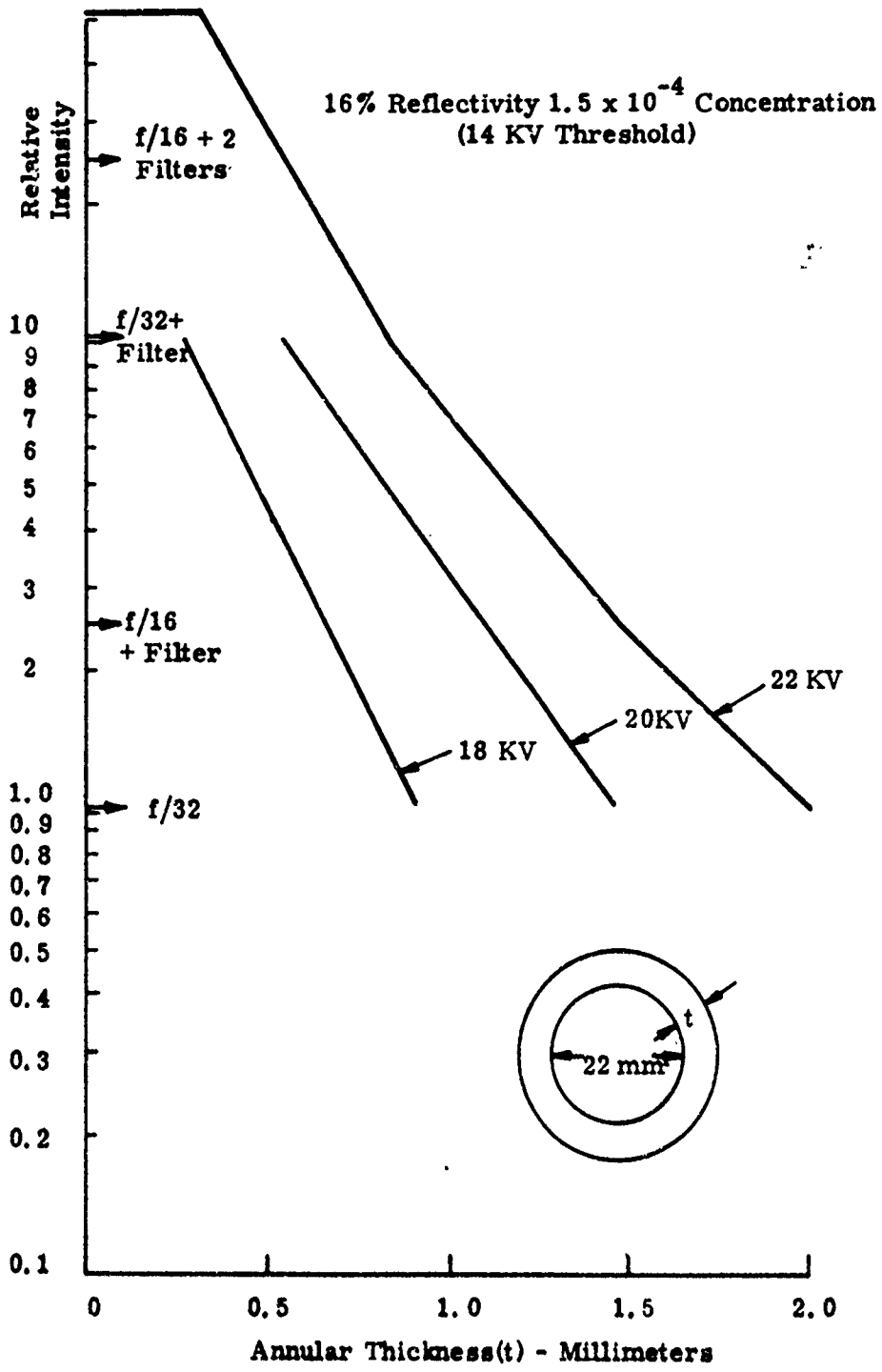

Figure 54. Intensity as a Function of Radial Distance from the Inner Diameter of the Gain Region for 16% End Mirror Reflectivity and 1.5×10^{-4} Dye Concentration

The laser output was recorded photographically to obtain near- and far-field quality. The near-field output of the laser is shown in Figure 55. A photo of the far-field intensity pattern is shown in Figure 56. The important thing to note is that there is no unusual structure in the far-field that would indicate dynamic or transient aberration due to the laser medium. As an example, transient effects due to absorbed infrared radiation would produce a radially propagating index gradient or discontinuity (shock). This would, in turn, yield an output wavefront with toric phase which would be evidenced by a ring focus. Such behavior was neither observed nor anticipated.

3. DYE-LASER HEAD MODIFICATION FOR USE WITH W-AXICON

The dimensions of the W-axicon element used with the HSURIA cavity configurations required a modification of dye-laser head dimensions in order to maintain the original design width of the cylindrical gain region. The original and modified head configurations are shown in Figures 57 and 58, respectively. The only dimension that has been altered is the diameter of the inner wall, which has been increased from 22 mm to 33 mm. The lines labeled "low gain region" in Figures 57 and 58 represent the outer rays from the cylindrical dye-laser region that reflect off of the W-axicon onto the axis of the compacted resonator region. The laser light intensity will be much lower in the "low gain region" of Figure 57 than in the "low gain region" of Figure 58 because it is more than twice as far from the "high gain region" which represents the inner radius of the cylindrical dye-laser volume. Increasing the inner radius of the cylindrical dye-laser gain region should have the effect of increasing the intensity of laser radiation on axis in the compacted gain region for the case where the laser intensity in the cylindrical gain region decreases faster than a linear function of the radius.

The radial extent and variation of the gain region during lasing was determined in the same manner as before. Photographs were taken of the laser output coupled out through the partially reflecting resonator end mirror while varying flash-lamp pumping power, dye concentration, end mirror reflection, and exposure time. The relative variation of light intensity in the outcoupled laser beam as determined from the photographs is plotted in Figure 59 as a function of radial distance from the inner diameter of the gain region.

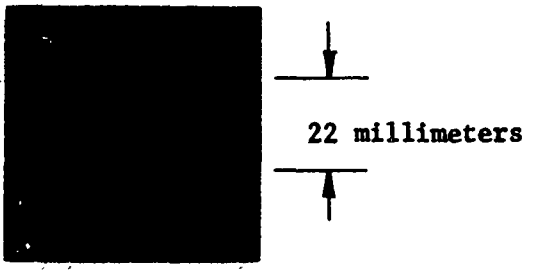

Figure 55. Near-Field Laser Output for a Plane-Parallel Resonator

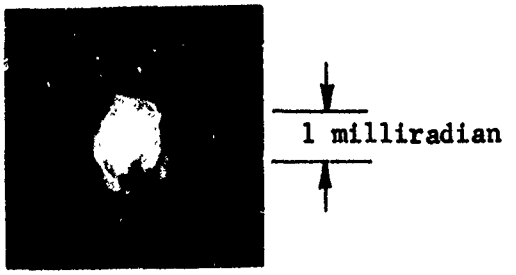

Figure 56. Far-Field Pattern Corresponding to the Near-Field Output of Figure 52

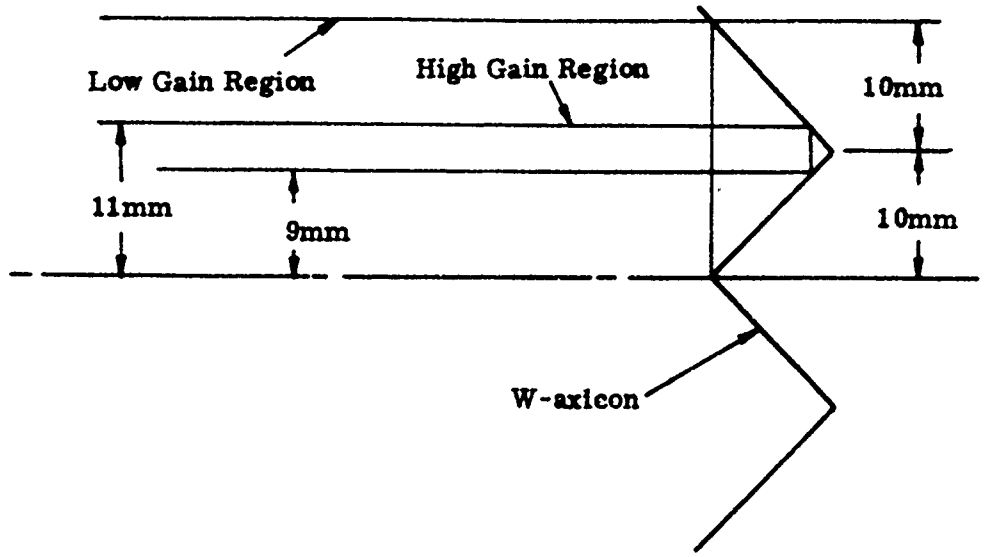

Figure 57. Gain Region Radial Dimensions with Original Head Design and Available W-axicon

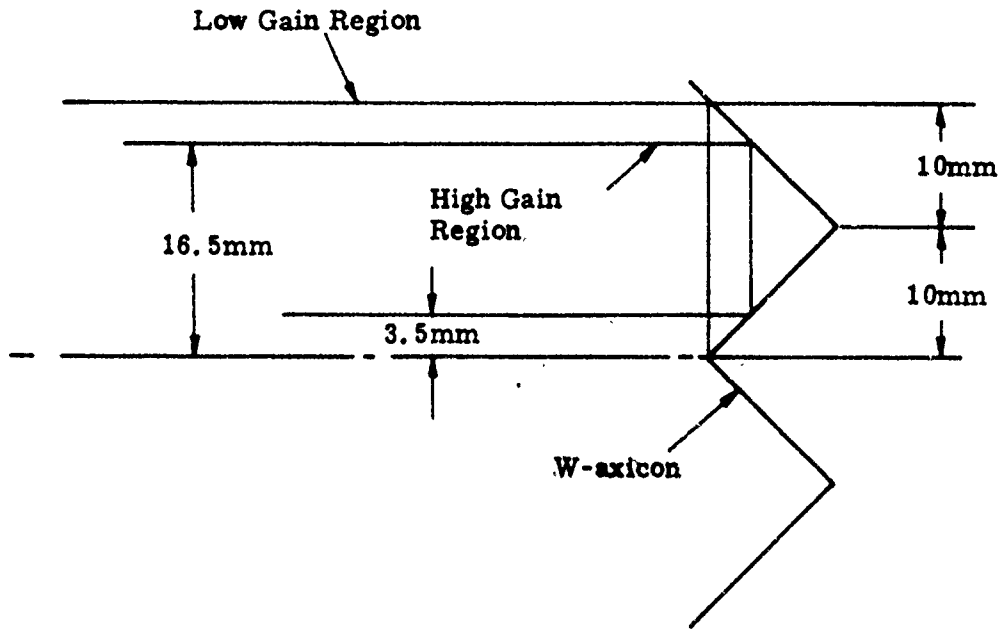

Figure 58. Gain Region Radial Dimensions with Modified Head Design

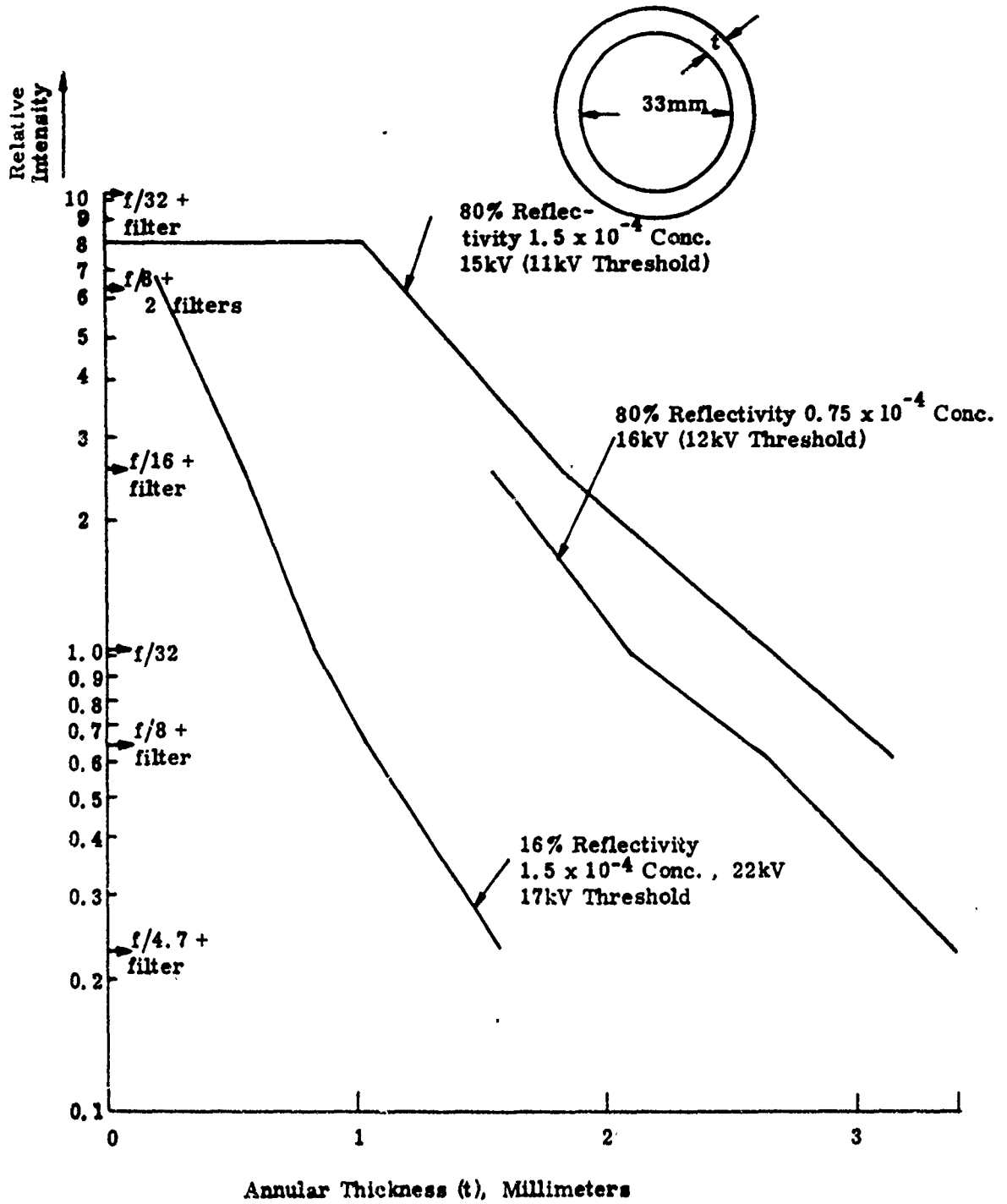

Figure 59. Intensity as a Function of Radial Distance from the Inner Diameter of the Gain Region

As before, a uniform gain across the dye medium is desired. The width of the region between the inner wall of the dye-laser head and the outer boundary defined by a line mapped from the axis of the W-axicon is 3.5 mm. The gain decreases by a factor of approximately 100 across this width for the dye concentration used in the spherical mirror tests. This means that the intensity on axis in the compacted beam will be very low. The inversion produced by the W-axicon gives a low percentage feedback and a high percentage of energy into the scraper, resulting in a high equivalent obscuration.

4. RESONATOR TESTS WITH THE DYE LASER

a. Spherical Mirror (Converging Wave) Resonator

(1) Resonator Design

The converging wave resonator configuration using two spherical mirrors and the predicted path of a ray in the resonant cavity for this configuration is shown in Figure 1. Since elements M_{1A} and M_{1B} are confocal, a ray parallel to the axis but at some radial distance from it should eventually work its way into coincidence with the axis. A classical geometrical ray would require an infinite number of reflections between M_{1A} and M_{1B} to arrive at the axis, but diffraction effects should actually result in a finite number of reflections before the ray returns on itself, and should spread the ray sufficiently to allow some energy to be coupled out of the cavity by the scraper. The diffraction spread would also result in azimuthal coupling within the resonator, which should tend to suppress high azimuthal order resonant modes.

The critical dimensions of the resonator design are shown in Figure 60. The inner diameter of the dye-laser head is 22 mm, and the diameter of the hole in the scraper is 30 mm. The resonator dimensions for the three configurations tested are listed in Table 2.

The spacing between convex and concave mirrors was designed to be 100 mm, but experiments were performed to determine the effect of varying the spacing around the nominal design value. The distance (L) determines the overall length of the resonator cavity and, hence, the diffraction losses, and the resonator was tested at lengths (L) of 50 cm, 1 m, and 6 m. A photograph of the assembled resonator at length L = 50 cm is shown in Figure 61.

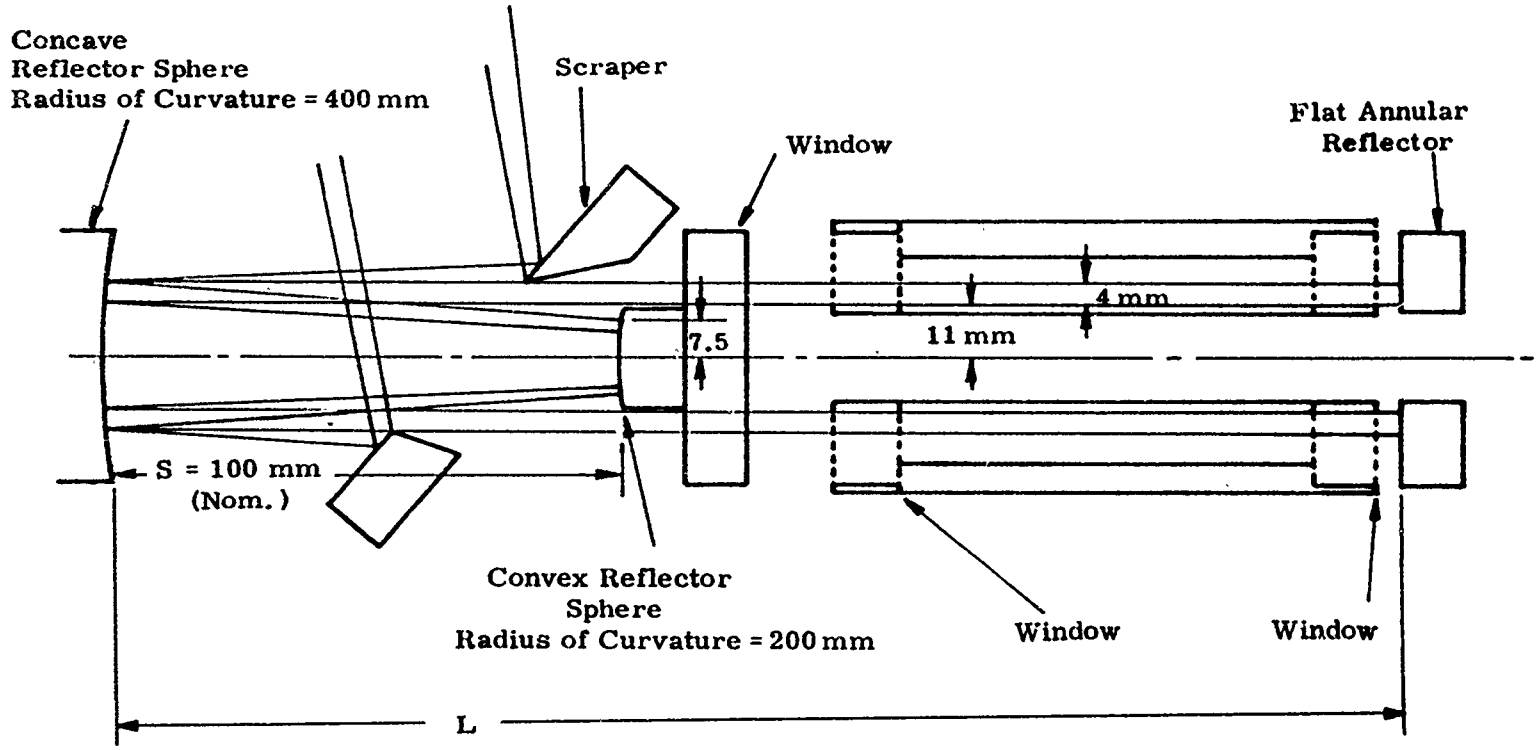

Figure 60. Spherical Mirror Resonator

TABLE 2. DYE-LASER SPHERICAL MIRROR RESONATOR DIMENSIONS

Configuration	Scraper Hole Radius a (mm)	Resonator Cavity Length L (cm)	Equivalent Fresnel Number	Spherical Mirror Spacing S (mm)
A	30	50	Not Defined for Spherical Mirror Resonator	100
B	30	100		100
C	30	600		100

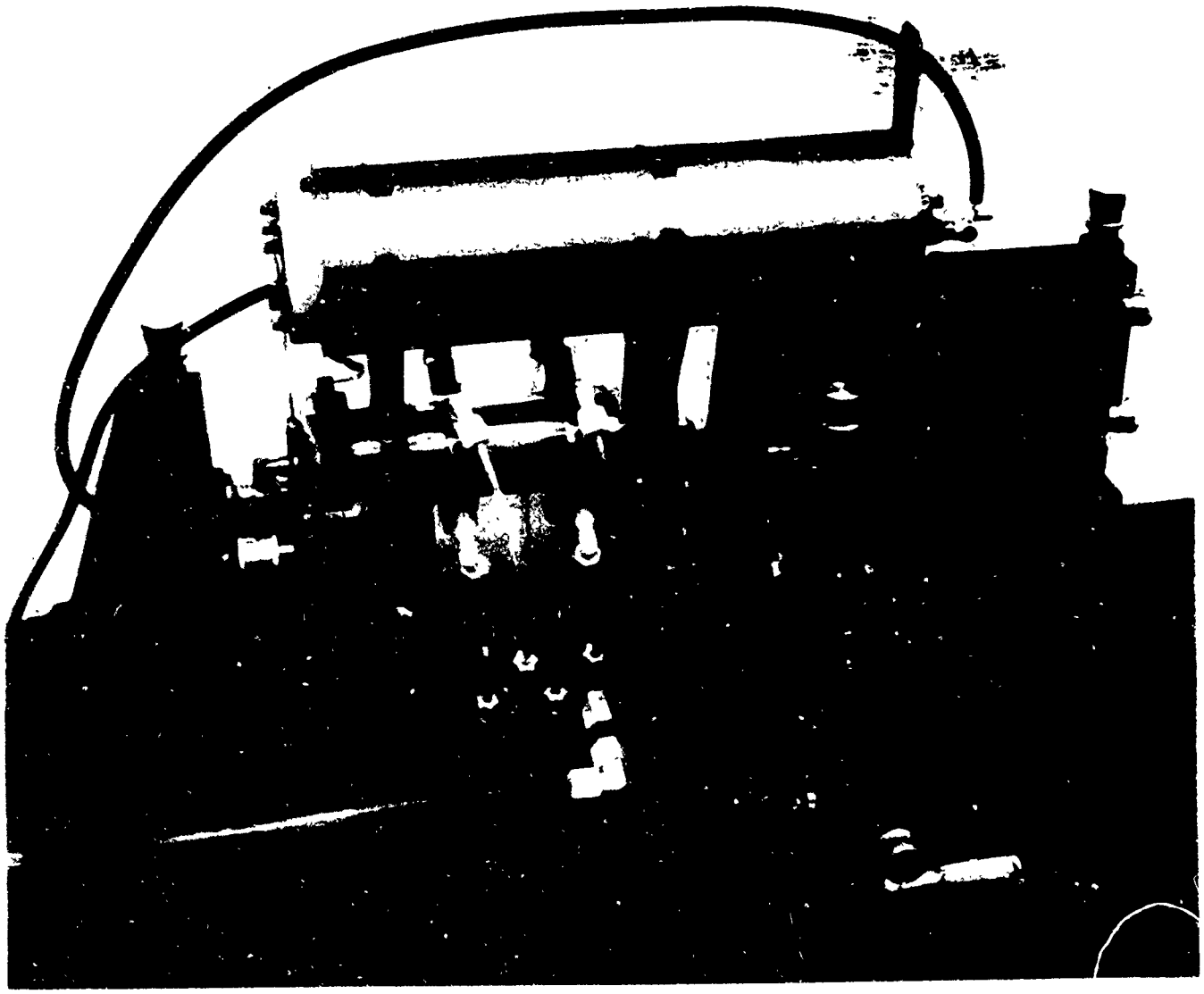

Figure 61. Spherical Mirror Dye-Laser Resonator Arrangement

(2) Spherical Mirror Alignment Procedure

(a) The dye-laser head containing the dye-laser medium was corrected to remove wedge by adjusting the tilt of the end windows to remove any tilt deviation introduced to the test wavefront when the head was inserted in one arm of a Twyman-Green interferometer.

(b) The boresighting of the head was checked by observing the symmetry of an extended collimated wavefront that was passed through the head perpendicular to the windows. The throughput was a uniform annulus with no apparent asymmetry due to vignetting at either the inside or outside diameters of the annulus, indicating that the windows were perpendicular to the axis of the inner and outer walls of the head.

(c) The dye-laser head was secured to the bench and served as the reference to which the rest of the resonator components were aligned.

(d) A Brunson focusing alignment telescope was aligned to the dye-laser head and was used as a secondary reference to implement most of the remaining alignment steps (Figure 62). The alignment telescope was on a cross slide that permitted it to be moved laterally so that it could be aligned on the axis of the dye-laser head or looking through any part of the gain medium, without losing its alignment perpendicular to the window of the dye-laser head.

(e) The flat, annular reflector was aligned to the dye-laser head using the alignment telescope. It was convenient to use the point-source arc-lamp telescope attachment to perform this step since the windows did not reflect much light, making the extended image of the internal telescope target difficult to see.

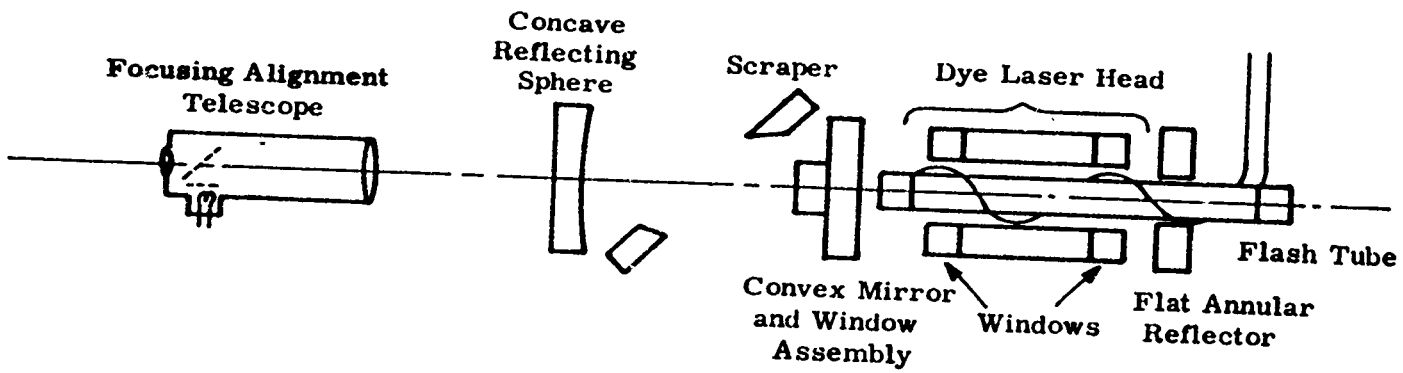

Figure 62. Spherical Mirror Alignment Arrangement

(f) The convex mirror and window assembly was aligned in tilt so that the reflected images of the point source arc lamp, from the window and from the flat annular reflector, were superimposed in the alignment telescope.

(g) The alignment telescope was placed on the axis of the dye-laser head. (This position was previously determined by centering the telescope on the image of the end of the dye-laser head and indexing the cross slide so that it could be reset easily to this point.) The convex spherical mirror and window assembly was translated laterally until the image of the telescope target reflected from the convex mirror was centered in the telescope.

(h) The scraper was adjusted to the design angle and was translated laterally so that the image of the scraper hole was centered in the telescope.

(i) The concave reflecting sphere was aligned in tilt so that the image of the telescope target reflected from the flat, back surface of the concave spherical element was centered in the telescope.

(j) The concave reflecting sphere was translated laterally until the image of the telescope target reflected from the convex back of the concave spherical element was centered in the telescope.

(3) Test Procedure

The test arrangement for observing near- and far-field patterns is shown in Figure 63. The near-field output was observed in a plane a few inches outside of the scraper, and the far-field pattern was observed at a distance of 4.5 meters from the scraper. In both cases photographs were taken of the illumination of a diffuse surface by the laser light.

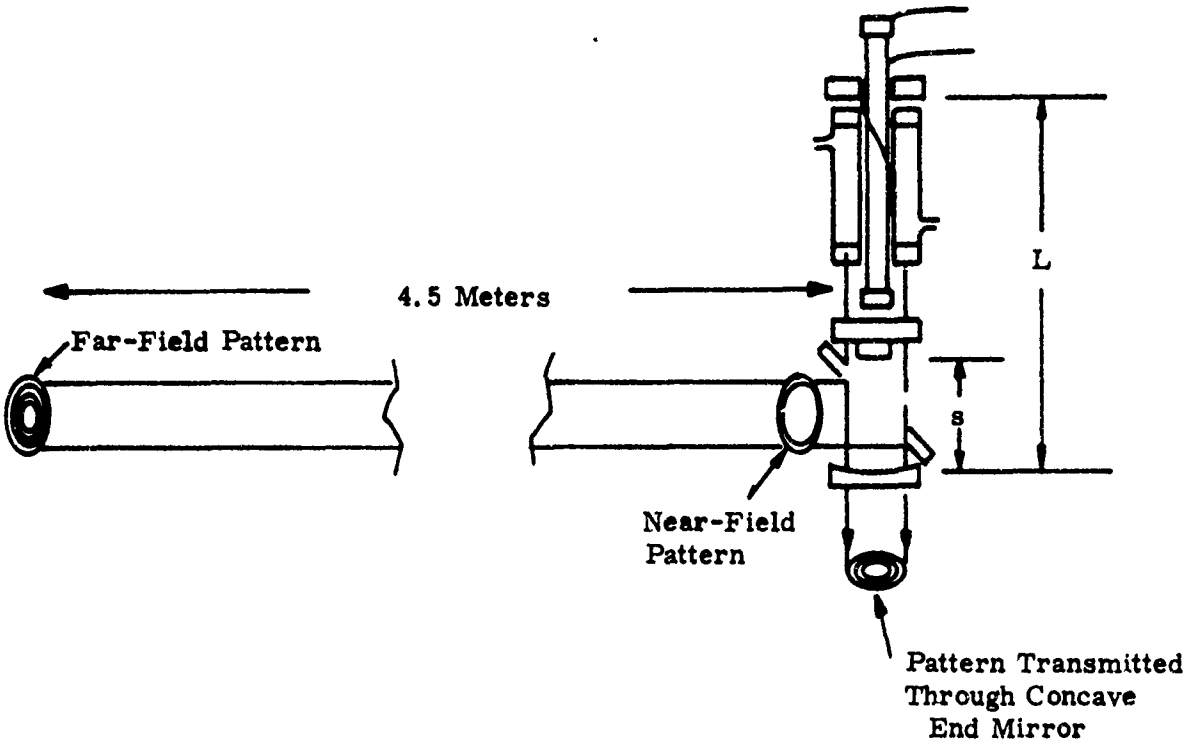

Figure 63. Far-Field Test Arrangement

Although the concave end mirror was very highly reflective at the lasing wavelength, the light transmitted through the mirror was intense enough to obtain photographs of the light impinging on a diffuse surface. These gave some indication of what was taking place in the space between the concave and convex mirrors where the beam was supposed to converge.

Figure 64 shows a second test arrangement for finding and observing the best focus of the output beam where the beam is brought to a "focus" by a two-element telescope arrangement.

(4) Intensity Distribution Test Results

The near-field intensity distribution was observed at a plane just outside the scraper; Figure 65 shows the near-field irradiance for the spherical resonator configuration of Figure 63, where L = 50 cm and S = 10 cm. The far-field intensity distribution observed at a distance of 4.5 meters from its scraper for the same resonator configuration is shown in Figure 65(b); the intensity distribution for the "focused" beam is shown in Figure 65(c). The distribution of energy transmitted through the concave end mirror for L = 50 cm and S = 10 cm is shown in Figure 66. Since the latter was taken close to the end mirror and since the distribution was observed to change very slowly as the observation point was moved farther away from the end mirror, the photograph shown effectively represents the energy distribution at the concave mirror surface itself. Figure 67 shows representative photographs of the intensity distributions in the far field and at the concave end mirror as the concave and convex mirror spacing (S) was varied around the nominal design value of 10 cm.

It is apparent from these results that the spherical mirror resonator is not performing as predicted. The pattern at the concave end mirror should show an energy flux distribution all the way to the center of the mirror corresponding to the converging ray path shown in Figure 1 for the condition that the convex and concave mirrors are confocal. If the mirror spacing is reduced, the ray path will not reach the axis before it starts to work its way back out; and if the mirror spacing is made greater, the ray path will overshoot the axis and work its way out the opposite side from which it entered. The proper spacing to achieve convergence on axis should be fairly critical. No such effects

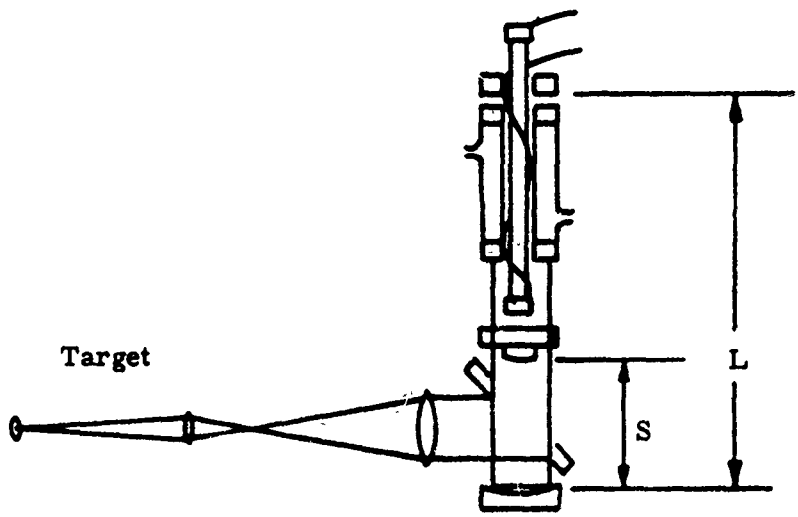

Figure 64. Test Arrangement for Finding Best Output Focus

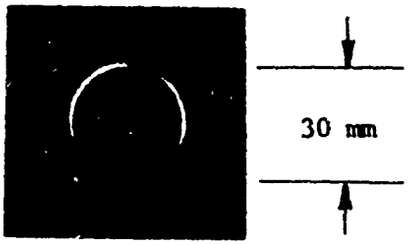

(a) Near-Field Pattern at Scraper

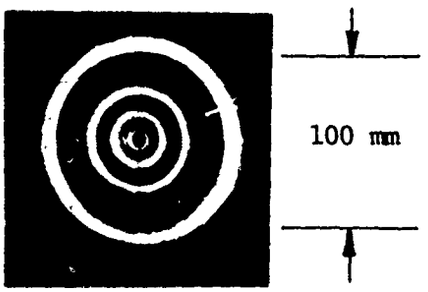

(b) Far-Field Pattern at 4.5 Meters from Scraper

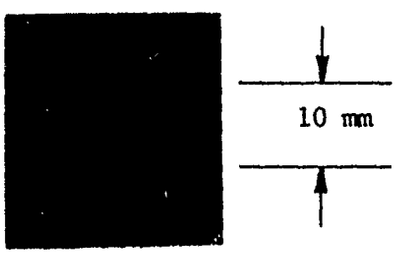

(c) Output Beam Brought to Best Focus

Figure 65. Intensity Distributions in Spherical Mirror Resonator Laser Output

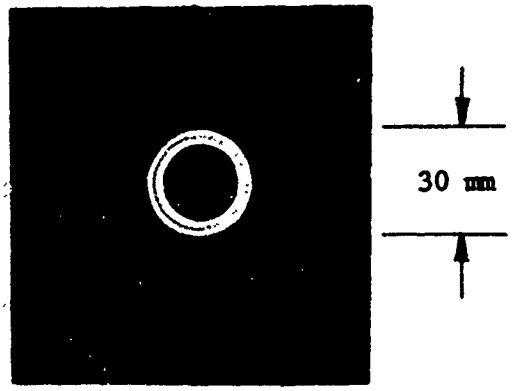

Figure 66. Intensity Distribution in Beam Transmitted Through Concave Laser End Mirror

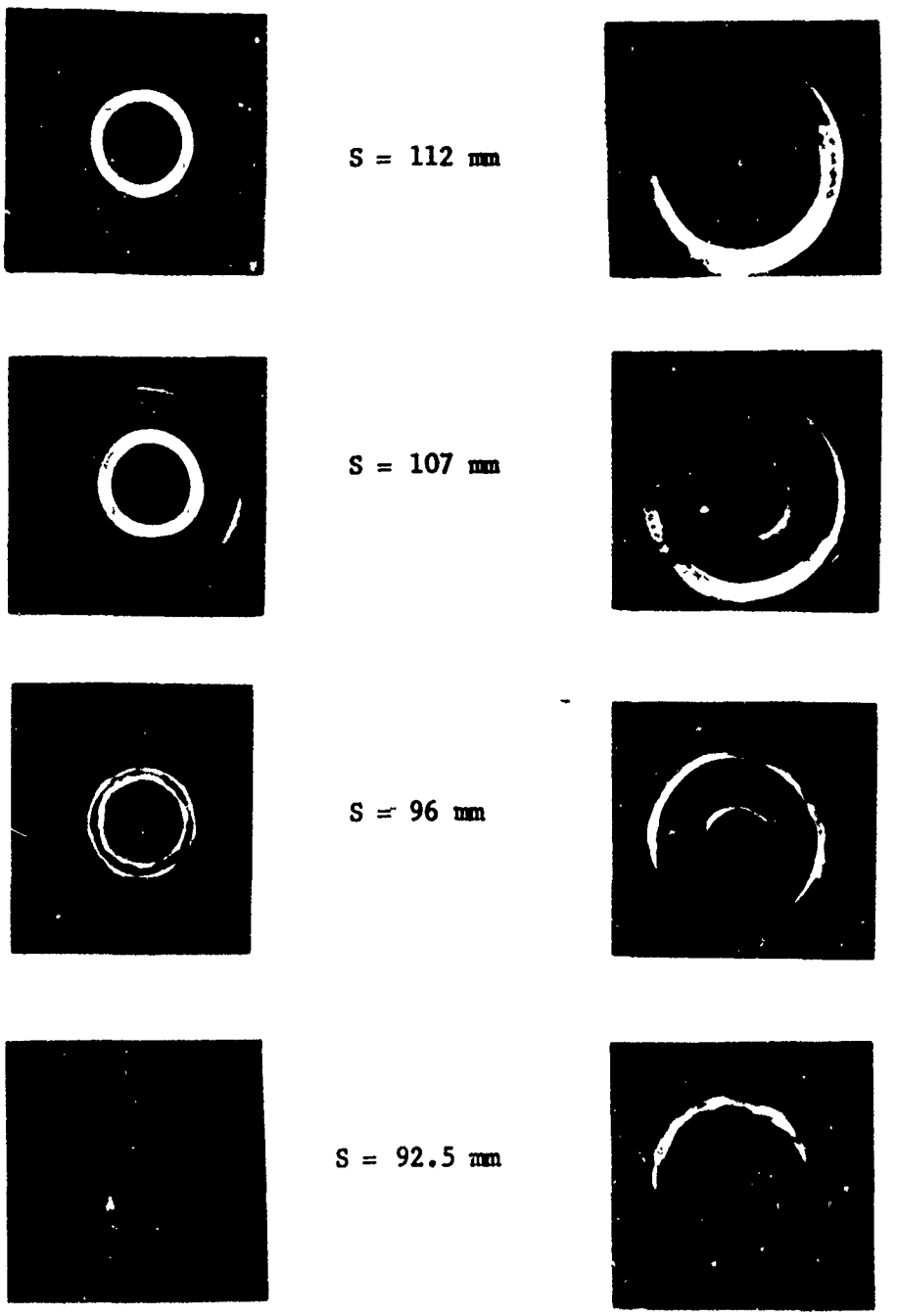

Figure 67. Energy Distribution in Far Field and at Concave End Mirror as Concave and Convex Mirror Spacing (S) is Varied

were observed as the spacing was changed; the energy distributions in the near and far fields and at the concave mirror stayed relatively constant over a change in spacing greater than plus and minus 1 centimeter.

The second anomalous effect observed was the energy pattern at the output beam "focus," which, at its smallest diameter, is a ring rather than a point, indicating some source of toroidal power in the resonator, also independent of concave and convex mirror spacing. Initially, it was suspected that the dye medium in the laser head might be the source of this toroidal power, but this possibility was eliminated by testing the head in a plane-parallel resonator, where the output was observed to focus to a "point." The source of the toroidal effect is therefore not known at this time.

An interesting characteristic observed in the intensity distribution at the concave end mirror was the breakup of the image into definite azimuthal modes at certain specific mirror separations. The modes observed had an odd number of azimuthal nodes. Figure 68 shows some of the modes observed. Blocking the convex mirror caused the lasing to stop; so there is evidence that at least one reflection from the convex mirror is taking place.

The spherical mirror resonator configuration with L = 50 cm was very short relative to the diameter of the gain region, so that the Fresnel number was much higher than desired and higher than that used in Chodzko's experiment (Ref. 2) with a spherical mirror resonator. The convex and concave spherical mirrors were moved farther away from the flat annular mirror to give a resonator length of L = 1 m. This increased diffraction losses but not enough to prevent lasing. The results were almost identical with the case in which L = 50 cm, although some falloff in laser energy output was observed (Figure 69).

In order to further increase the diffraction losses for high-order transverse resonator modes, the spherical and concave mirrors were moved still farther away to make L = 6 m. At this distance, it was not possible to obtain lasing, presumably because the diffraction losses were too great. Resonator lengths of L greater than 1 meter and less than 6 meters were not tried at

2. R.A. Chodzko, S.B. Mason, and E.F. Cross, "Annular Converging Wave Cavity," SAMSO-TR-76-115 (June 1976).

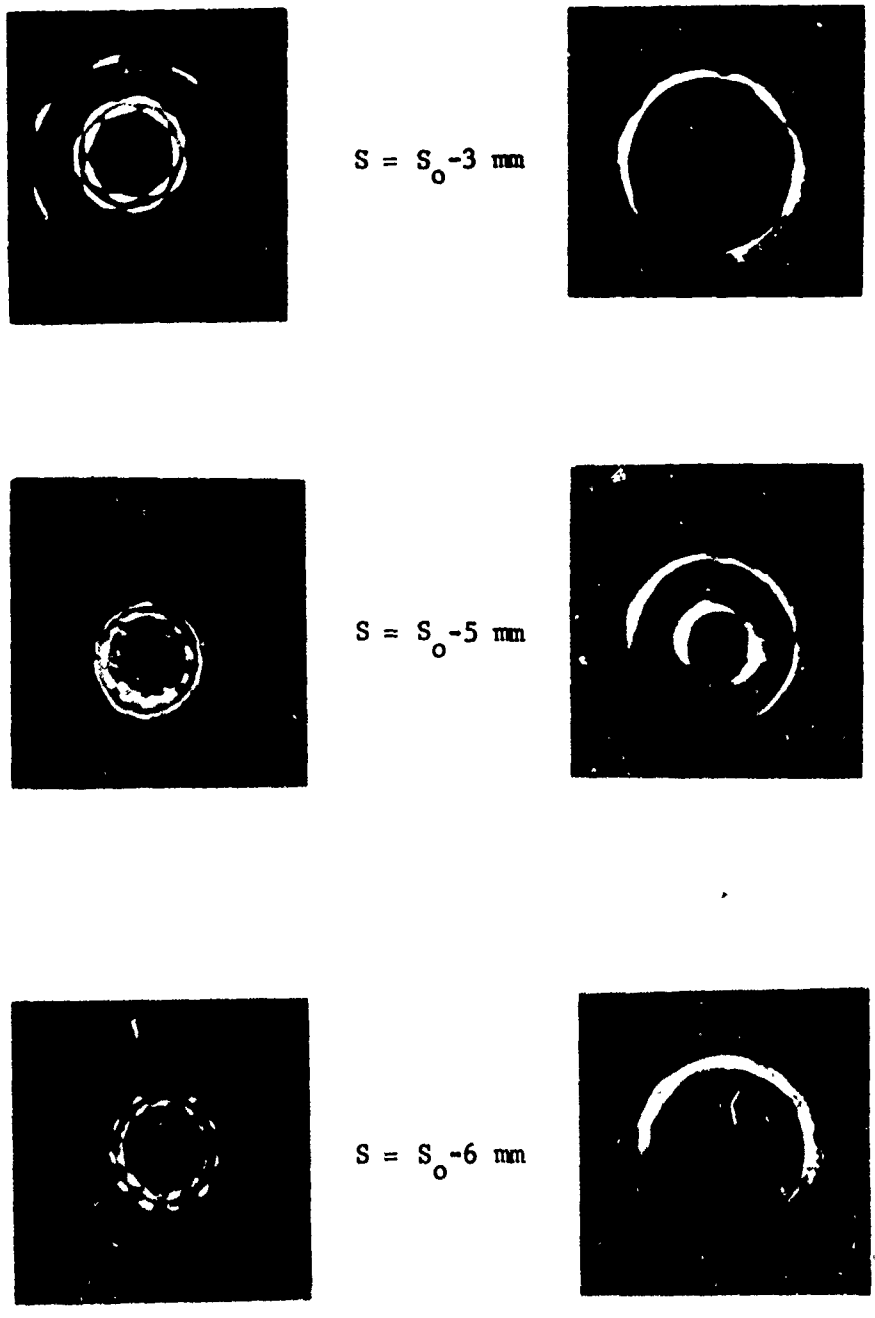

Figure 68. Some High-Order Azimuthal Modes Observed for Different Spherical Mirror Separations

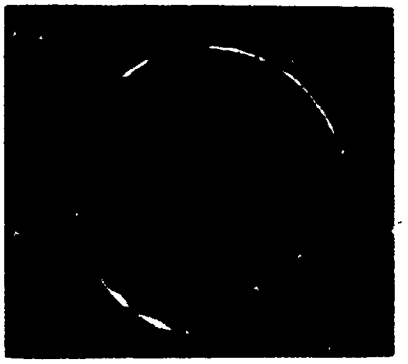

(a) Far-field Pattern at 4.5 Meters from Scraper

(b) Energy Pattern Through Concave End Mirror

Figure 69. Energy Distribution in Far-Field and at Concave End Mirror for 1-Meter Resonator Length (L)

this time because of the available bench arrangement and because of time and the priority of other resonator tests.

Tilt alignments of the flat end mirror and the convex and concave mirrors were not extremely critical to obtain the results observed; misalignments of up to 20 arc-seconds in tilt could be introduced without defeating the lasing and with little effect on the nature of the output. It may be, however, that the alignment is extremely critical to obtain the desired mode of operation. The alignment of the resonator for which L = 50 cm was therefore checked and readjusted using interferometric techniques. The tilt alignments were then estimated to be accurate to approximately 1 arc-second. No change in performance was observed. The possibility still exists, however, that the alignment required to obtain the desired performance is supercritical and was not achieved. In that case, much more sensitive alignment techniques, that is, techniques that would provide better than 1 arc-second accuracy in tilt adjustment, would be necessary.

(5) Conclusions

The spherical mirror resonator lased, but not in the desired mode. Increasing the resonator length to suppress higher order modes did not reveal the existence of the desired low-order modes. The dye-medium gain distribution would appear to have a strong negative influence in the production of power output in these low-order modes. The alignment accuracy required to obtain the desired mode may be more critical than present techniques can provide.

b. Half-Symmetric Unstable Resonator with Internal Axicon (HSURIA)

(1) Resonator Design

Figure 70 shows the basic HSURIA arrangement with a convex spherical element. Figure 71 shows the HSURIA with a corner cube and spherical lens feedback arrangement. The axicon is an axially symmetric conical beam compactor that converts a circular beam with a large central obscuration to a smaller beam with a smaller central obscuration. The ratio of the diameter of the beam to the diameter of the obscuration is increased in the output from the compacted beam relative to the beam in the gain region so that

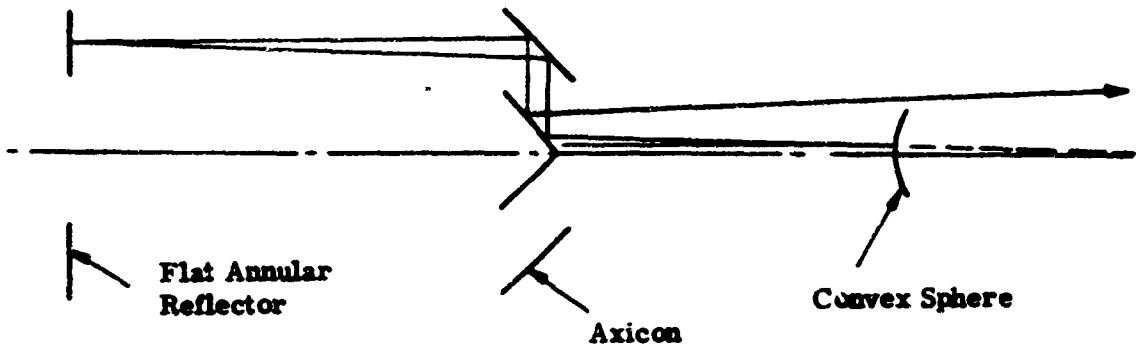

Figure 70. HSURIA with Convex Spherical Feedback Element

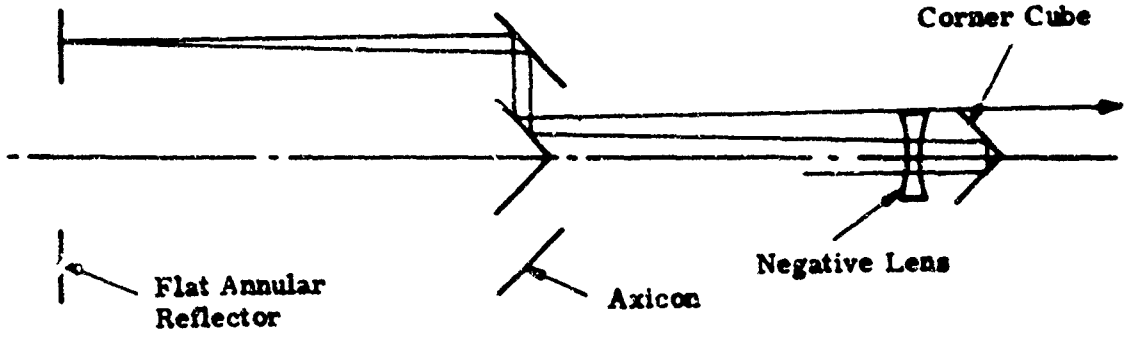

Figure 71. HSURIA with Corner-Cube and Negative-Lens Feedback

improvements in the intensity distribution of the far-field pattern can be realized. Another feature is that smaller optics can be used to project the output obtained from the compacted beam. The primary purpose of the axicon is to obtain mode discrimination in the annular resonators. The portion of the resonator between the axicon and the feedback mirror looks very much like a conventional unstable resonator. It was hoped that some of the mode discrimination properties of these resonators would result in mode discrimination in the annular resonators. In Figure 70, the convex spherical feedback element provides the optical power required to spread the beam so that energy can be coupled out either past the edge of the convex spherical mirror or by means of a scraper. In Figure 71, the feedback is provided by a corner cube, and the optical power needed to couple energy out is provided by a negative lens in front of the corner cube. The corner cube is expected to decrease sensitivity to mirror misalignments.

Figures 2 and 3 show HSURIA arrangements using a W-axicon, which is also an axially symmetric conical beam compactor. The W-axicon differs from the axicon in that it gives a radial inversion of the compacted beam with respect to the beam in the expanded gain region. In Figure 2 the convex spherical feedback element provides the optical power required to spread the beam so that energy can be coupled out of the resonator. In Figure 3, the feedback is provided by a negative lens and a corner cube. Figure 72 is a photograph of the dye-laser HSURIA experimental arrangement per Figure 3.

Resonator dimensions for two configurations attempted are shown in Table 3. Resonator cavity lengths were determined for equivalent Fresnel numbers selected to minimize diffraction losses.

The Fresnel number is a dimensionless parameter for expressing the size of the mirrors in an optical resonator. For a plane-mirror optical resonator:

$$N = \frac{a^2}{L\lambda},$$

where N equals the number of Fresnel zones which can be seen over the surface of one plane mirror of diameter 2a when viewed from the center of the other mirror, and L is the spacing between the two mirrors.

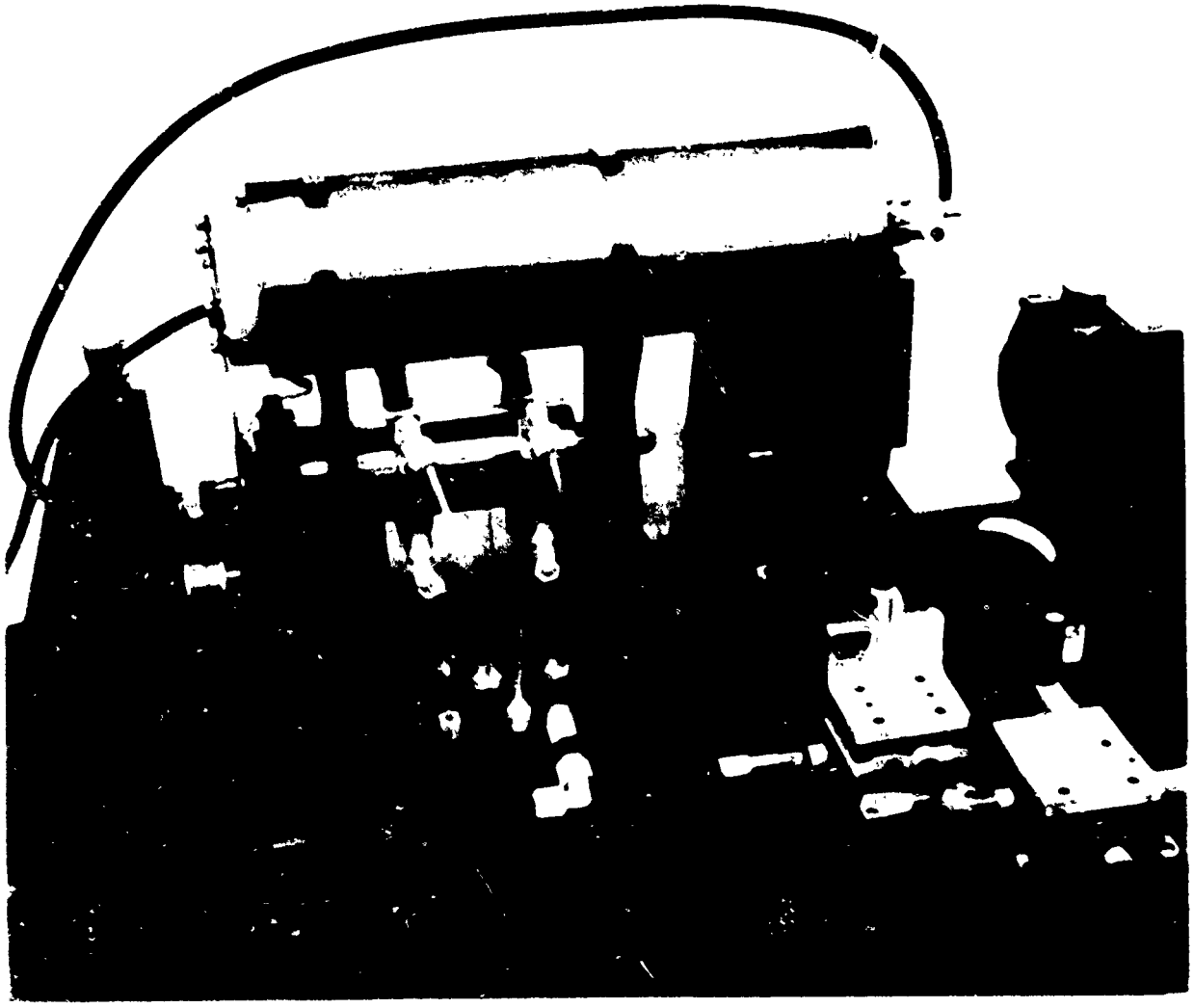

Figure 72. Dye-Laser HSURIA Arrangement with Corner Cube

TABLE 3. DYE-LASER HSURIA DIMENSIONS

Configuration	Equiv. Fresnel Number N_{eq}	Scraper Hole Radius a (mm)	Equiv. Focal Length of Feedback Element (meters)	Resonator Cavity Length L (cm)	Compacted Beam Length L_c (cm)	Beam Magnification M	Output Beam Obscuration (%)
A	3.5	2	-4	50	18	1.64	37
B	4.5	2	-2	66	34	2.21	20

The larger the Fresnel number, the smaller the diffraction losses.

For the HSURIA configurations used in this study an "equivalent Fresnel number" can be determined from the relation:

$$N_{eq} = \frac{a^2}{2L\lambda}\left(\frac{M^2-1}{2M}\right)$$

where

a = radius of the compacted resonator region

f = diverging element equivalent focal length

L = resonator cavity length

M = beam magnification ratio

and

$$M = C + \sqrt{C^2-1} \qquad \text{where } C = 1 - \frac{L}{f}$$

(2) Test Results

In operation, the HSURIA configurations shown in Figures 2 and 3 did not produce lasing action. The observations made on the gain distribution in the dye-laser head, described in paragraph 2.b. of this section of this report, lead to the conclusion that the gain drops off too rapidly with radius and that this adversely affects the feedback ratio for the given configuration to the extent that lasing is not supported.

c. HSURIA with Compacted Gain Region

In order to obtain a qualitative indication of the performance limits imposed in the visible by the HSURIA resonator optics, the HSURIA resonator configurations were then set up using a compacted dye-gain medium.

(1) Resonator Design

The two configurations tested are shown schematically in Figure 5. The compacted gain region gives a higher conversion efficiency and a uniform gain distribution so that lasing was easily achieved. Although this was not the gain medium geometry desired, the experiment was useful to check the feasibility of the HSURIA resonator configuration and to get a qualitative

indication of the performance limits imposed by the W-axicon optical figure. Figure 5(a) shows the HSURIA with compacted dye-gain region and feedback element composed of a negative lens and a corner cube. Figure 5(b) shows the configuration with a convex mirror feedback element. The resonator dimensions for the two configurations are listed in Table 4.

(2) Test Procedure

The test arrangement for observing near-field and far-field intensity distribution is shown in Figures 73 and 74. The near field was observed in a plane approximately 6 inches from the scraper as shown in Figures 73(a) and 74(a). The far field was observed where the beam was brought to a focus by the telescope formed by diagnostic lenses 1 and 2 in Figures 73(b) and 74(b). The lasing energy levels were sufficient to produce burn patterns on developed Polaroid film in the near field and in the far field at low magnification. Photographs were taken of the far-field pattern at a higher magnification.

(3) Intensity Distribution Test Results

Burn patterns produced in the near field, just outside the scraper, are shown in Figure 75(a) for the corner-cube feedback configuration and in Figure 75(b) for the convex mirror feedback configuration. Burn patterns in the far field are shown in Figures 76(a) and 76(b) for the corner cube and the convex mirror, respectively. Photographs of the far-field pattern imaged on a diffuse surface are shown in Figure 77.

The alignment was observed to be very sensitive to adjustment in tilt of the W-axicon and convex mirror. Small translations of the W-axicon and tilt or translation of the corner cube, however, caused relatively little variation in the laser output observed. There was no discernible difference between the intensity distributions for the two different feedback configurations when aligned.

(4) Conclusions

The far-field patterns obtained from the configurations tested show several times the diffraction-limited spread at 5900 Å, and the primary source

TABLE 4. DYE-LASER HSURIA WITH COMPACTED GAIN REGION - DIMENSIONS

Configuration	Equiv. Fresnel Number	Scraper Hole Radius a (mm)	Equiv. Focal Length of Feedback Element (cm)	Resonator Cavity Length L (cm)	Compacted Beam Length L_c (cm)	Beam Magnification M	Output Beam Obscuration (%)
A	3.69	2	-200	107	7	2.70	13.7
B	6.17	2	-90	107	7	4.14	5.8

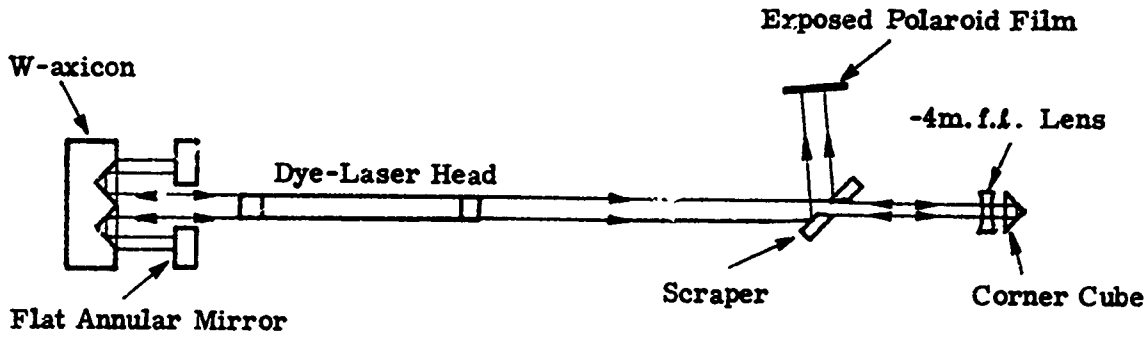

(a) Arrangement for Near-Field Observation

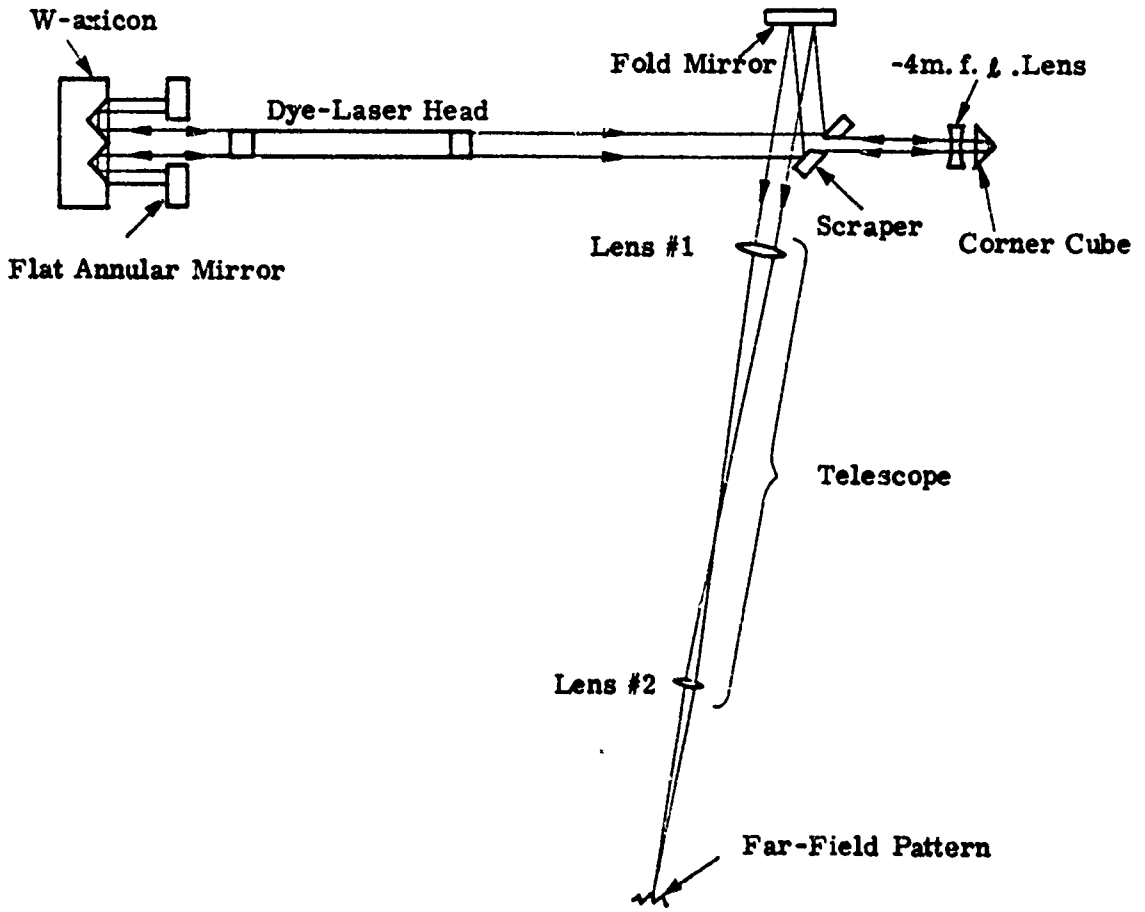

(b) Arrangement for Far-Field Observation

Figure 73. HSURIA with Corner Cube, Test Arrangements for Observing Near- and Far-Field Patterns

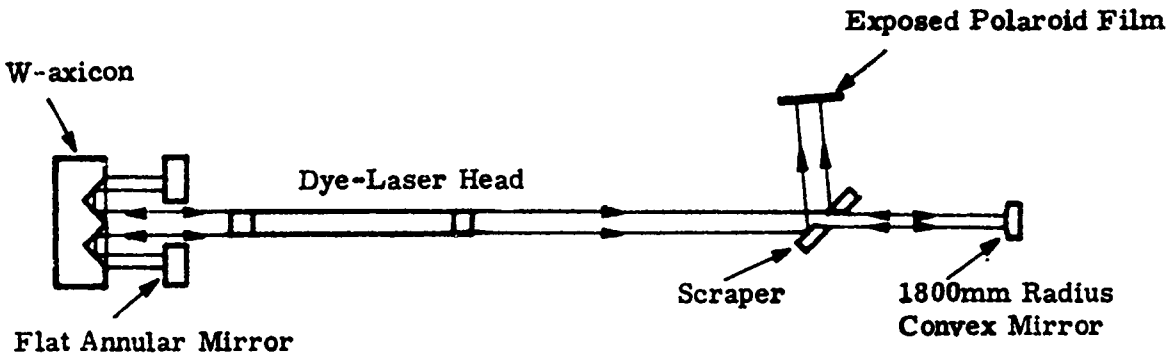

(a) Arrangement for Near-Field Observation

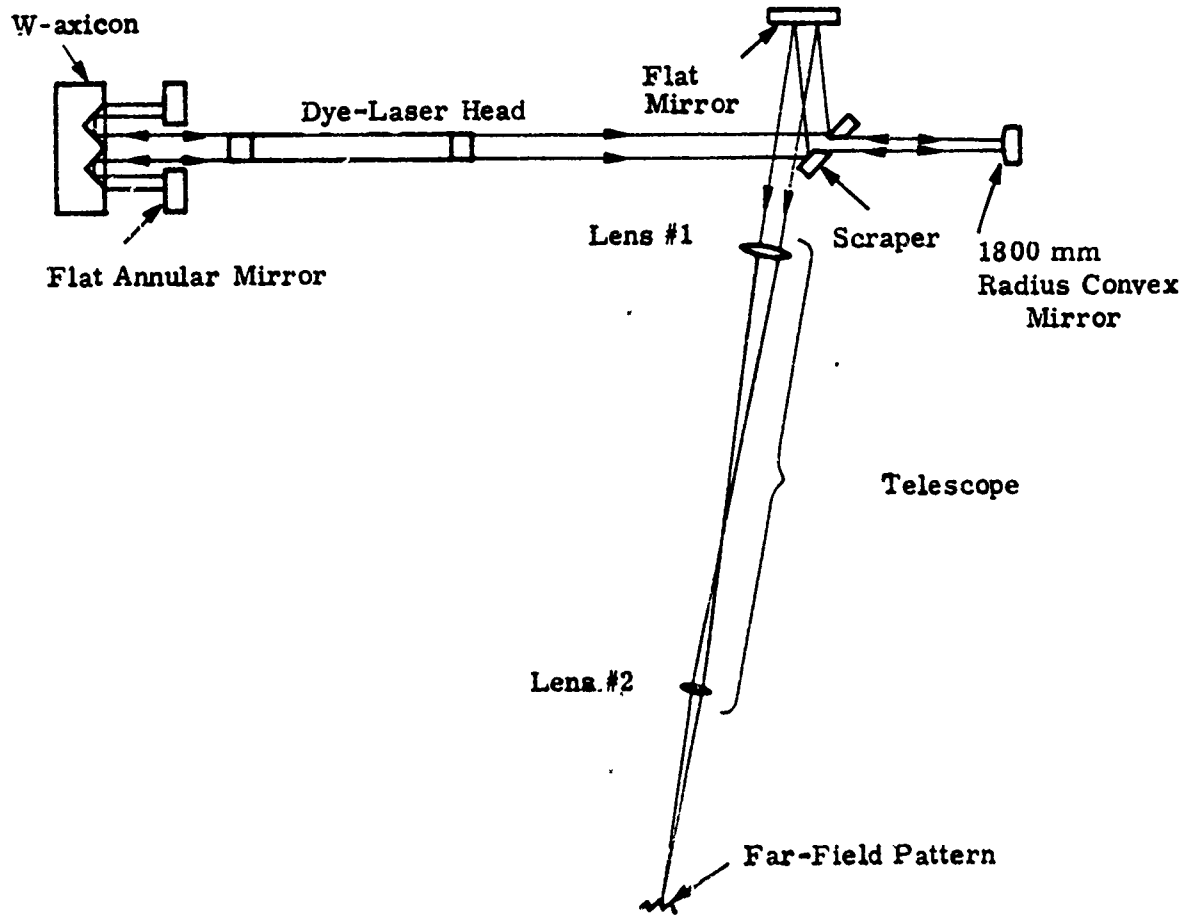

(b) Arrangement for Far-Field Observation

Figure 74. HSURIA with Convex Spherical Mirror Feedback Element, Test Arrangements for Observing Near- and Far-Field Patterns

(a) HSURIA with Corner Cube

(b) HSURIA with Convex Mirror

Figure 75. Near-Field Burn Patterns

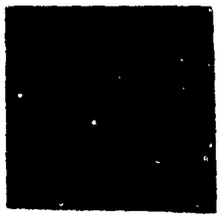

(a) HSURIA with Corner Cube

(b) HSURIA with Convex Mirror

Figure 76. Far-Field Burn Patterns

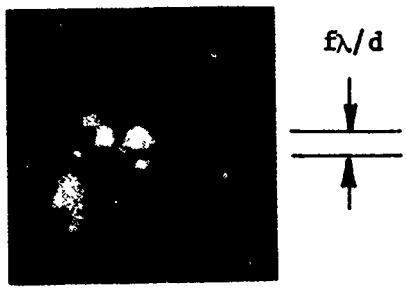

(a) HSURIA with Corner Cube

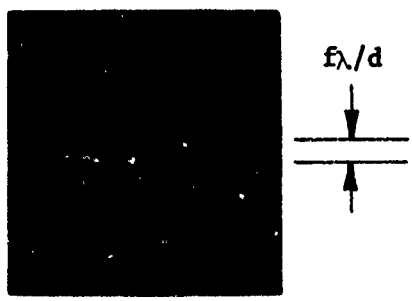

(b) HSURIA with Convex Mirror

Figure 77. Far-field Pattern Imaged on a Diffuse Surface
(f = Lens Focal Length)

of aberration is attributed to the figure quality of the W-axicon. For this reason, it was decided to make tests at a longer wavelength using an HF/DF laser, where the W-axicon figure error would be a smaller fraction of a wavelength and where the gas laser would provide better medium gain distribution.

SECTION IV

HF/DF LASER EXPERIMENTS

1. HF/DF LASER HEAD

The HF/DF laser head was subcontracted to Rocketdyne* for fabrication to Perkin-Elmer-supplied specifications compatible with the resonator optics used in the dye-laser experiments.

a. Design

The geometry of the laser head was chosen to be compatible with the dye-laser resonator optics, including the W-axicon already available for the HSURIA resonator tests. The inner dimension of the active region of the annular gas cell was therefore chosen to be 33 mm in diameter, and the outer diameter was required to be greater than 40 mm. Details of the actual geometry and construction techniques are contained in Appendix A -- Rocketdyne's final report, submitted to Perkin-Elmer, which covers design and construction of the HF/DF laser head.

Two versions of the HF/DF laser head were actually designed and delivered by Rocketdyne. The preliminary model allowed initial setup, test, and measurement of gain distribution while the second model, which required a longer construction schedule because of fabrication time involved in obtaining high optical precision windows, was being prepared.

b. Gain Distribution Test

Measurements of the gain distribution of the DF laser head were made using part of the annulus as an oscillator to probe a different amplifier region whose radial position could be varied. The oscillator provided a reference signal that could be used to remove the effects of variations in the output due to pumping energy variations and small variations in the gas mixture. Figure 78 shows the experimental arrangement for the gain measurements. The 1-mm diameter beam generated by the oscillator was amplified as

*Rocketdyne Division of Rockwell International

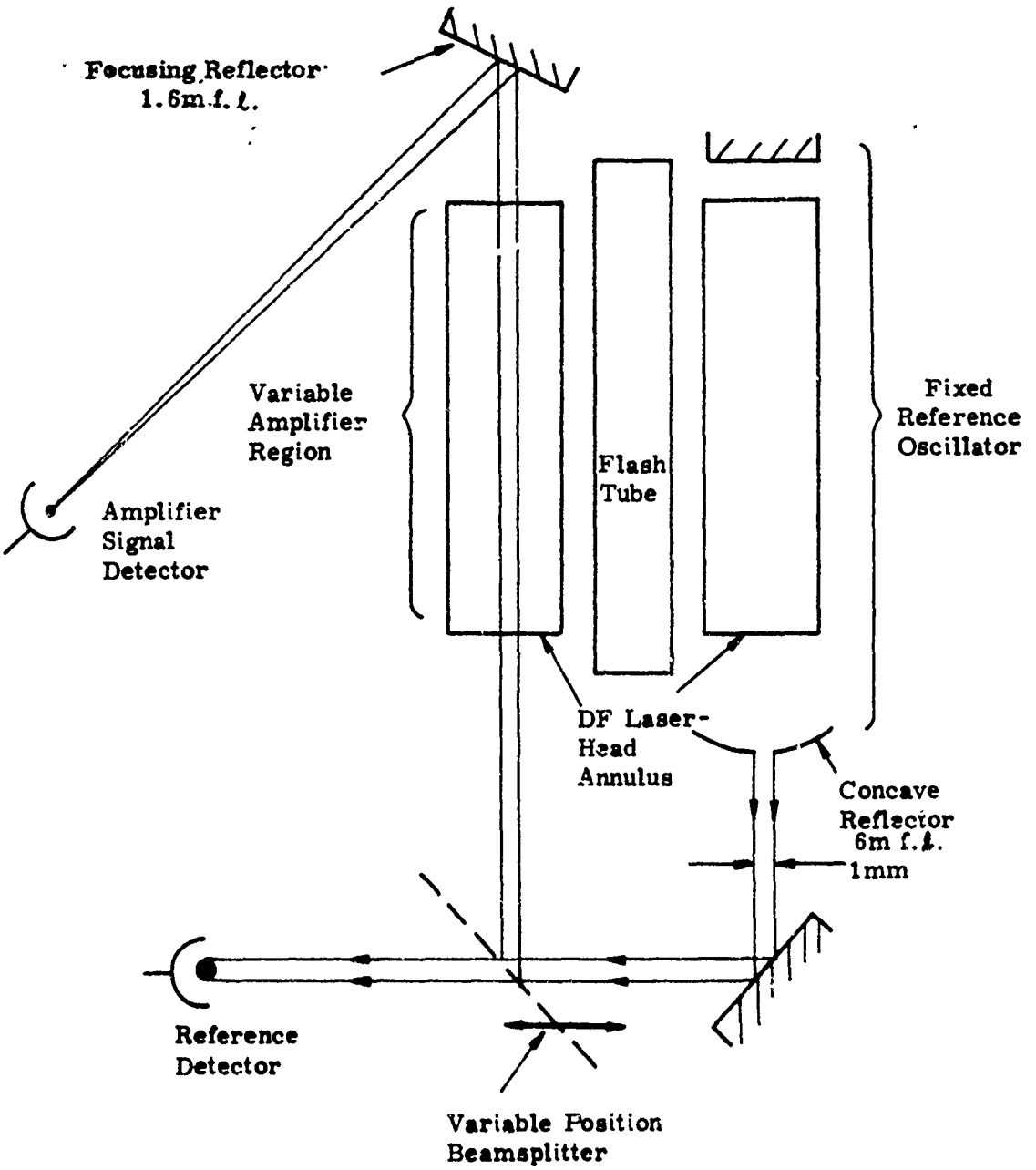

Figure 78. Test Arrangement for Measurement of DF Laser-Head Gain Distribution

it passed through the amplifier region. The distance of the amplifier region being probed, from the center of the annulus, was varied by changing the position of the beamsplitter. Pyroelectric detectors were used for both signals. The ratio of the amplified signal to the reference signal was plotted as a function of radial position, and the results are shown in Figure 79 for three different gas mixture ratios.

The gain measurements were made with the preliminary DF laser-head setup, which uses different windows and a slightly different assembly technique than the second DF laser head, which was subsequently set up for far-field measurements in the HSURIA resonator configuration. However, the gain medium dimensions are the same, and the results should apply to either head. One difference is that the preliminary head setup has glue lines, where the windows are cemented, that extend somewhat past the inner wall into the gain region; this, as well as the finite 1-mm size of the probe beam from the reference oscillator, may be responsible for the drop in gain observed in Figure 79 for positions near the inner wall.

The gain at the outer wall corresponding to a line that will fold into the center of the axicon in the HSURIA resonator configuration is approximately 10 percent of the maximum gain observed. This represents more than an order-of-magnitude improvement over the gain distribution observed with the dye-laser head and was adequate to obtain lasing with the designed HSURIA resonator configurations.

2. HSURIA RESONATOR TESTS WITH THE HF/DF LASER

a. Alignment Procedure

The DF laser was set up in the HSURIA arrangement with a reflective corner cube as shown in Figure 6. The alignment procedure is described in the following paragraphs.

(1) The laser head windows are aligned parallel to each other and perpendicular to the laser head tube walls using a Brunson alignment telescope [Figure 80(a)].

Total Head Pressure = 150 Torr
Partial Pressure of N_2F_4+D_2 = 1 Torr

Run #	Relative Flowmeter Readings*		
	N_2F_4	D_2(8%)He(92%)	He
1	58	75	950
2	91	84	1000
3	30	84	1000

*Matheson Flowmeter #600 (Not Calibrated For Absolute Readings With Gases Used)

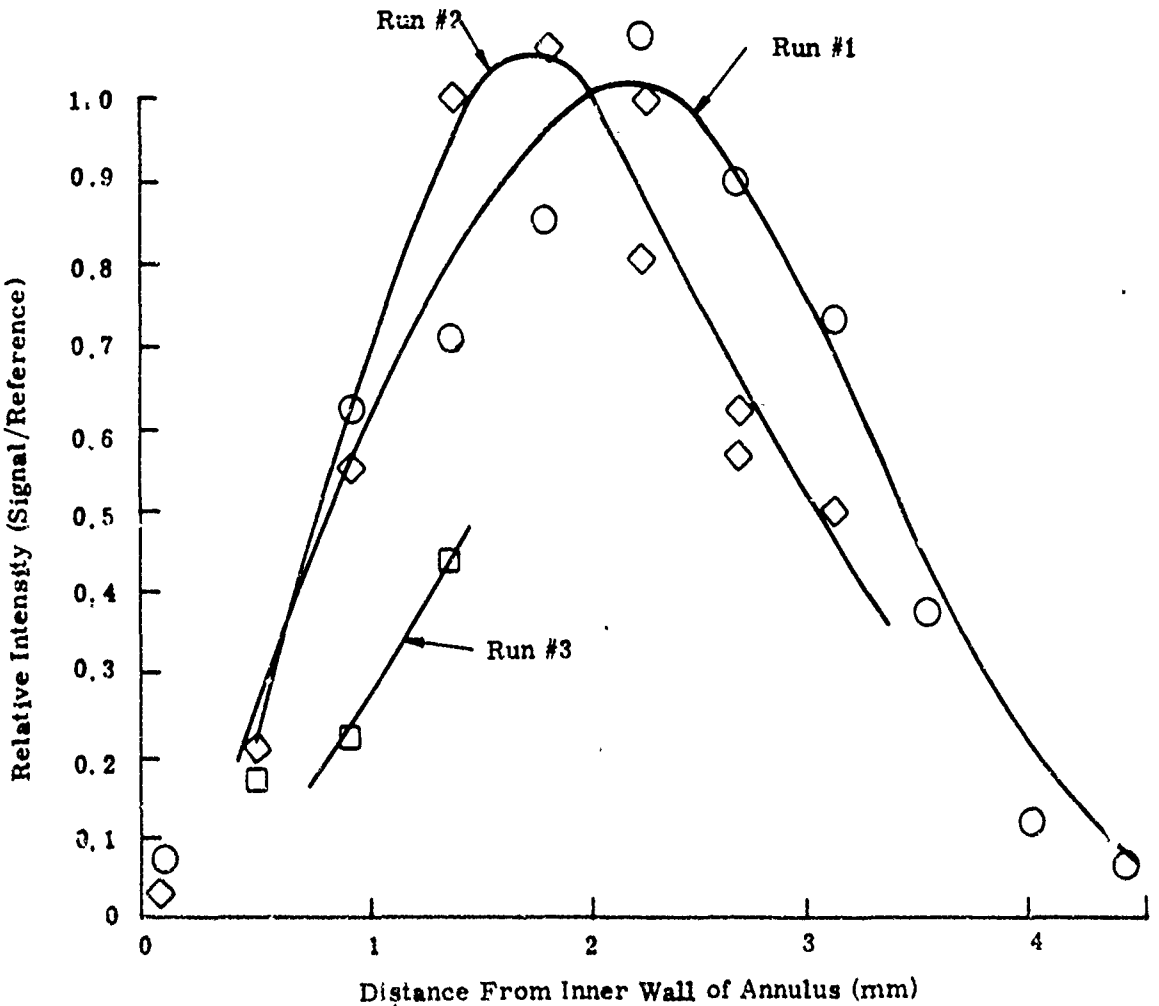

Figure 79. Radial Gain Distribution for DF Laser Head

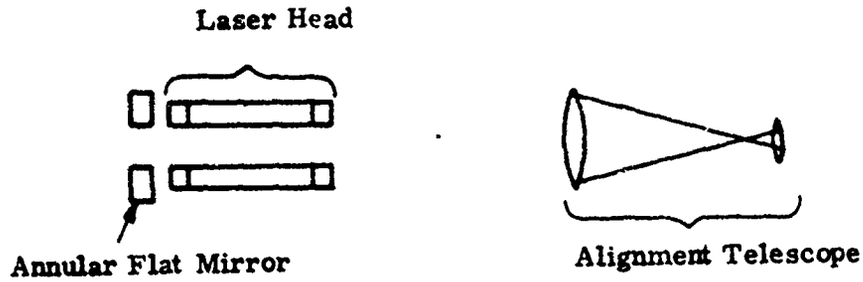

(a) Laser Head Aligned to Alignment Telescope

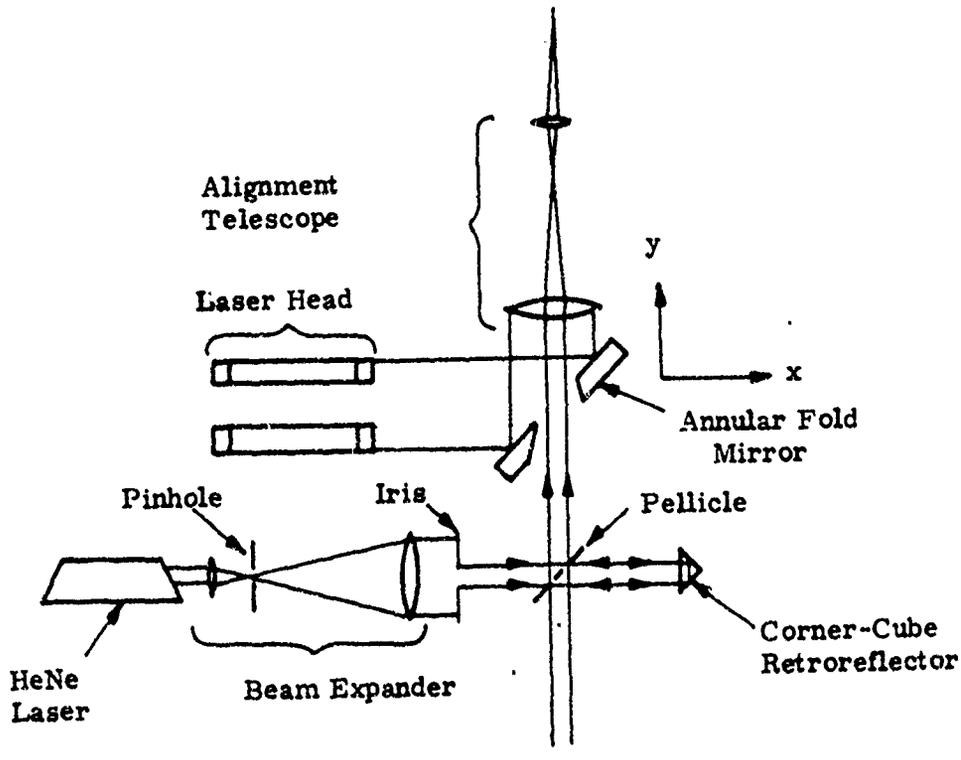

(b) HeNe Reference Beam Aligned to Laser Head

Figure 80. Steps in Alignment Procedure of HF/DF Laser HSURIA (Sheet 1 of 3)

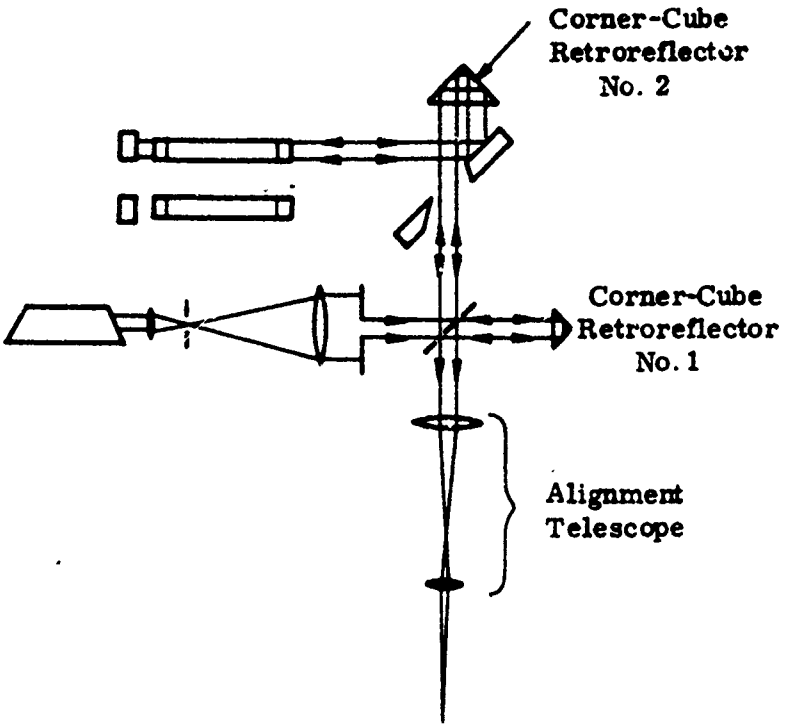

(c) Annular Flat End Mirror and Fold Mirror Aligned to HeNe Reference Beam

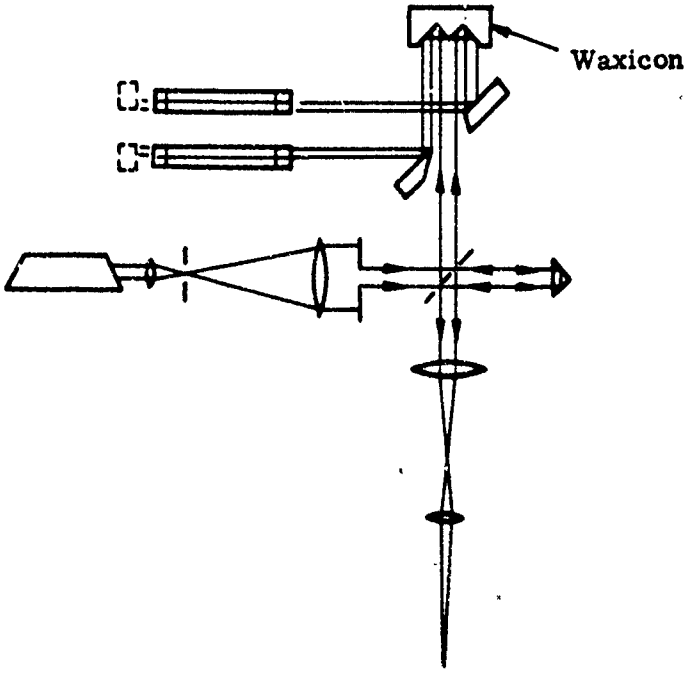

(d) W-axicon Aligned to HeNe Reference Beam

Figure 80. Steps in Alignment Procedure of HF/DF Laser HSURIA (Sheet 2 of 3)

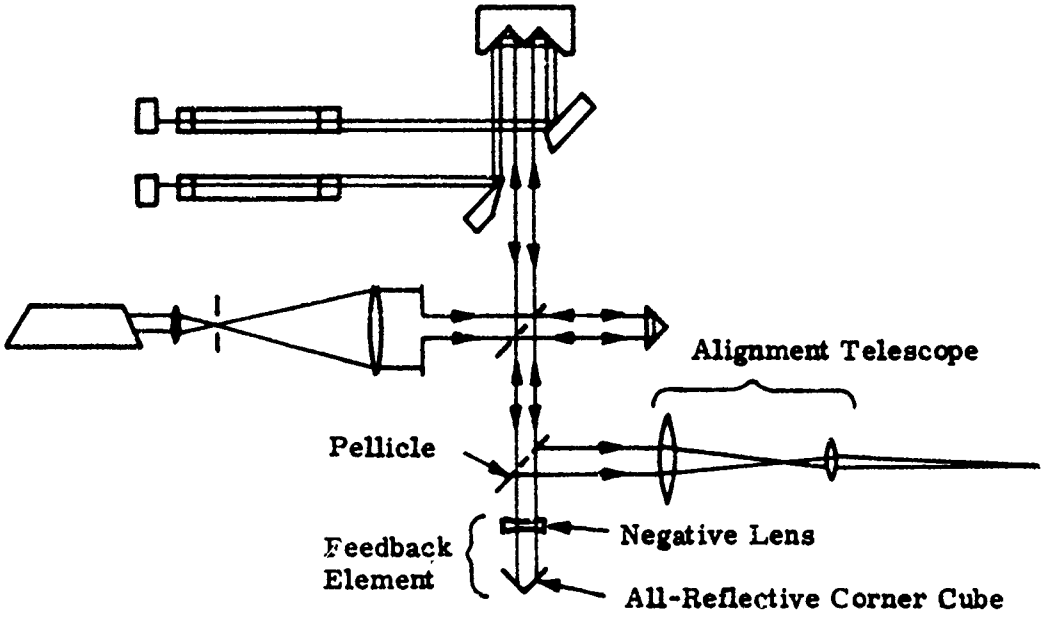

(e) Feedback Element Aligned to HeNe Reference Beam

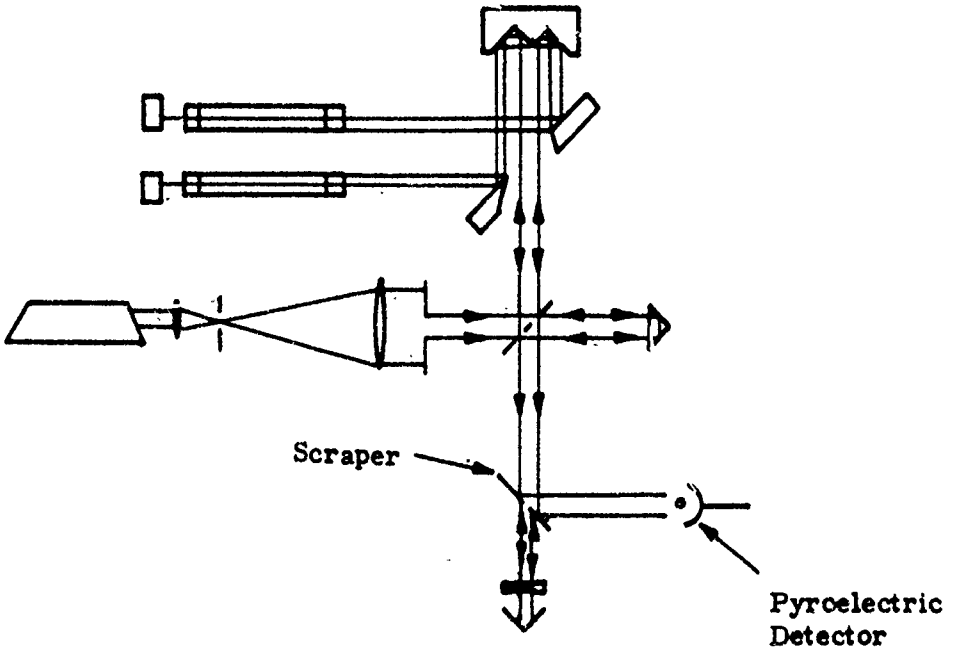

(f) Scraper Aligned to HeNe Reference Beam

Figure 80. Steps in Alignment Procedure of HF/DF Laser HSURIA (Sheet 3 of 3)

(2) A collimated HeNe beam was set up parallel to the bench at the same height as the axis of the laser head [Figure 80(b)]. An alignment telescope was set up on the axis of the HeNe reference beam. The fold mirror was aligned laterally in the x direction so that its aperture was centered in the alignment telescope and was adjusted in tilt and in the y direction so that the images of the two laser-head windows, observed in the alignment telescope after reflection off the fold mirror, were both concentric with the aperture of the fold mirror.

(3) A corner-cube retroreflector (No. 2) was used [Figure 80(c)] to monitor fine adjustment of the fold mirror tilt, which was adjusted so that reflection of the HeNe beam from the laser head windows coincided with the reference beam from corner cube No. 1, as observed in the alignment telescope.

(4) With the annular end mirror temporarily removed, the W-axicon was put in place [Figure 80(d)] and aligned in tilt and translation to give a uniform annular HeNe wavefront exiting the laser head.

(5) The W-axicon tilt was precisely adjusted to align the far-field pattern of the beam reflected from the laser-head windows with the far-field pattern of the reference beam from the corner-cube retroreflector.

(6) The annular mirror was replaced and adjusted so that the far-field pattern of the HeNe beam reflected from it coincided with the reference far-field pattern from the corner cube.

(7) The feedback element was added to the resonator, and a second pellicle was inserted to observe the reflected beams from the feedback element [Figure 80(e)]. The near-field image of the beam observed through a telescope allowed the lateral alignment of the feedback corner cube to be checked.

The far-field pattern was used to adjust the tilt and lateral position of the negative lens in front of the corner cube, or of the convex mirror in the alternate resonator configuration.

(8) The scraper was aligned in the beam so that the HeNe light reflected from the reference beam was a round, uniform annulus at the scraper design angle [Figure 80(f)]. A detector was centered on the HeNe output beam, and the pellicles were removed from the resonator.

b. Test Configuration

Figure 81 shows the diagnostic arrangement for making measurements of the intensity distribution in the far field. Integrated irradiance as a function of diameter at the far-field beam focus (energy in the bucket) was determined from the ratio of the signal, as measured through various pinhole apertures, to the total energy in the beam, as measured at a reference detector. Figure 82 is a photograph of the laser resonator and test arrangement.

The reference detector received a part of the beam that had been extracted from the main beam by means of a beamsplitter. Both detectors were pyroelectric. The signal-to-reference ratios obtained were normalized to the signal-to-reference ratio observed without the pinhole mask. The pinhole diameters used in the variable pinhole mask were 13, 20, 30, 40, 50, 60, 70, and 80 mils or 0.65, 1.0, 1.5, 2.0, 2.5, 3.0, 3.5, and 4.0 times the calculated diameter of the first dark ring in the diffraction-limited Airy pattern at the beam focus.

The diagnostic arrangement was aligned in focus by:

(1) Stopping down the diameter of the HeNe alignment reference beam to less than the diameter of the scraper hole so that the beam had to make a double pass through the cavity and be diverged by the feedback element in order to be seen at the output of the scraper.

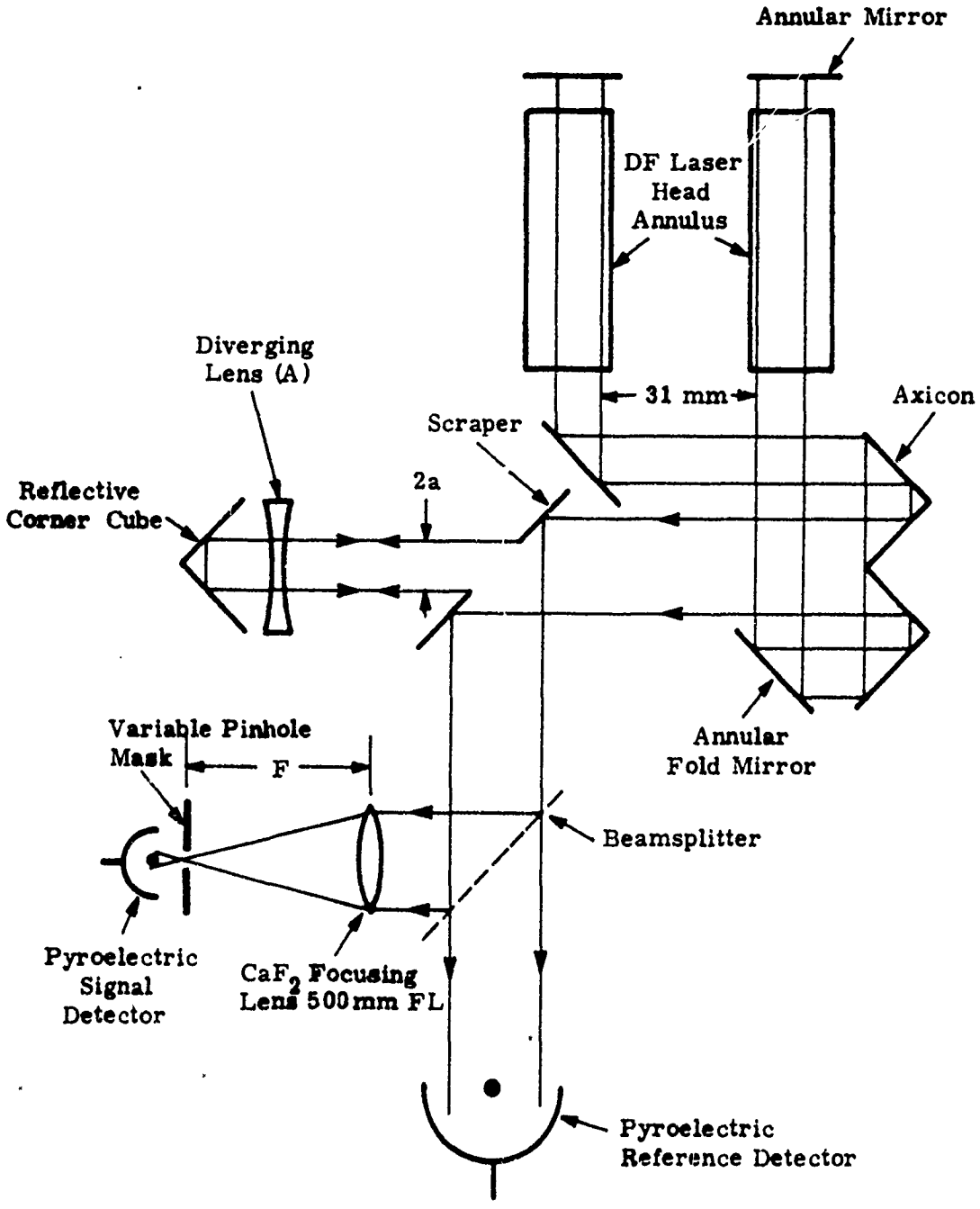

Figure 81. DF Laser HSURIA with Corner-Cube Experimental Arrangement for Measurement of Energy in Far-Field

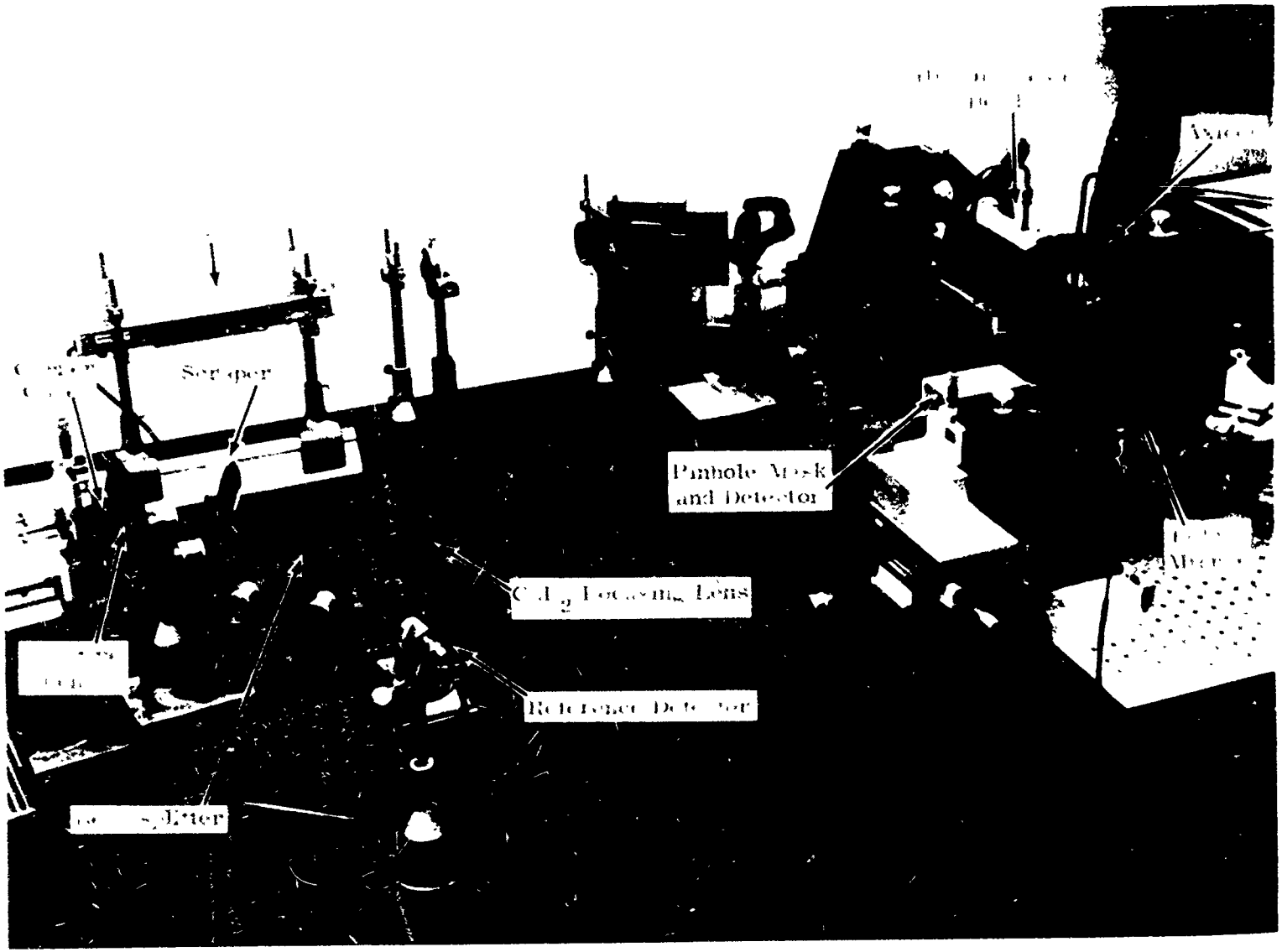

Figure 82. HF/DF Laser HSURIA Diagnostic Arrangement

(2) Observing the focus of the HeNe alignment beam at the variable pinhole mask with a microscope to determine the distance between the 50-cm CaF_2 lens and the pinhole mask for best focus in the visible.

(3) Adjusting the distance between the pinhole mask and the CaF_2 lens to correct for the difference in refractive index of CaF_2 between 6328 Å and 3.8 μm.

(4) Taking energy-in-the-bucket measurements with the pinhole at several different distances from the CaF_2 lens to determine the position of optimum focus.

The HF/DF laser output was quite variable so that the reference detector was a necessity for canceling at least some of the effects of the variations. Even with the reference detector, the variation in the ratios of the signal to reference for a given pinhole aperture was larger than desired so that many readings were required at each setting to provide a good average. The laser output decreased and the variation between pulses increased if the time between pulses was decreased so that the gases in the laser head had less time to be replaced. A time in excess of 1 minute was required between pulses to allow the spent gases to be flushed out and replaced. Since energy-in-the-bucket measurements required as many as 100 pulses per run, this increased the time required to obtain data.

The flashtube pumping energy varied as the flashtube aged. The xenon flashtubes required quite a high voltage to break down, and the breakdown voltage became higher as a function of the number of times the tube was flashed. Consequently, the lifetime of some of the tubes was only several hundred flashes. Flashtube replacement required some realignment, and in some cases, diagnostic runs that had been interrupted by tube failure had to be repeated.

The output of the two detectors was displayed simultaneously on a storage oscilloscope. A photograph of a typical oscilloscope display is shown in Figure 83. The detectors response is too slow to resolve the pulse, but the relative amplitude of the two signals could be inferred from the maxima of the two traces. The lower trace is the inverted reference.

Pinhole Throughput
Detector Output
(2 mV/cm)

Reference Detector
Output (Inverted)
(10 mV/cm)

100 μs/cm ⟶

Figure 83. Storage Oscilloscope Display of Detector Output for Energy-in-the-Bucket Measurements

c. Test Results

Three different combinations of resonator length, beam magnification, and output coupling for the resonator arrangement shown in Figure 81 were tried, as listed in Table 2. The three combinations were derived from the following formulas.

$$A = N_{eq} \frac{2\lambda}{a^2} \tag{1}$$

$$L = \frac{-2/f}{A^2 - 1/f^2} \tag{2}$$

$$M = C + \sqrt{C^2 - 1}, \text{ where } C = 1 - \frac{L}{f} \tag{3}$$

where N_{eq}, a, L, and M are as defined on page 83 in Section III. Values for available scraper diameters and diverging lens focal lengths were plugged into Equations (1), (2), and (3) along with the desired 1/2 integral values for the Fresnel number to obtain the resonator cavity length and beam magnification.

The results of energy-in-the-bucket measurements for configuration A are shown in Figure 84. This was the first configuration tried, and no attempt was made to optimize the focus. Two measurement runs are shown; the system was realigned between runs.

With configuration B, lasing was extremely weak--even with 9 kV (800 J) into the flash excitation lamp--apparently because of the output coupling level with the 3.2 magnification being used. It was not possible to obtain meaningful measurements with the signal level available with this configuration.

The results of energy-in-the-bucket measurements for configuration C are shown in Figure 85. The curve for the analytically derived performance of a diffraction-limited system with the same obscuration is shown with each set of curves for energy-in-the-bucket measurements to allow a comparison of actual performance with the ideal. Each point on the experimental curves is the average of several readings, and the standard deviations are tabulated on

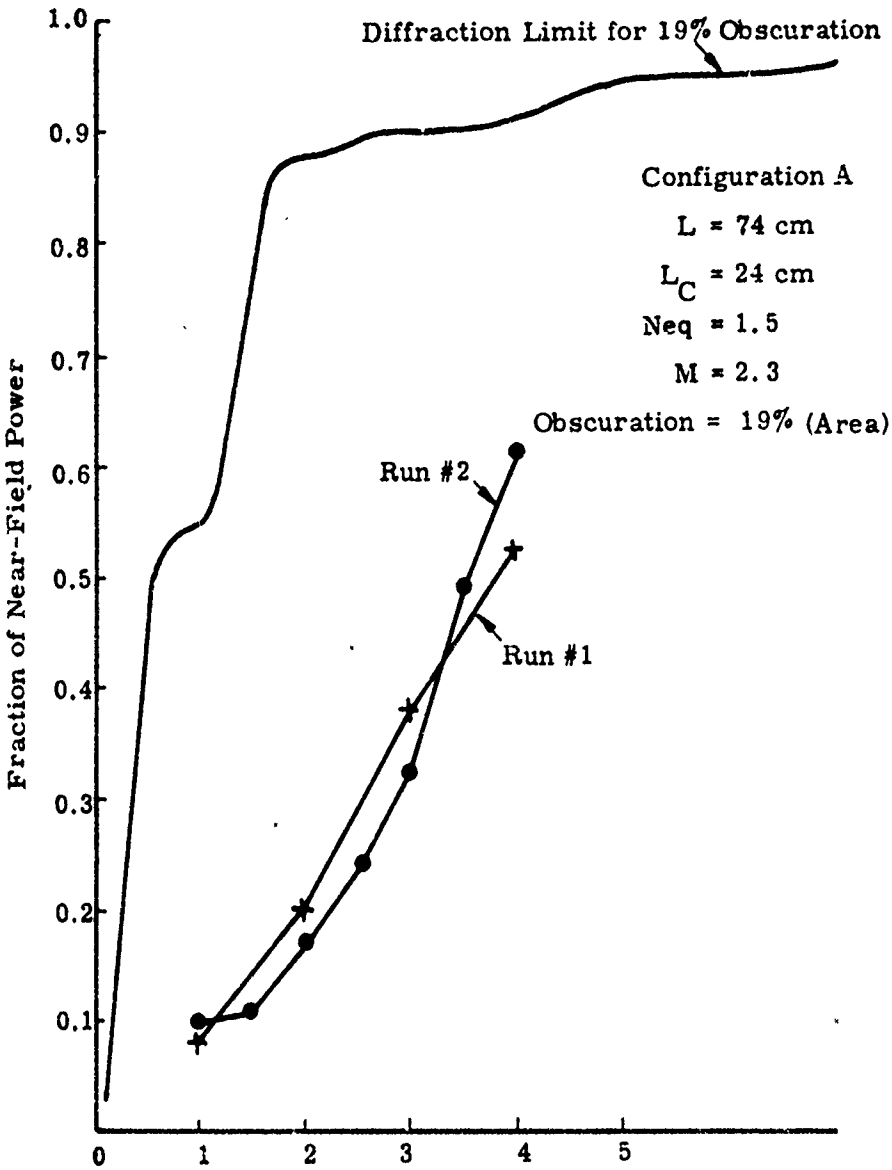

	θ =	1.0	1.5	2.0	2.5	3.0	3.5	4.0
Run #1	Mean (Norm) =	0.082		0.202		0.380		0.527
	Stand. Dev ± =	0.007		0.026		0.036		0.054
Run #2	Mean (Norm) =	0.094	0.103	0.165	0.233	0.324	0.498	0.603
	Stand. Dev ± =	0.004	0.012	0.008	0.017	0.037	0.035	0.066

Figure 84. Integrated Irradiance as a Function of Diameter at the Far-Field Beam Focus for 74-cm Resonant Cavity

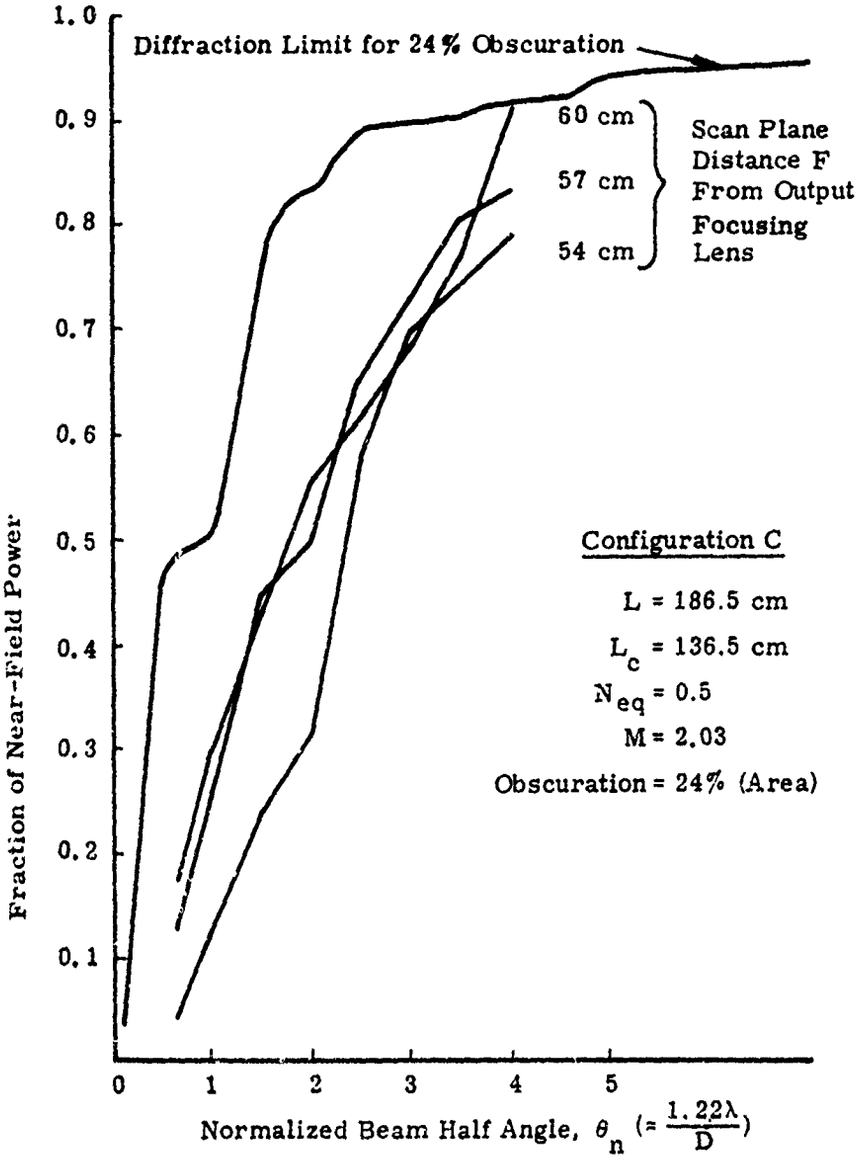

	θ =	0.65	1.0	1.5	2.0	2.5	3.0	3.5	4.0
Stand. Dev. ±	F = 54 cm	0.004	0.016	0.016	0.054	0.036	0.071	–	0.063
	F = 57 cm	0.010	0.044	0.061	0.055	0.054	0.093	0.055	0.056
	F = 60 cm	0.045	0.073	0.139	0.123	0.033	0.104	0.101	0.174

Figure 85. Integrated Irradiance as a Function of Diameter at the Far-Field Beam Focus for 186.5-cm Resonant Cavity (Superposition of measurements taken at three different positions near the focal plane)

each figure. Figure 86 shows a profile scan of the far-field pattern at best focus for configuration C, obtained by scanning the 0.013-inch pinhole across the spot diameter.

d. Conclusions

The far-field pattern obtained at best focus with configuration C begins to approach the ideal diffraction-limited performance analytically predicted. However, it was relatively difficult to extract data from the HF/DF laser test bed because the output was pulsed and variable and was not visible. Further investigation of the HSURIA configurations is therefore recommended, but not with the HF/DF laser.

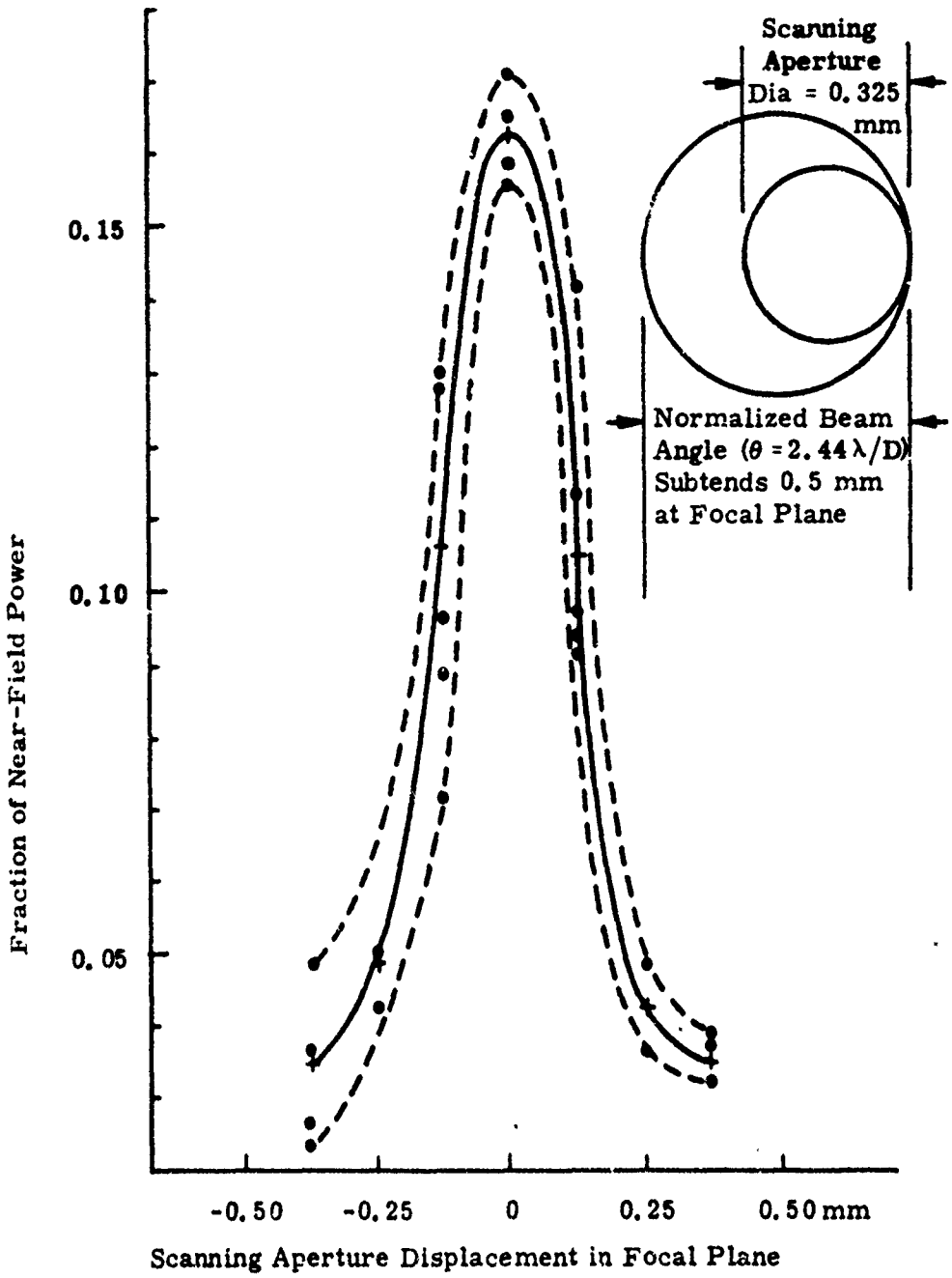

Figure 86. Intensity Profile Obtained by Scanning a 0.325-mm Diameter Aperture Across the Far-Field Pattern at 57 cm from the Output Focusing Lens

SECTION V

SUMMARY AND CONCLUSIONS

Several annular mode volume resonator experiments were performed. The spherical mirror (converging wave) resonator was tested using a dye-laser annular gain medium and results were at variance with the geometric model of Chodzko (Ref. 2). Several configurations of the half-symmetric unstable resonator with internal axicon (HSURIA) were tested using both visible (dye medium) and IR (deuterium fluoride) gain cells with pulsed flash lamp excitation. Visible wavelength results show poor beam quality, which appears to be attributable to the poor optical quality of the W-axicon. The IR experiments yield beam quality better than 2X diffraction limited with no evidence of higher order modes (based upon far-field profile scans).

Further investigation of the HSURIA configurations is recommended but not necessarily with the HF/DF laser test-bed which was inefficient in obtaining data. Recent advances made with a xenon laser test-bed operating continuously at 3.5 μm indicate that this would be a better medium for further investigations.

REFERENCES

1. H.W. Furumoto and H.L. Ceccon, "Optical Pumps for Organic Lasers," Appl. Opt. 8, 1613 (1969).

2. R.A. Chodzko, S.B. Mason, and E.F. Cross, "Annular Converging Wave Cavity," SAMSO-TR-76-115 (June 1976).

APPENDIX A

HF/DF ANNULAR LASER HEAD (ROCKETDYNE FINAL REPORT)

by

J. Novak and G. Simpson

ABSTRACT

Two versions of an annuiar HF/DF flash-pumped laser head were designed, constructed and delivered to Perkin-Elmer Corporation, Electro-Optics Division, along with the required support systems. Both versions use a linear xenon flash, 12-inch arc length, 7-mm bore, positioned axially in a 2-inch inner diameter cylinder, for photolysis of the N_2F_4:H_2/D_2:He mixture. One version is made of quartz tubing and uses stationary CaF_2 windows (1 λ visible), and the other is constructed of a stainless-steel cylinder and has adjustable CaF_2 ($\lambda/10$ visible) windows. Both versions passed acceptance testing easily, the criterion being demonstration of laser output using a 50% outcoupler in a plane-parallel resonator.

INTRODUCTION

This is a final report for Subcontract #21910PT from the Perkin-Elmer Corporation, Electro Optics Division, let to Rocketdyne for the construction of an HF/DF laser head that produces a beam having an annular shape. The most important requirements placed on this annular beam are that it exhibit a smoothly-varying radial intensity distribution and a uniform azimuthal output, and that the gain length be sufficient to produce laser output when using a 50% outcoupler. The RFP stipulated that this be a flash-photolysis device because the prime contractor felt that this is the best means to achieve radial and azimuthal intensity uniformity.

It should be stated here that it was requested of and agreed to by Rocketdyne that this item, plus the required support systems, be designed, fabricated, tested and delivered to Perkin-Elmer in a period of six weeks from go-ahead. This time constraint necessitated certain compromises between delivery on schedule and performance of the overall system, the specifics being self-explanatory as the text proceeds.

A large number of HF/DF flash-photolysis systems have demonstrated laser output exhibiting varying degrees of efficiency and practical operating requirements (Refs. 1-3). The system selected by Rocketdyne is the N_2F_4:H_2/D_2: He, and it was chosen for a number of reasons. First of all, it is a "clean" system, requiring no cleaning or bake out of solid reaction products which can adhere to the inside of the laser head and windows. N_2F_4, while certainly not benign, is less hazardous and corrosive than F_2, and far more acceptable from the safety standpoint. N_2F_4 is a versatile fluorine atom source, allowing the use of CH_4, C_2H_4, CH_3I and others, as well as H_2/D_2 to produce working

1. C.E. Wiswall, D.P. Ames and T.J. Menne, "Chemical Laser Bibliography," IEEE Quant. Elec., Vol. 9, p. 181 (1973).
2. L.E. Brus and M.C. Lin, "Chemical HF Lasers from Flash Photolysis of various N_2F_4 + RH Systems," J. Phys. Chem., Vol. 75, p. 2546 (1971).
3. T.D. Padrick and G.C. Pimentel, "Hydrogen Fluoride Elimination Chemical Laser from N,N-Difluoromethyl-amine," J. Chem. Phys., Vol. 54, p.720 (1971).

laser systems. The absorption bands of N_2F_4 and NF_2 lie in the 2000-2800 Å region, making it an efficient source of fluorine atoms when photolyzed by a xenon flash lamp.

Having selected the N_2F_4:H_2/D_2:He system, the question of the best pumping configuration for uniform output was approached. The possibilities include the use of a linear xenon flash lamp placed axially in the 2-inch outer diameter laser head (Figure A-1); the use of a helical xenon flash lamp having an inner diameter of 2 inches, placing the laser head inside the helix; or the use of a cylindrical xenon flash lamp having ring electrodes, with the lamp placed coaxially over the outer diameter of the laser head with a gap of 4 to 6 mm between the walls.

During the design stages of this contract, the ring-electrode configuration was tested at another Rockwell facility, since a working device of this type was available for use, and it was found likely that the flash uniformity from this type of device would be inconsistent, both from shot to shot, and from one azimuthal region to another. The use of a helical lamp remains a viable alternative, having the advantage that a high flux is available for N_2F_4 photolysis, but having the disadvantages of long procurement times for a necessarily custom lamp and of high operating voltage, > 20 KV, due to the extremely long arc length. The linear xenon lamp configuration was therefore chosen and constructed having the dimensions shown in Figure A-1.

It was requested by Perkin-Elmer after the start of the contract that the laser head be constructed so that the windows could be aligned parallel to each other within 30 arc-seconds. This necessitated the design of a second laser head shown in Figure A-2. It is essentially the same as that shown in Figure A-1, except that the overall length required shortening to accommodate the already-purchased flash lamps, and that the outer tube is made of stainless steel instead of quartz. The windows in this configuration are adjustable, rather than rigid as in the quartz configuration, by virtue of a set-screw actuated pressure ring on each window and the compressibility of the "O" rings. Wilson seals are used to seal the axial flash lamp envelope.

The mechanism of operation of the N_2F_4:H_2/D_2 system is thought to proceed via the following reactions (Ref. 2):

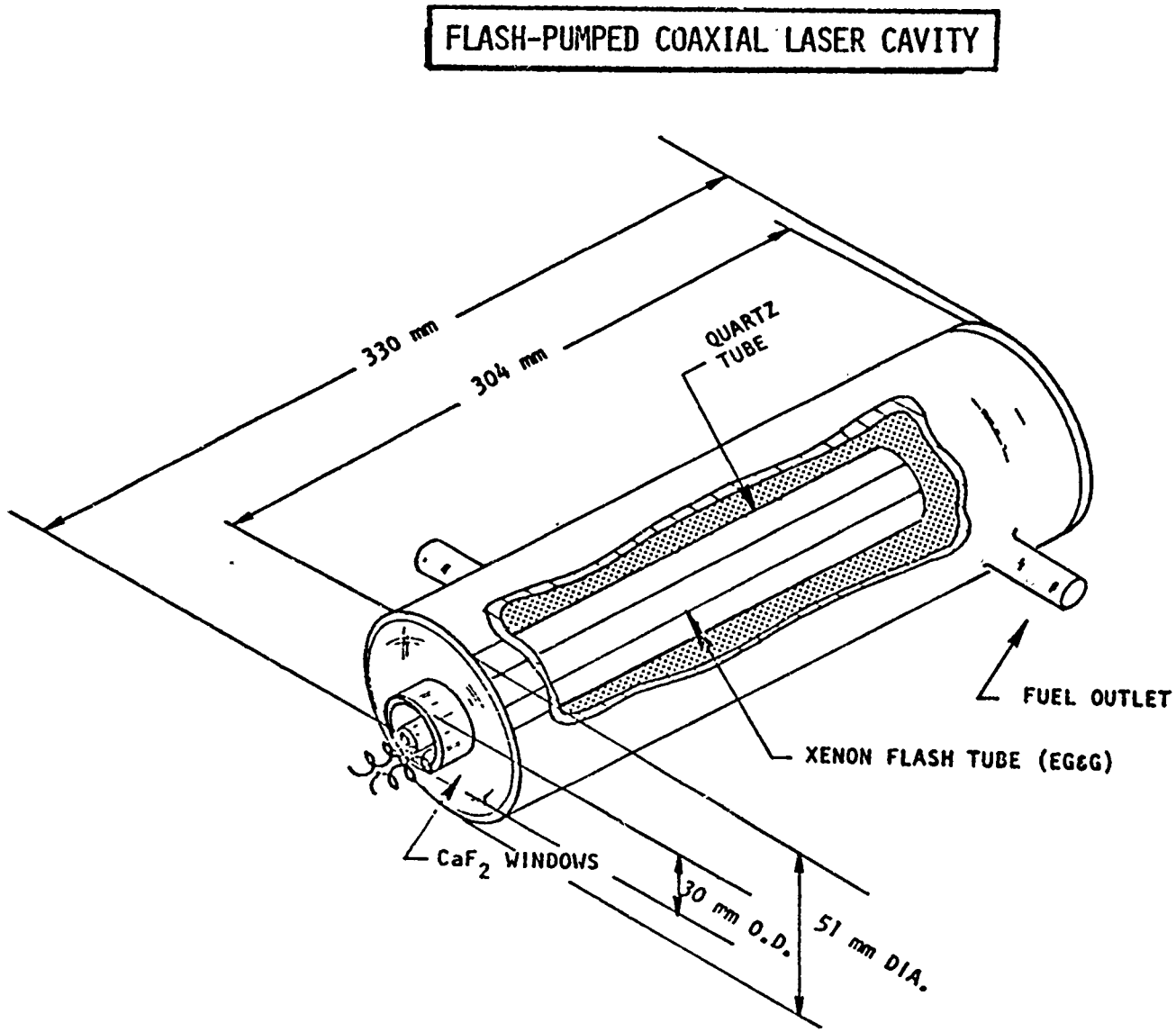

Figure A-1. Quartz Configuration

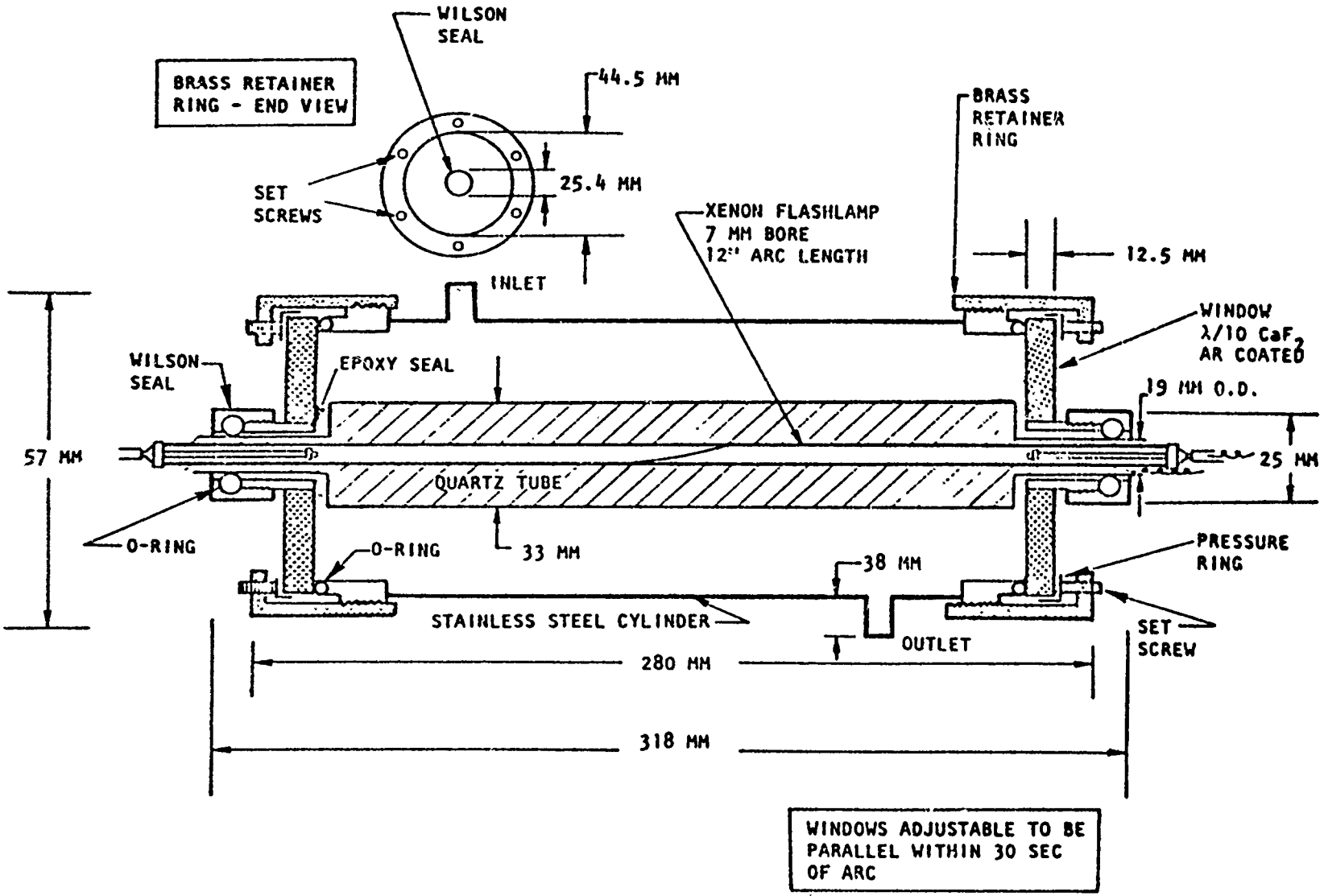

Figure A-2. Stainless Steel Configuration

$$N_2F_4 \rightleftharpoons 2NF_2 \qquad (2\% \text{ at } 300^\circ K)$$

$$N_2F_4 \xrightarrow[(2000\ \text{Å})]{h\nu} N_2F_3 + F$$

$$NF_2 \xrightarrow[(2600\ \text{Å})]{h\nu} NF + F$$

$$2NF \longrightarrow N_2 + 2F$$

$$F + N_2F_4 \longrightarrow NF_3 + NF_2$$

$$NF + N_2F_4 \longrightarrow NF_2 + N_2F_2 + F$$

$$2F + M \longrightarrow F_2 + M$$

and including H_2/D_2 in the system,

$$F + H_2 \longrightarrow HF^* + H \qquad (HF^* \equiv HF(\nu),\ \nu = 1,\ 2,\ 3)$$

EXPERIMENTAL

DESCRIPTION OF COMPONENTS

The HF/DF Annular Laser Head System consists of the quartz (Figure A-3) or stainless-steel laser head, including a 12-inch arc length 7-mm bore linear xenon flash lamp supplied by ILC; the flash lamp power supply, a Model 472 from Xenon Corporation, rated at 10 kV, 200-2000 J; and a self-contained portable gas-handling console, containing flow-meters, pressure gauges, regulators, gas cylinders and control valves (Figures A-4 and A-5).

Gas handling components were purchased from Matheson: #600 and #610 rotameters with stainless-steel construction and Viton seals, regulators for He, H_2/D_2 and N_2F_4. Valves are of three types: Whitey stainless-steel "shut-off" valve, with a kel-F seat for helium; two Monel Control Components valves for precise metering of N_2F_4 and H_2/D_2; and one all stainless-steel Whitey metering valve for control of system pressure. The pressure gauge is a 0 to 200 mm Wallace and Tiernen.

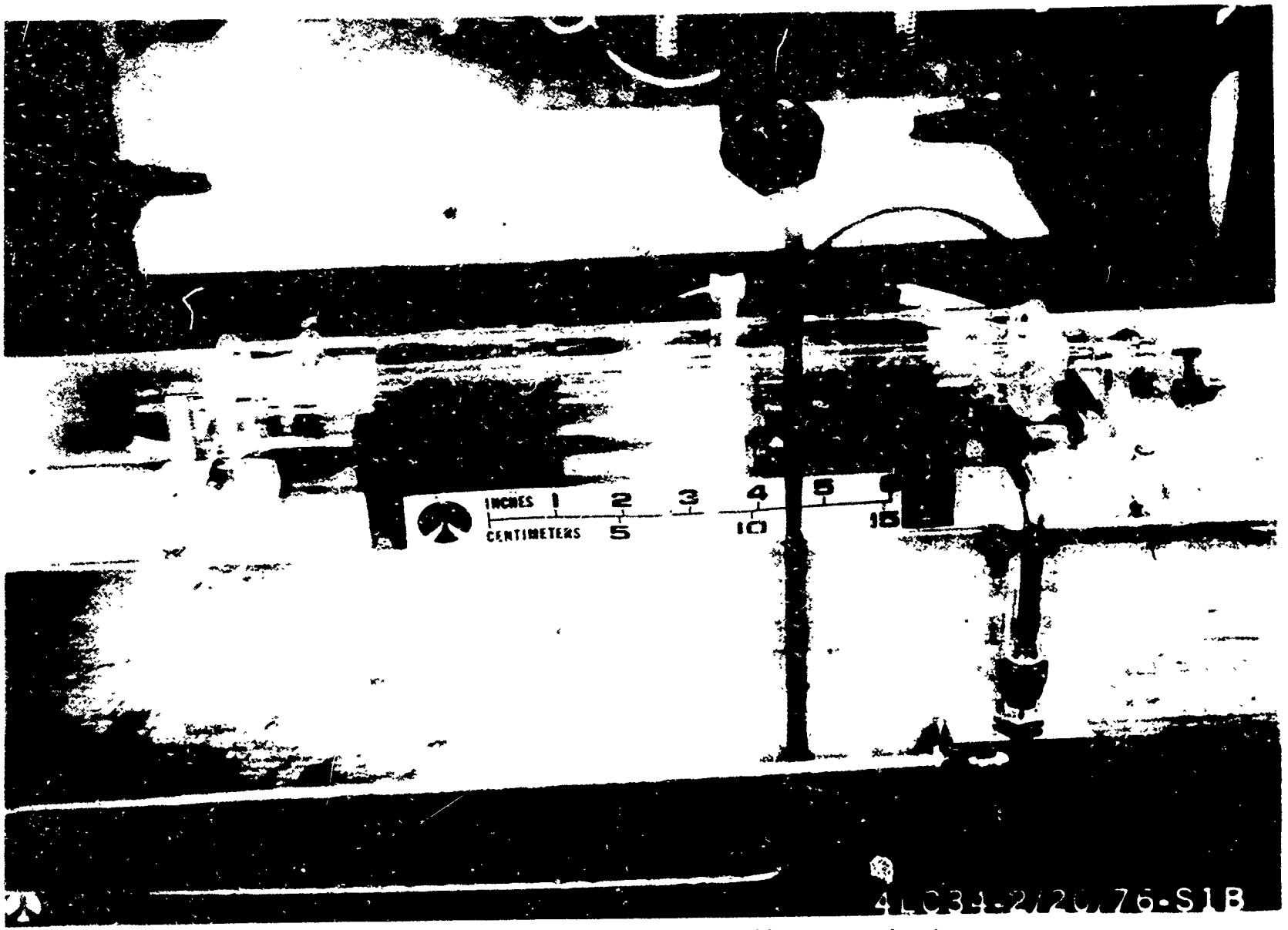

Figure A-3. Quartz Laser Head Installed at Rocketdyne

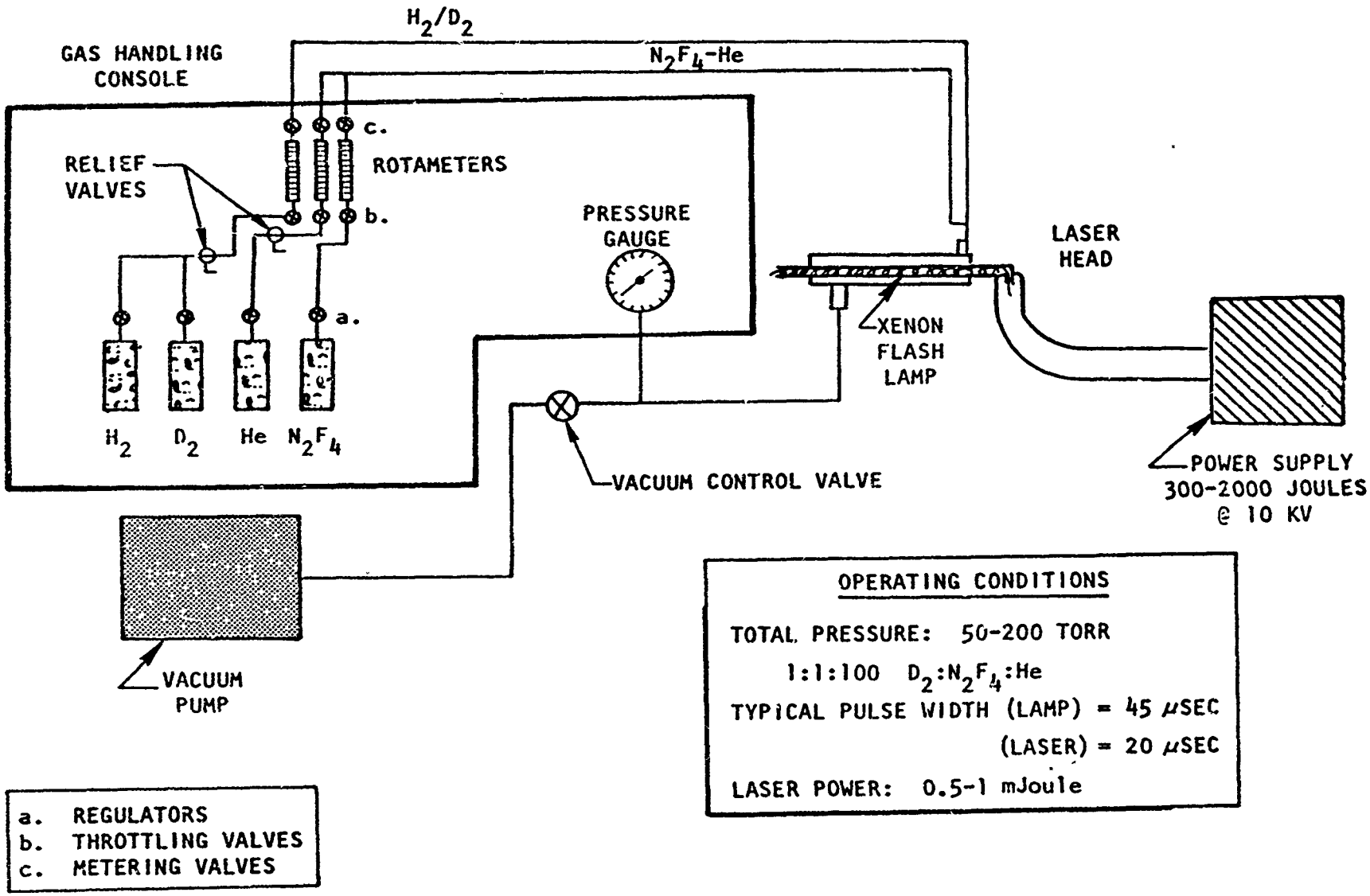

Figure A-4. Schematic of HF/DF Laser System

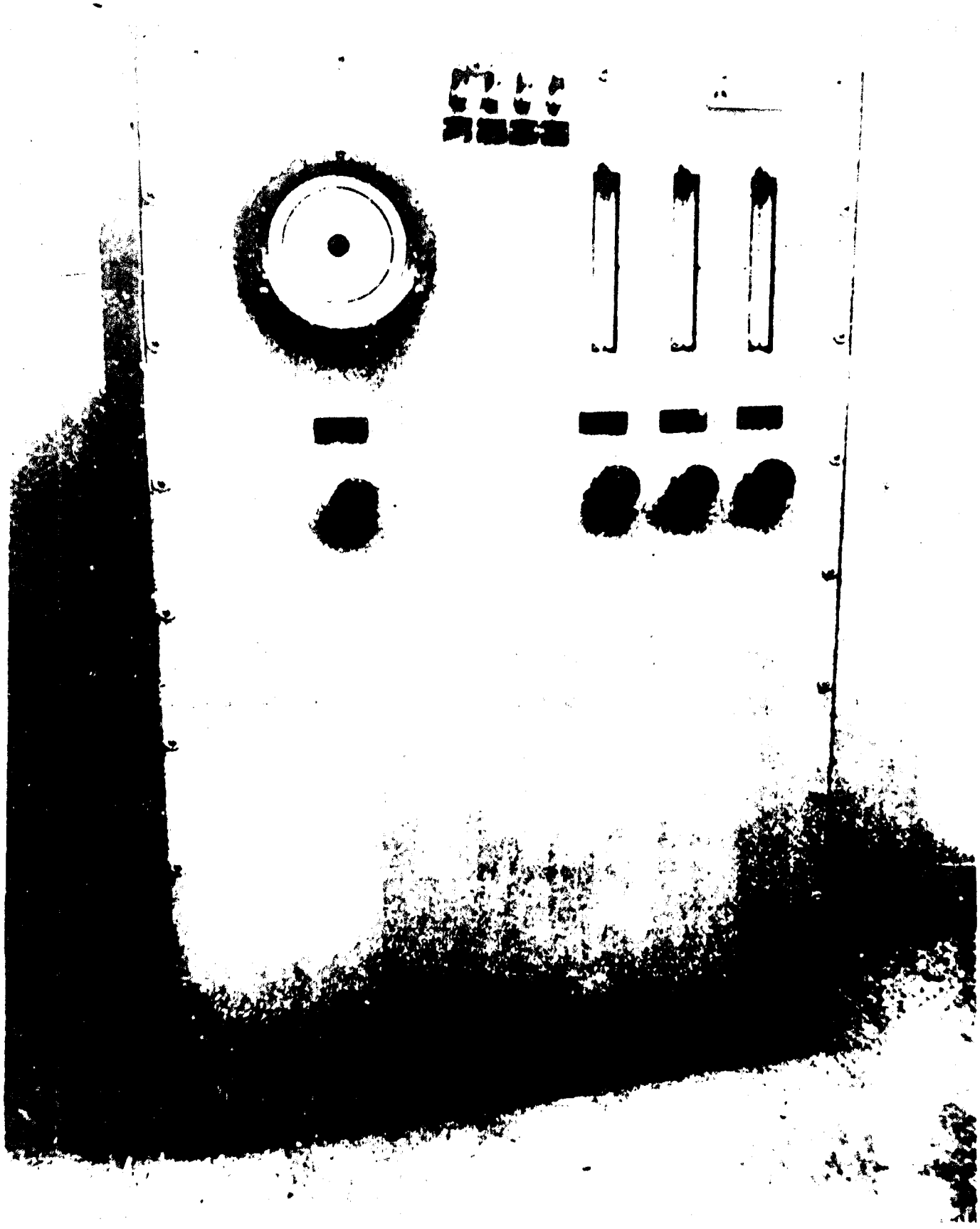

Figure A-5. Gas-Handling Console (Complete with appropriate gas cylinders)

Shortly after receiving the flash lamp power supply, inconsistent firing of the lamp occurred as an apparent failure of the ignitron. To remedy this an EG & C series-injection transformer was placed in series with the thyratron, providing a high-voltage pulse to aid in ignitron breakdown. This solved the problem; however, the time required for the modification greatly limited experimental evaluation of the laser head because of the tight delivery schedule.*

Initial experiments were performed with the quartz laser head, 12-inch long, 42-mm ID, with a 19-mm OD center tube. The experimental arrangement is shown in Figures A-3 and A-6. The windows were 10 λ(visible) calcium fluoride, 2 inches in diameter, 1/4 inch thick, cored to 19 mm and cemented on the quartz cylinder with G. C. Electronics Epoxy, #347. The windows were adjusted for parallelism to ± 1 arc-minute with the reflections of an alignment laser while the epoxy was curing.

A second laser head was designed, constructed, and delivered to Perkin-Elmer which accommodates $\lambda/10$ calcium fluoride windows which are 2 inches in diameter and 1/2 inch thick. This head has a gain region 9 inches long while that of the quartz head is 12 inches long. The main difference between the two, however, is that the former incorporates a mechanism that enables the windows to be moved relative to each other, and thereby achieving parallelism to within 30 arc-seconds. This is necessary in order to facilitate resonator alignment, which is very critical when an axicon is incorporated into the system.

FLOW OPTIMIZATION

Using the quartz laser head, initial lasing experiments were run with flows set at 20:20:80 (scale readings) H_2:N_2F_4:He using #610 rotameters for N_2F_4 and H_2 and a #600 for He. All flows were regulated with the metering valves on the rotameter, with throttling valves wide open and system pressure

*Similar difficulties were experienced with the power supply subsequent to delivery, and were finally remedied by Xenon Corporation upon installing a capacitor across the ignitron, eliminating the need for the high-voltage transformer modification.

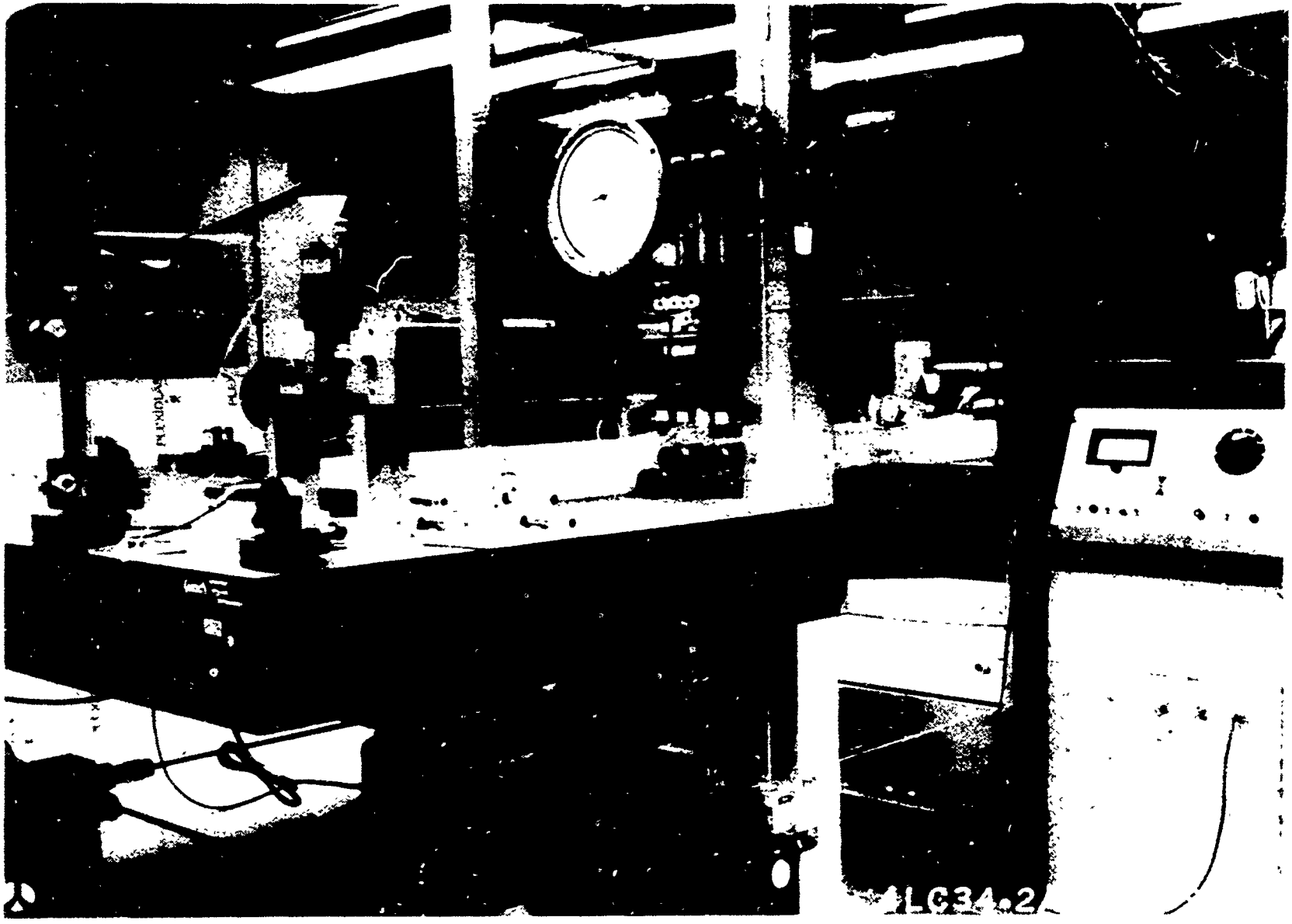

Figure A-6. HF/DF Laser Head - Experimental Apparatus at Rocketdyne

of 150 torr. The flash lamp was fired with 250 joules and the resonator consisted of a 2-inch diameter, 3-m total reflector and a 1-inch diameter sapphire flat with 98% reflectivity at 2.7 μm. The detector used was a Santa Barbara Research Model #9550 InSb operating near 77°K photovoltaically, the output of which was displayed on a Tektronix 7844 dual beam oscilloscope. Another identical InSb detector monitored the flash lamp pulse and was displayed on the second beam of the scope.

Using these conditions, lasing was observed immediately; however, the lasing pulse was about 10 times shorter than the flash lamp pulse. Reduction of the H_2 flow greatly increased the pulse length, but after several flashes, a green luminescence appeared throughout the gain region of the laser head, and the system no longer lased. It was found that, in order to eliminate the reaction producing this green flame, the H_2 and N_2F_4 flows had to be greatly reduced. This was done by opening the metering valves of the N_2F_4 and H_2 rotameters fully and controlling the flows by the throttling valves. Using these valves then the flows were set at 30:5:100 N_2F_4:H_2:He and consistent laser action resulted. The laser pulses follow the flash lamp envelope closely, and are consistent in intensity output, at a flash rep rate of 1/30 seconds. The optimum flash energy was found to be 600 to 800 joules. Figure 7(a) shows a typical HF trace. These lamps are rated at 1580 joules in a 10-μs pulse, this figure being the explosion energy limit.

ACCEPTANCE TESTING

Acceptance of the laser head by Perkin-Elmer required laser demonstration using a 50% outcoupler for both HF and DF. Since procuring such optical elements designed for specific wavelengths involved unacceptable delivery times, it was decided to use an uncoated sapphire flat as one resonator element and a 100% reflecting flat mirror as the other element. Uncoated sapphire transmits ~ 90% of the incident radiation, so that the 50% outcoupling requirement is greatly exceeded. Figures A-7(b) and A-7(c) show the lasing pulses recorded using this 90% outcoupler. Figure A-8 shows a schematic of the experimental setup. Typical output powers, as measured with a Molectron Joule Meter, are 200 μJ, and since only a portion of the annulus was used, this represents approximately 1/8 of the total power extractable from this

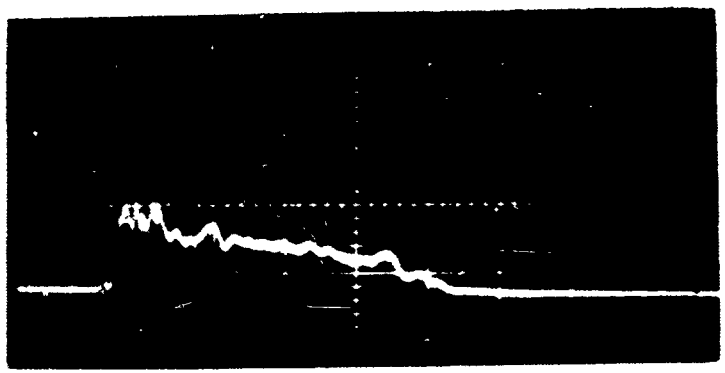

(a) HF, 2% Outcoupler
(5 μs/Div)

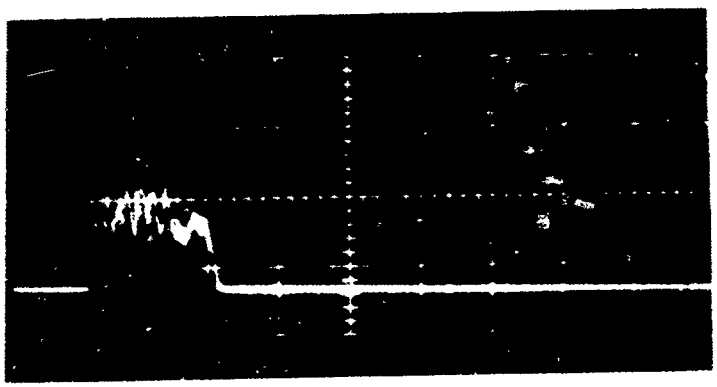

(b) HF, 90% Outcoupler
(10 μs/Div)

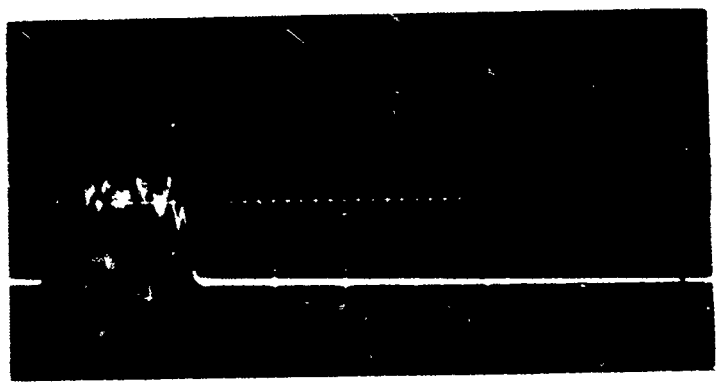

(c) DF, 90% Outcoupler
(10 μs/Div)

Figure A-7. Oscilloscope Traces of Laser Output

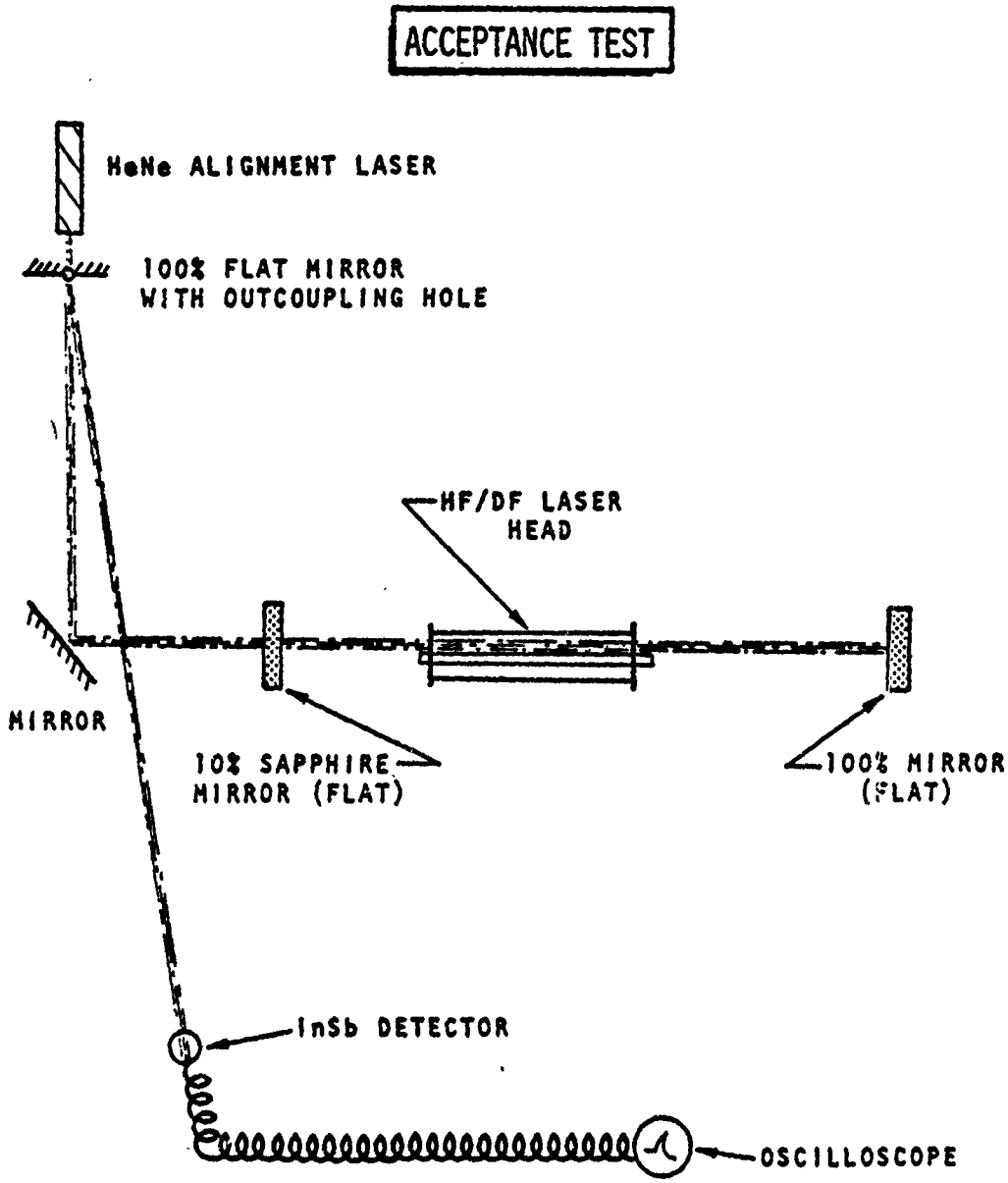

Figure A-8. Experimental Arrangement for Acceptance Testing

head. The shot-to-shot reproducibility of the laser output, both for HF and DF, is well within 5% assuming a rep rate of one shot every 30 seconds. Time, unfortunately, did not permit measurement of spectral content; however, earlier work shows that similar systems lase on the P branch lines of 1-0, 2-1, and 3-2 bands (Ref. 1).

OPERATING INSTRUCTIONS

GENERAL

Prior to operation, ascertain that the entire system has been pumped out to at least 10 millitorr, all the way up to the various gas regulator shutoff valves. It is advisable in fact to pump to 10^{-4} torr or lower for a full 12 hours prior to operation in order to thoroughly clean the system.

REGULATORS AND GAS CYLINDER INSTALLATION

All gas lines must be evacuated up to the regulator shutoff valves in order to minimize any possible atmospheric reactions. For helium and H_2 or D_2, initial regulator hook-up unavoidably traps air in the line and it may be removed by simply flowing the gases through the head for $\sim$ 15 minutes. Since the in-line pressure relief valves are set for 20 psi, this pressure should not be exceeded on the output gauge of the regulator.

For N_2F_4 initial hook-up, air will be trapped in the cylinder-to-regulator section as well as in the regulator itself. After connections are made, the line is evacuated up to the regulator shutoff valve, as above, after which this valve is slowly opened, thus pumping down the regulator output stage. Care should be taken not to peg the needle. This procedure will minimize the amount of trapped air to be mixed with N_2F_4 as the cylinder is opened. N_2F_4 reacts with air and the products can contaminate the rotameter causing the balls to stick and give inaccurate readings. Should this occur, it is easily remedied by breaking the connections at both ends of the rotameter and flushing it out with Freon, drying with clean N_2 and reconnecting using new conical seals.

GAS FLOWS

With the system pumped out, the diffusion pump off and cooled, admit helium to the laser head by turning off both the appropriate throttling and metering valves, opening the regulator valves and setting pressure at 15 to 18 psi (Figure A-3) and then opening the throttle valve fully with the metering valve off. The head pressure is still at less than 1 torr, or the minimum roughing pump pressure, and the vacuum control valve is fully open. Slowly open the He metering valve to obtain a scale reading of 100 with the stainless-steel ball, which will raise the pressure to ~ 50 torr. Slowly close the vacuum-control valve in order to adjust head pressure to 150 torr.

Close N_2F_4 throttling valve, leaving metering valve on rotameter fully open. Open regulator valves and set pressure at 10 to 12 psi. Very slowly open throttling valve to obtain scale reading of 60 with glass ball (dark in color, rests on top of stainless-steel ball). No detectable pressure rise will result.

Repeat N_2F_4 procedure for H_2/D_2, also leaving the metering valve fully open and adjusting flow with throttling valve to obtain a scale reading of 25 to 30, with the regulator set at 15 to 18 psi. These instructions apply to the use of diluted H_2 or D_2, which is supplied as a 92:8 mixture of either H_2 or D_2 in helium. If undiluted H_2/D_2 is used, a #610 rotameter tube must be installed in place of the #600 tube in order to control the flow more precisely. With a #610 tube installed the flow is also adjusted with the throttling valve, metering valve open, for a scale reading of 5 for either H_2 or D_2.

FLASH LAMP AND POWER SUPPLY

The power supply requires several minutes warm-up after the main toggle switch is turned on. An audible click occurs, which is a thermo-sensitive relay, when the circuitry is ready for charging the main capacitors. The red "on" button is then pushed which raises the capacitor shorting bar. The appropriate voltage is selected on the meter dial, the variac is turned to a level that just allows the selected voltage to be reached, and the "charge" button is pushed. An amber ready light comes on when charging is complete.

The lamp is flashed by pressing the button on the trigger box, connected to the power supply by a 5-foot coaxial cable. The energy input to the lamp, an ILC #7D12, should not exceed 1500 joules, although these have been successfully run at 2000 joules. The usual operating range is 600 to 900 joules for this system. If the lamp is not to be fired subsequent to charging the capacitors, the energy may be dumped by pressing the black "off" button, which lowers the shorting bar. It is good practice to minimize the time during which the capacitors remain charged.

SAFETY PRECAUTIONS

The primary hazard associated with operation of this system is the potentially explosive nature of N_2F_4 under certain conditions. The flash lamp power supply poses an electrocution hazard, and of more minor importance are the toxicity of N_2F_4 and the flamability of H_2 and D_2. Considering such potential dangers, the system must not be operated by or worked on by anyone not entirely familiar with its operation.

For general information on N_2F_4, see "Dangerous Properties of Industrial Materials," fourth edition, by N. Irving Sax (Ref. 4). Specific information on the explosive reaction of N_2F_4 with H_2 can be found in references 5 and 6. Care should always be taken to insure that N_2F_4 does not come in contact with organic materials or reducing agents, which requires all lines and fittings to be scrupulously clean. Initial charging of a line should be proceeded by either evacuation or GN_2 purge, and then only 10 psi should be admitted and allowed to stand for several hours in order to passivate the surfaces exposed to pure N_2F_4. Materials successfully used with N_2F_4 include copper, brass, stainless steel, Monel, Viton A, Teflon, and quartz. Since N_2F_4 and H_2 are known to form explosive mixtures at room temperature, certain design precautions in the present system have been incorporated to minimize

4. N.I. Sax, Dangerous Properties of Industrial Materials, 4th edition, Van Nostrand Reinhold, New York, 1975

5. L.P. Kuhn and C. Wellman, "The Explosive Reaction Between Tetrafluorohydrazine and Hydrogen," Inorg. Chem., Vol. 9, p. 603 (1970).

6. J.L. Lyman and R.J. Jensen, "Laser Driven Chemical Reactions of Dinitrogen Tetrafluoride with Hydrogen and Sulfur Hexafluoride with Hydrogen," J. Phys. Chem., Vol. 77, p. 883 (1973).

catastrophic failures. It is known that the expected pressure rise from an N_2F_4-H_2 detonation is 30:1 (Ref. 7). Therefore, if the total pressure of the system cannot exceed 760 torr, assuming a partial pressure of reactants of 1 torr each, no damage will result if detonation occurs. In the present case 2 torr → 60 torr if detonation occurs and 60 torr plus 150 torr of helium diluent yields 210 torr, well below the damage threshold. Dilution of N_2F_4 with helium reduces the likelihood of detonation (Ref. 6); thus in this system helium and N_2F_4 are mixed at least 100:1 He:N_2F_4 immediately upon passing through the rotameters. Further, the laser head should be enclosed by a Lucite scatter shield, 1/4 inch minimum thickness, to protect personnel in the event of explosion.

Since N_2F_4 is considered toxic, to the same degree as HF (Ref. 4), care must be taken to provide proper exhaust facilities whenever N_2F_4 escape is possible. Ideally, the gas console, laser head, and vacuum pump exhaust should be connected to a high-capacity fume hood type exhaust system.

Pressure relief valves have been built into the gas-handling console, and are set to exhaust to the atmosphere at 20 psi. These are placed in series with the feed lines for H_2/D_2 and helium, and will prevent overpressure on the laser head should regulator failure occur. There is no relief valve in the N_2F_4 line. The console is set up to use either pure H_2 and D_2 or H_2 and D_2 that is diluted with helium, depending on the choice of gas cylinders. Should the pressure relief valves vent pure H_2 or D_2 to the atmosphere, an explosion hazard definitely would exist; however, use of diluted H_2 or D_2 (92% He, 8% H_2/D_2) will eliminate any such probability.

The electrocution hazard is always present when using high-energy storage capacitors, and it is particularly evident in a breadboard system such as this. Great care must be taken to discharge the main capacitors before approaching any electrical components of the system. The flash lamp power supply is a commercial unit and therefore has interlocks that dump the capacitors when the black "off" button is pushed or when the rear door of the cabinet is opened. It is always wise to ground the capacitors a second time before

7. Reed Jensen, Los Alamos Scientific Labs, Los Alamos, NM, private communication.

touching anything electrical, because the energies here are lethal. The Lucite scatter-shield mentioned earlier must be set up so as to make inadvertent contact with the flash lamp leads impossible. Proper operation and technical information on the power supply is to be found in the instruction manual delivered with the system.

FAILURE MODES

GAS HANDLING CONSOLE AND LASER HEAD

Possible trouble spots that can be anticipated with extended use of this system, and which relate primarily to exposure of the components to HF, are:

(1) N_2F_4 rotameter metering valve seals

(2) Degradation of window coatings, both from contamination and etching

(3) Vacuum pump oil contamination and corrosion of moving parts

(4) Degradation of epoxy seals.

Flash Lamp and Power Supply

(1) Lamp life > 1000 pulses at 600-800 joules

(2) Ignitron - metallic head must be baked periodically at 150°C for 6 to 8 hours to remove mercury condensate from top electrode. Should be baked after transport or shipment of power supply prior to use.

REFERENCES

1. C. E. Wiswall, D. P. Ames and T. J. Menne, "Chemical Laser Bibliography," IEEE Quant. Elec., Vol. 9, p. 181 (1973).

2. L. E. Brus and M. C. Lin, "Chemical HF Lasers from Flash Photolysis of various N_2F_4 + RH Systems," J. Phys. Chem., Vol. 75, p. 2546 (1971).

3. T. D. Padrick and G. C. Pimentel, "Hydrogen Fluoride Elimination Chemical Laser from N,N-Difluoromethyl-amine," J. Chem. Phys., Vol. 54, p. 720 (1971).

4. N. I. Sax, Dangerous Properties of Industrial Materials, 4th edition, Van Nostrand Reinhold, New York, 1975.

5. L. P. Kuhn and C. Wellman, "The Explosive Reaction Between Tetrafluorohydrazine and Hydrogen," Inorg. Chem., Vol. 9, p. 603 (1970).

6. J. L. Lyman and R. J. Jensen, "Laser Driven Chemical Reactions of Dinitrogen Tetrafluoride with Hydrogen and Sulfur Hexafluoride with Hydrogen," J. Phys. Chem., Vol. 77, p. 883 (1973).

7. Reed Jensen, Los Alamos Scientific Labs, Los Alamos, NM, private communication.